SCOUR AT THE BASE OF RETAINING WALLS AND OTHER LONGITUDINAL STRUCTURES

FINAL REPORT

Prepared for
NCHRP
Transportation Research Board
of
The National Academies

Author
Dr. Fotis Sotiropoulos
Stony Brook University
Stony Brook, NY

Dr. Panos Diplas
Lehigh University
Bethlehem, PA

April 2017

ACKNOWLEDGEMENT OF SPONSORSHIP

This work was sponsored by one or more of the following as noted:

X American Association of State Highway and Transportation Officials, in cooperation with the Federal Highway Administration, and was conducted in the **National Cooperative Highway Research Program**,

☐ Federal Transit Administration and was conducted in the **Transit Cooperative Research Program**,

☐ Federal Aviation Administration and was conducted in the **Airport Cooperative Research Program**,

☐ Research and Innovative Technology Administration and was conducted in **the National Cooperative Freight Research Program**,

☐ Pipeline and Hazardous Materials Safety Administration and was conducted in the **Hazardous Materials Cooperative Research Program**,

☐ Federal Railroad Administration and was conducted in the **National Cooperative Rail Research Program,**

which is administered by the Transportation Research Board of the National Academies.

DISCLAIMER

This is an uncorrected draft as submitted by the Contractor. The opinions and conclusions expressed or implied herein are those of the Contractor. They are not necessarily those of the Transportation Research Board, the National Academies, or the program sponsors.

Contents

List of Figures

Author Acknowledgements

The research reported herein was performed under NCHRP Project 24-36 by the St. Anthony Falls Laboratory at the University of Minnesota. Lehigh University and the Virginia Polytechnic Institute and State University (Virginia Tech) were subcontractors to the University of Minnesota.

Dr. Fotis Sotiropoulos, Professor of Civil Engineering and Director of the St. Anthony Falls Laboratory (SAFL) at University of Minnesota, currently dean of College of Engineering & Applied Science and Professor of Civil Engineering Department at Stony Brook University, is the Project Director and the Principal Investigator. The other authors of this report are Dr. Panos Diplas, Civil and Environmental Engineering Dept. of Lehigh University, Dr. Ali Khosronejad, Research Associate at SAFL (currently Assistant Professor at Civil Engineering Department of Stony Brook University), Dr. Jessica Kozarek, Research Associate at SAFL, Phairot Chatanantavet, Post-Doctoral Associate at Lehigh University, Nasser Heydari, Ph.D student at Lehigh University, Colleen Turley, M.S. Student at Lehigh University, Polydefkis Bouratsis, Ph.D Student at Virginia Tech, and Nikos Apsilidis Ph.D Student at Virginia Tech. The work was completed under the general supervision of Dr. Fotis Sotiropoulos and Dr. Diplas at Lehigh University.

Abstract

We carried out a series small- and large-scale experiments at Lehigh University and the Outdoor StreamLab (OSL) of University of Minnesota, respectively, to obtain datasets for maximum scour depth at the base of longitudinal walls. These datasets are used to validate the coupled flow and morphodynamics model of Virtual Flow Simulator (VFS-Rivers). The dataset of the small-scale experiments, which contains 64 data points, is employed to present an empirical relationship for maximum scour depth due to local scour near the leading edge of longitudinal walls with different bank and wall configurations. The validated numerical model is run for more than 20 test cases to obtain more data for the maximum scour depth in the large-scale meandering rivers due to general scour. Combining the maximum scour data from large-scale experiments at the OSL (four data points) and numerical simulations (20 data points), we obtained a dataset that was used to produce another empirical relationship to estimate the maximum scour depth at the base of longitudinal walls due to general scour in meandering rivers. The maximum scour depths obtained from the two presented equations can be linearly added to give the total maximum scour depth at the base of longitudinal walls in meandering rivers. The presented equations are valid within a specific range of data for sediment material, flow field, and waterway characteristics.

Executive Summary

The current state-of-the-art for the scour depth prediction near longitudinal walls is be limited to two empirical equations, which are obtained from a limited number of experimental and field data. These existing methods of prediction do not take into account some important properties of flow, sediment and waterway geometry, including, for instance: median grain size of sediment material, mean-flow depth and velocity, and sinuosity of meandering rivers.

To fill the gap and develop a more comprehensive relationship for estimating the total scour depth at the base of longitudinal walls, we carried out a series of experimental (large- and small-scale) and numerical investigations encompassing most of the important characteristics of the sediment, flow and waterway geometry. In these investigations, we studied the effect of turbulence, sediment material, roughness of the structures, and river geometry on the scour depth at the base of longitudinal walls.

A series of small-scale laboratory experiments were conducted at Lehigh University to produce 64 data points for the local scour depth occurring at the leading edge of longitudinal walls. Based on these data points, we obtained a relationship for estimating the maximum scour depth in the vicinity of longitudinal walls due to *local scour* process. This dataset was also used to validate the numerical model.

A series of large-scale experiments were also carried out at the Outdoor StreamLab of St. Anthony Falls Laboratory at the University of Minnesota to produce large-scale physical data for the validations of numerical model. The large-scale experiment data (four data points) were also combined with 20 data points obtained from numerical simulations to develop a relationship for estimating the maximum scour depth at the base of longitudinal walls due to *general* scour.

The *total* maximum scour depth at the base of longitudinal walls is considered to be a linear combination of *local* and *general* scours. Thus, the scour depth values obtained from the two equations for the local and general scours, respectively, can be linearly combined to obtain the *total* maximum scour depth at the base of longitudinal walls in meandering waterways.

1 Introduction

Longitudinal walls are widely used to enhance the slope stability of earth material and protect bridge abutments and other longitudinal structures that encroach into waterways. When installed at riverbanks, their base becomes subject to erosion due to the action of water. Even partial exposure of the foundation may result in the failure of the longitudinal wall. Thus, longitudinal walls on the river banks require to be protected against scour that can lead to structure undermining and failure by designing and installing countermeasures to mitigate erosion along the face and/or at the bottom of the structure. In meandering rivers flowing through urban areas or along roadways, retaining walls are commonly used as a countermeasure to prevent streambank erosion (HEC-20). Such longitudinal countermeasures include vertical and/or sloping walls that are constructed of rocks, cable-tied blocks, geo-bags, steel sheet pile, etc. (Martin-Vide et al. 2011). These walls generally form a vertical or sloping surface where scour takes place with the purpose of withstanding high shear stresses encountered during high flow events. The presence of the longitudinal structure provides an armoring layer that protects underlying bed material from being eroded (Lagasse et al. 2004).

A critical component missing from the design, installation, and monitoring of these structures is the ability to accurately determine the maximum depth of scour along the base of the retaining wall or longitudinal structure to ensure that their foundations are set at elevations below maximum expected scour depths, thereby preventing failure due to undermining. Therefore, to date, the maximum scour depth along the base of retaining wall structures and longitudinal walls is either not considered or estimates are made based on unreliable "rule-of-thumb" guidance. For instance, the most commonly utilized relation to compute the local scour depth around vertical and sloping longitudinal walls is an analytical-empirical equation employed in HEC-18 and HEC-23 in which the scour depth at the base of longitudinal walls is related to the flow depth, Froude number and the angle that flow impinges on the wall (HEC-23).

Due to the lack of a unified and reliable guideline to calculate the scour depth along the base of a longitudinal structure, some practitioners utilize the general (contraction) scour relation of abutment design to provide an order-of-magnitude estimate of potential scour. Scour along the base of such longitudinal structures is a result of a combination of processes including: (1) general scour caused by the 3D curvature effect of meandering; and, (2) local scour due to the presence of the complex large-scale energetic coherent structures at the leading edge of the retaining wall and/or around larger rocks occasionally used in constructing the wall.

Scour depth prediction at the base of longitudinal walls becomes even more intricate considering the fact that maximum scour events often occur during peak flood stage when field observations are both difficult and dangerous, and the resulting scour holes may be partially or completely filled during the recession of the passing flood (HEC-18). This process results in maximum scour depths often going unobserved without a costly and potentially dangerous effort. Some of the typical engineering approaches used today (mainly by geotechnical engineers) is to estimate the scour depth based on empirical guidance to ensure that maximum scour depths do not reach the base of the longitudinal structure to avoid failure. For instance, it is recommended that for walls constructed along rivers and streams where the depth of scour has been determined, a minimum embedment of 0.6 m below this depth should be considered as the foundation level (HEC-23).

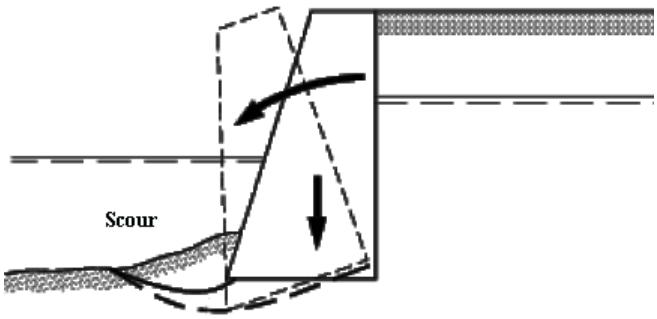

Figure 2. Illustration of overturning and structure failure of a retaining wall due to scour along the base.

Development of a set of reliable and comprehensive relationship to accurately predict the maximum scour depth at the base of longitudinal walls in rivers and waterways is therefore essential. In order to develop such relationship, one needs, however, to take into account all of the effective parameters including turbulent flow, sediment, and waterway characteristics. It is also critical to understand the complex environments and dynamic interaction between the hydrodynamic and geomorphic systems in the vicinity of the longitudinal walls. Current guidelines detailed in HEC-23 are often challenged and considered excessively conservative and lack many of the effective parameters including the soil characteristics, wall roughness and slope, flow discharge, and meander characteristics.

An adequate relationship for predicting maximum scour must take into account both local and general scour processes. Local scour along the base of longitudinal walls occurs either under clear water conditions (i.e. no active sediment transport from upstream into the scour zone) or live bed conditions (i.e. active sediment transport from upstream). Local scour can also result from the acceleration of the flow around the wall leading edge and along the base of the longitudinal structure, the roughness transition imposed by the presence of the wall, and the generation of large-scale energetic vortices shed from the wall. Additionally, longitudinal walls installed along both inner and outer banks throughout meandering rivers may also experience significant scour and deposition along the meander wave length. This phenomenon, known as general scour, occurs along the base of the longitudinal walls, increasing the risk of structure failure. During flooding events, the hydrodynamic processes accelerate these local and general scour mechanisms and endanger the structural integrity of retaining wall structures by reducing the passive resistance and overall bearing capacity of the foundations (Fig. 1) (HEC-23).

Abrupt change in river-bank roughness and stepped transitions at the leading edge of the retaining walls or longitudinal structures can introduce complex large-scale energetic coherent structures in the surrounding flow environments. The vortices give rise to complex sediment transport phenomena and scouring dynamics originating at the exposed upstream edge of the structure. This means that one needs to take into account the effective roughness height of the longitudinal walls in order to predict the local and general scour at the base of these structures.

We employ a set of science-based predictive engineering tools to develop two relationships for predicting the maximum scour depth at the base of longitudinal walls by considering most of the effective flow, sediment, and waterway parameters, including: sediment particle median grain size, mean-flow velocity, mean-flow depth, angle of installation, effective roughness of longitudinal walls, and sinuosity of the waterway. We develop two separate equations. One equation is developed based on our indoor flume experiments at Lehigh University to represent the maximum scour depth at the leading edge of the longitudinal wall due to local scour. The other equation is developed base on the numerical simulation and Outdoor StreamLab (OSL) of St. Anthony Falls Laboratory (SAFL) data to represent the maximum scour depth at the base of the longitudinal wall due to general scour process. A linear combination of the

two maximum scour depths yields the total scour depth at the base of longitudinal walls. Use of the two equations in this study will ensure that engineering standards remain at a high level while minimizing the economic impact of design, installation, monitoring, and maintenance of retaining walls and other longitudinal structures.

2 Background

Scour along the base of longitudinal structures has been a growing focal point in many engineering practices. Most practitioners are well aware of the paucity of suitable design guidelines that can be used to prevent and halt scour development along major embankments and retaining walls. Because literature in this sector is very limited, many structures are designed by empirical methods and are based on previous experiences rather than well founded and tested engineering techniques.

At the beginning of this study, we identified and evaluated the scour prediction guidelines that are currently used by practitioners. By determining the effectiveness of these guidelines and identifying the potential gaps, the research plan for the development of successful scour prediction methodologies in this study was refined and finalized.

Among the limited number of studies (see, e.g., Carriaga (2000), Davies and Carriaga (2001), Anderson and Williams (2002), Kearney and Gloonan (2005), Martin-Vide (2010), McKelvey (2011), Giró and Schleiss (2012)), the HEC-23 manual, which is provided by the Federal Highway Administration, contains the most popular guidelines for engineers and practitioners in the field. More specifically, HEC-23 provides guidance for engineers through the design and monitoring process to determine depth of scour at the base of longitudinal retaining walls. The guidelines for predicting local scour depths are resulted from analytical simplifications to evaluate potential scour along a vertical wall (HEC-23). In this simple formula, the depth of maximum scour (H_s) is related to the mean flow depth (H), Froude number (Fr), and the angle between the impinging flow direction and the vertical wall (α) as follows:

$$\mathrm{H_s}/H = (0.73 + 0.14\pi F_r^2)Cos\alpha + 4F_r^{0.33}Sin\alpha \qquad (1)$$

in which α varies from 0 to 90 degrees for flow parallel and perpendicular to the side wall, respectively. Other references, such as the "Handbook of Geotechnical Investigation and Design Tables" (Look, 2007), suggest that the minimum embedment for retaining walls should be 20% of their height, without explicitly stating whether this guideline incorporates the effect of scouring or not.

Maynord (1996) presented an empirical method for determining scour depths on a typical bend with sand bed materials. Maynord's method of estimating scour depth is based on a regression analysis of 215 data points extracted from laboratory investigations and field observations with return period of one to five years. Maximum scour depth at the base of a retaining wall as defined in Maynord's best-fit equation for scour depth estimation is a function of mean-flow depth (H), radius of curvature to width ratio (R_C/W), and width to depth ratio (W/H), which reads as follows:

$$(\mathrm{H} + \mathrm{H_s})/H = 1.8 - 0.051(R_C/H) + 0.0084(W/H) \qquad (2)$$

It is noteworthy to mention that the correlation coefficient of this proposed equation is relatively low (r^2=0.49). In a separate study by Zimmerman (1997), it is noted that Eq. (2) does not take into account critical parameters such as the flow velocity and the size of sediment materials. In his closure, Maynord (1997) acknowledged the need for more elaborate, physics-based studies of the phenomenon that could provide more accurate descriptions and estimates of the scour compared to the purely empirical derivations.

We also note that both Eq. (1) and (2) are applicable for clear-water scour conditions. For live-bed conditions, HEC-23 suggests that the maximum scour depth caused by bedforms should be added to these calculated scour depths (HEC-23). It can be clearly seen that current relationships for predicting the scour depth (e.g. Eqs. (1) and (2)) suffer from the lack of important influential parameters including flow velocity, sediment material cohesiveness, meander characteristics, retaining wall slope, and wall roughness.

To identify the most common practices in scour prediction and provide useful insight on the scour phenomenon at the base of longitudinal structures, we also designed a comprehensive survey to document the current-state-of-practice used by engineers and practitioners dealing with longitudinal structures. Responders and interviewees in this survey include engineers and practitioners from all the State Departments of Transportation (DOTs), a few private companies and several state and federal organizations, such as the US Forest Service (USFS), Departments of Natural Resources (DNRs), Departments of Environmental Quality/Protection (DEQs/DEPs), the US Geological Survey (USGS) and the US Army Corps of Engineers (USACE).

The major findings of the survey confirmed our findings from literature review regarding the need to (a) better understand the scour mechanisms at the base of the retaining walls and (b) develop a set of comprehensive relationships for estimating scour depth at the base of longitudinal walls. These finding are summarized as follows: (1) current methods to design longitudinal structures and evaluate scour are sparse, general, and untested; (2) practitioners reported longitudinal structure failure due to excessive scour; (3) scour countermeasure use was based on practitioner preference; (4) current longitudinal structure guidelines were considered inadequate by practitioners because they were too general and do not include “soil” conditions; (5) HEC-23 was the most used design methodology, often combined with a supplemental method (HEC-18, and local methods); (6) longitudinal structure effectiveness is dependent on site-specific characteristics; (7) practitioners recommended research that incorporates longitudinal structure roughness and sediment material characteristics.

Given the enormous challenges of predicting the maximum scour depth along the base of longitudinal walls, it is the basic premise of this study that major advances need to be made in our ability to predict scour depths along the base of longitudinal wall structures. In this study, we employ an innovative research approach that integrates experiments across a range of scales with state-of-the-art numerical simulations to produce adequate number of data point for developing a set of equations to estimate the maximum scour depth at the base of longitudinal walls.

3 Research Approach

Our research approach uses a combination of innovative physics-based state-of-the-art computational methods and multi-scale experimental datasets to investigate the complex relationships between total scour at the base of longitudinal walls and other critical parameters such as flow, sediment material, and waterway characteristics. To accomplish this goal, we couple an in-depth literature assessment and survey of the needs and scour research challenges (Appendices A and B) with a comprehensive study of scour processes using field-scale experiments (Appendix C), indoor laboratory experiments (Appendix D), and numerical simulations (Appendix E).

The indoor flume experiments at Lehigh University are used to investigate scour at the leading edge of longitudinal structures due to local scour. These experimental data are also used to validate the numerical model (Appendix E).

The OSL experiments at SAFL are carried out to produce data points for numerical model validations (Appendix E). These data are also combined with the numerical simulations data to develop an equation for maximum scour depth at the base of the longitudinal walls due to general scour.

4 Compilation of Experimental and Numerical Results to Develop Scour Relations

The results obtained from small-scale indoor experiments, listed in Table 2 of Appendix D, are used to develop an empirical relationship for estimating the maximum scour depth in the vicinity of a retaining wall due to local scour. It is found that in all experiments the maximum scour depth occurs near the leading edge of the wall, which is due to the abrupt contraction from the channel bank to the vertical wall (see Fig. 2). The abrupt contraction results in pronounced local flow separation and intense vorticity. The formulation presented here will provide practitioners with a scour evaluation methodology at the base of the leading edge of longitudinal walls, especially during flood conditions. The analysis below provides significant improvement for the case of scour near the base of longitudinal retaining walls, currently not available in the literature. Fig. 2 shows a schematic of the area near the leading edge of the retaining wall in the flume experiments at Lehigh.

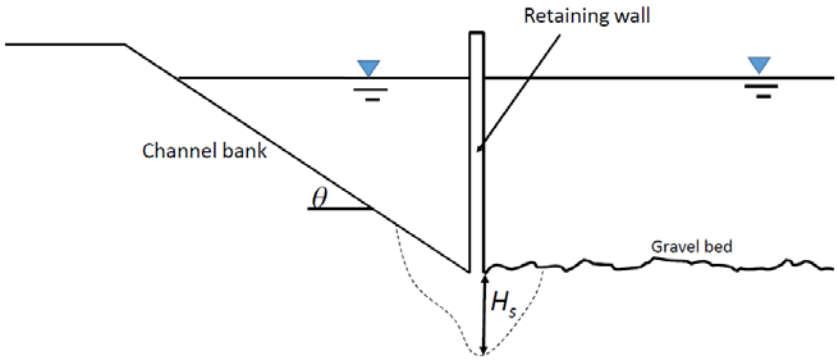

Figure 2. Schematic of cross-section at the transition from a sloping bank to rectangular section within the retaining wall area. Flow direction out of the paper.

Considering dimensional analysis, the maximum scour depth due to local scour (H_{sl}) can be written as a function of other independent dimensional variables. One possible set of such variables is included in Eq. (3):

$$H_{sl} = f(H, d_{50}, U, \theta, g, \upsilon, R) \tag{3}$$

where H is the mean-flow depth, d_{50} median grain size of the sediment material, U is the mean-flow velocity, θ is the bank slope (shown in Fig. 2), g is the acceleration of gravity, υ is the kinematic viscosity of water, and $R = (\rho_s - \rho)/\rho$ is submerged specific density; where ρ_s is the density of sediment and ρ is the density of water). By selecting d_{50} and g as the repeating variables, and following standard dimensional analysis procedures, Eq. (3) can be recast in terms of dimensionless parameters in the following way:

$$H_{sl}/d_{50} = f\left(H/d_{50}, Fr_d, \theta, Re_p, R\right) \tag{4}$$

Where Re_p is particle Reynolds number ($=Ud_{50}/\nu$) and $Fr_d = U/\sqrt{gd_{50}}$ is the "grain-size Froude number". Re_p is not as important for a fully rough boundary, where the friction factor (and critical Shields stress) becomes independent of particle Reynolds number. Additionally, for natural rivers, R is approximately constant. Therefore, Eq. (4) can be reduced to:

$$H_{sl}/d_{50} = f\,(H/d_{50}, Fr_d, \theta) \tag{5}$$

This analysis is limited to non-cohesive bed material. Using all 64 data points (Table 2 in Appendix D) obtained from the experiments, and employing forward multiple regression analysis, the following expression is obtained:

$$H_{sl}/d_{50} = 0.0178(H/d_{50})^{1.24}\left(cot(\theta)\right)^{1.325} Fr_d^{1.108} \tag{6}$$

This equation has a goodness of fit $r^2 = 0.63$ and covers considerable range of bank slopes ($28° \leq \theta \leq 70°$), bed slopes ($0.09 \leq S \leq 0.6\%$), relative roughness values ($17.9 \leq H/d_{50} \leq 62.5$) and grain size Froude number ($1.59 \leq Fr_d \leq 3.89$).

Figure 3 depicts the best-fit curve between the measured values of scour depth due to local scour and the combination of independent variables with the exponents obtained from the multiple regression analysis. All the variables in the model were statistically significant, the p-value of the exponents were less than 0.005.

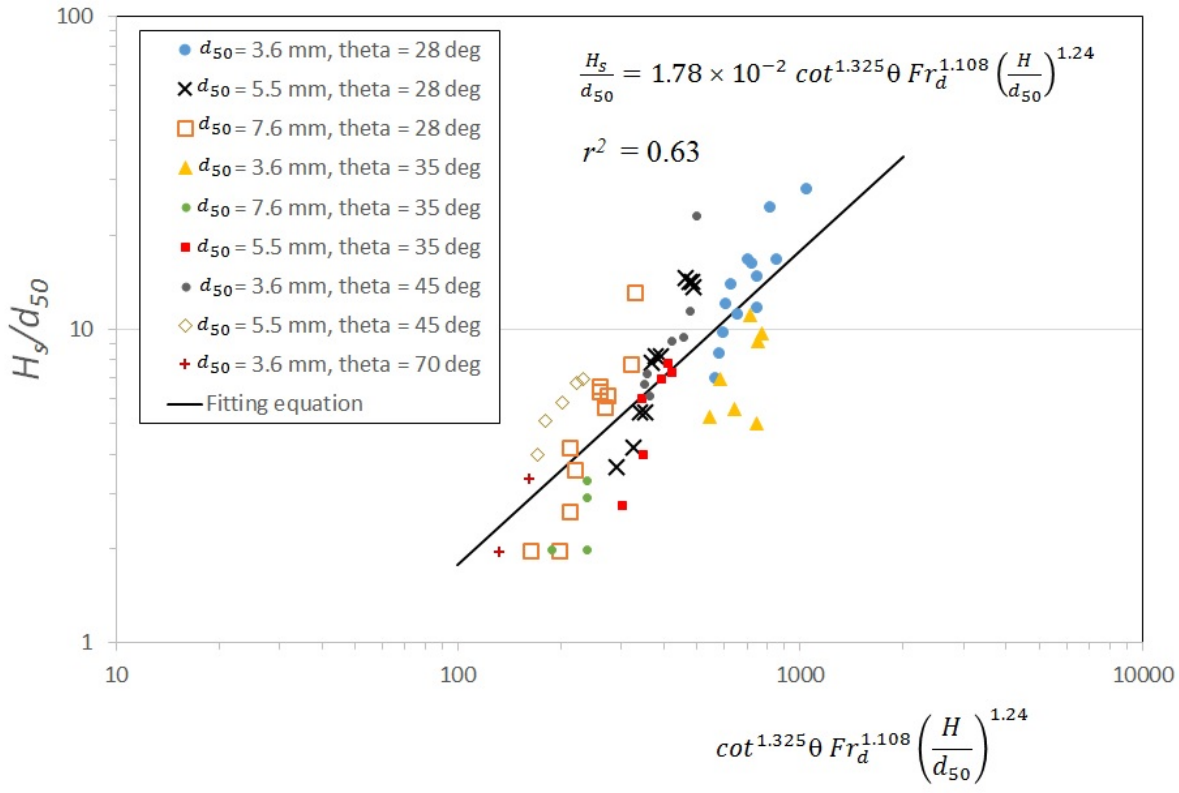

Figure 3. Regression equation to estimate maximum scour depth due to local scour at the leading edge of the retaining wall.

The results obtained from large-scale physical modeling in the Outdoor StreamLab of SAFL (four data points) (Appendix C) are combined with the numerical simulations results (20 data points) (Appendix E) to develop an empirical relationship for estimating the maximum scour depth at the base of longitudinal walls due to general scour. It is found that for most cases the maximum scour depth due to general scour occurs near the mid-length of the longitudinal walls.

Similar to the analysis for the local scour data, via dimensional analysis, parameters influencing the maximum scour depth due to general scour along the length of the walls are as follows:

$$H_{sg} = f(d_{50}, U, H, S, \lambda_m, A_m, Q, g, k_s, \psi) \quad (7)$$

where H_{sg} is the maximum scour depth due to general scour, S is the channel bed slope, λ_m is the wavelength of the meander bend, A_m is the amplitude of the meander bend, Q is the flow discharge, k_s is the effective roughness height on the longitudinal wall, and ψ is the angle of installation of the longitudinal wall (Fig. 4). Angle of installation, ψ, is the angle that longitudinal wall makes with the tangent to the river bank at its apex. Therefore, ψ for a straight channel is zero.

Effective roughness height is measured as the mean of intrusion length of roughness elements into the channel. For instance, assume that a longitudinal wall is constructed using rock structures. If the average intrusion length of rocks into the channel is 10 cm, then k_s will be 10 cm, as well.

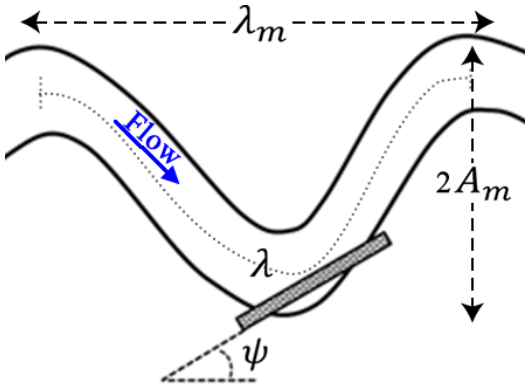

Figure 4. Schematic of a meander bend showing the installation angles (ψ) of the longitudinal wall, wavelength (λ_m), arc-length (λ) and amplitude (A_m) of the meander.

The maximum scour depth due to general scour can be best found if scaled with d_{50} (which, in this study, varies between 0.1 mm to 32 mm) (see Table 2 of Appendix E). The characteristics of a meander bend can also be best expressed via its sinuosity (s)($= \lambda_m/\lambda$), which is a function of λ_m and λ (see Fig. 4). Therefore, Eq. (7) in its non-dimensional form can be rewritten to obtain:

$$H_{sg}/d_{50} = f(Fr, Fr_d, tan(\psi), s, k_s/H) \quad (8)$$

We analyzed numerous methods to best represent the bulk of these data in one empirical relationship (see Fig. 5) and found that the following equation provides the best overlap:

$$H_{sg}/d_{50} = 1909\,(Fr\ s\ \vartheta)^{-10/9} + \frac{8}{5}\,Fr_d - \frac{3\pi}{2}\mathrm{e}^{(k_s/H)^{1/10}} \quad (9)$$

in which ϑ for the gravel (G) and sand (S) bed rivers (for more details on the two G and S rivers see Appendix E) is defined in Eqs. (10) and (11), respectively:

$$\vartheta = Max\{150, (\tan\psi)^{-2}\} \quad (10)$$

$$\vartheta = Max\{100, (\tan\psi)^{-2}\} \quad (11)$$

Equation (9) has a correlation coefficient of r^2 = 0.821 with the following important limitations:

1- It is only applicable for rivers and streams with non-cohesive material;

2- It is developed for rivers under bankfull flow conditions and thus use of this equation for base-flow condition can result in misleading predictions;

3- It is best applicable for the rivers that have geometry, flow, and sediment characteristics within the range of the rivers we studied in this project (see Table 2 of Appendix E);

4- Scour hole due to the intrusion of the upstream edge of the longitudinal wall is not considered in obtaining the dataset for developing Eq. (9) and such scour depth needs to be determined based on the small-scale laboratory experiments (Eq. 6);

Hence, we propose the use of Eq. (9) as a formula to calculate the maximum scour depth at the base of longitudinal walls in meandering rivers due to general scour process. To avoid misleading predictions, it is important, however, that the four abovementioned limitations to be considered. A linear combination of the two scour depths obtained from Eqs. 6 and 9 can obtain a conservative value for the maximum scour depth (H_s) at the base of longitudinal walls:

$$H_s = H_{sl} + H_{sg} \quad (12)$$

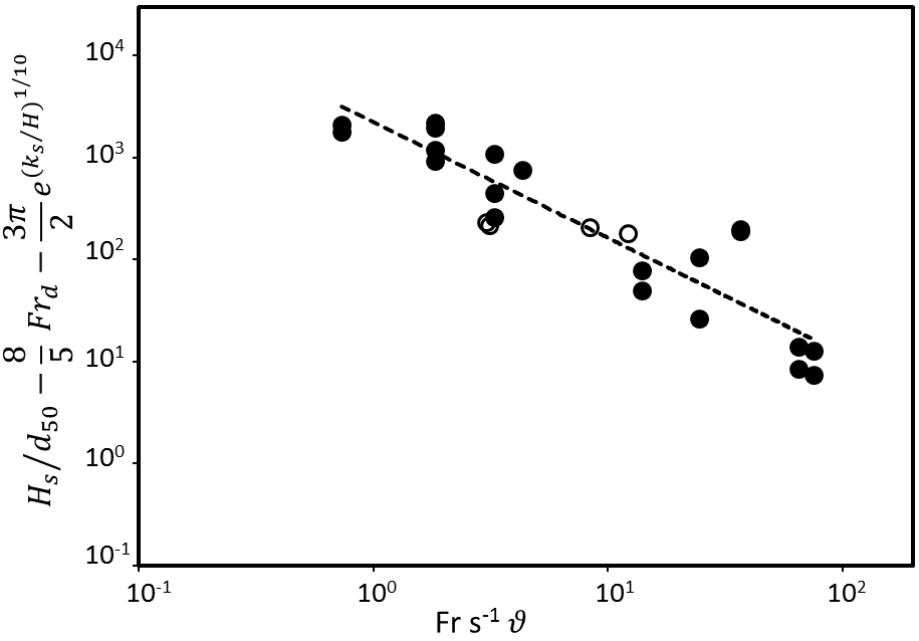

Figure 5. Maximum scour depth data obtained from large-scale experiments (hollow circles) and numerical simulations (bold circles) for general scour and the regression equation overlapping the data points (dashed-line). r^2 of the regression is 0.821.

5 References

Anderson, S., and Williams, J. (2002). "Road Stabilization, Reconstruction, and Maintenance with a Combined Mechanically Stabilized Earth and Secant Pile Wall: Zion National Park, Utah." Transportation Research Record: Journal of the Transportation Research Board, 1808(-1), 76-83.

Bouratsis, P., Diplas, P., Dancey, C.L., and Apsilidis, N. (2013). "High-resolution 3-D monitoring of evolving sediment beds". Water Resources Research, 49(2): 977-992.

Carriaga, C.C. (2000). "Scour Evaluation Program for Toe-Down Depth Assessment." Building Partnerships, 1-10.

Davies, R., and Carriaga, C.C. (2001). "Scour Evaluation Procedure for Determining Toe-Down Depths of Hydraulic Structures." Bridging the Gap, 1-9.

Federal Highway Administration, (2001). "Evaluating Scour at Bridges." Hydraulic Engineering Circular No. 18 (HEC-18). 4th Edition, Washington D.C. – U.S. Department of Transportation.

Federal Highway Administration, (2001). "Bridge Scour and Stream Instability Countermeasures," Hydraulic Engineering Circular No. 23 (HEC-23). Washington D.C. – U.S. Dept. of Transportation.

Federal Highway Administration, (2001). "Stream Stability at Highway Structures," Hydraulic Engineering Circular No. 20 (HEC-20). Washington D.C. – U.S. Department of Transportation.

Giró, A.V., and Schleiss, A.J. (2012). "Bank protection at the outer side of curved channels by an undulated macrorough concrete wall." Proc., 4th IAHR International Symposium on Hydraulic Structures.

Kearney, P.G., and Gloonan, J.F. (2005). "Scour analysis evaluation for the proposed Indian River inlet bridge at Sussex County, Delaware." Duffield Associates Inc., 10.

Lagasse, P.F. Spitz, W.J., Zevenbergen, L.W., and Zachman, D.W., 2004, "Handbook for Predicting Stream Meander Migration using Aerial Photographs and Maps," Report for the National Research Council, Trans Res. Board, Natl. Cooperative Highway Research Council, NCHRP Report 533.

Martin-Vide, J.P. (2010). "Local Scour in a Protruding Wall on a River Bank." J. Hydraul. Res., 45(5), 710-714.

Maynord, S. T. (1996) "Toe scour estimation in stabilized bendways." J. of Hydraul. Eng., ASCE, 122(8).

Maynord, S.T. (1997). "Closure: Toe-Scour Estimation in Stabilized Bendways." J. Hydraul. Eng., 123(11), 1048-1050.

McKelvey, J.A. (2011). "Lessons Learned from Failures: The Wall of Shame." Geo-Frontiers 2011, 3235-3244.

Martin-Vide, J. P., Roca, M. and Alvarado-Ancieta, C. A. (2011) "Bend scour protection using riprap." Water Management, 163(WM10):489-497

Appendix A

State of the Art Review

A.1 Introduction

Retaining walls are widely used to enhance the slope stability of earth material. When installed at riverbanks, their base becomes subject to erosion due to the action of water. Even partial exposure of the foundation often results to the failure of the wall. Identifying the mechanisms responsible for the failure of a wall is an area of active research in the fields of geotechnical and hydraulic engineering and depends greatly on the topography of the eroded river bed, among other parameters (see for example Huang and Chen, 2012). Scouring is also a problem affecting other longitudinal structures (e.g. embankments) that built on floodplains and adjacent to riverine systems. Despite the popularity of these types of structures, we still lack a comprehensive understanding of the mechanisms that drive scouring phenomena at the water-soil-structure interfaces. While manuals dealing with retaining walls provide extensive description about geotechnical design aspects, they do not include any meaningful and specific guidelines when it comes to proper construction for protecting the wall from scour, even though the latter represents a prevalent mechanism of failure. As a result, critical information about the design, installation, and performance of retaining walls and longitudinal structures is incomplete, scarce, and scattered among various sources. This document summarizes the major findings of a thorough literature review on scouring at the base of retaining walls, embankments and other structures of similar type.

A.2 Design standards

Scour at the base of retaining walls and longitudinal structures is typically being evaluated using a combination of empirical equations and "rule-of-thumb"-type of recommendations. The Hydraulic Engineering Circular No. 23 (HEC 23) provides the following equation for the computation of the terminal scour depth (y_s) at the toe of a retaining wall:

$$\frac{H_s}{H} = (0.73 + 0.14\,\pi\, Fr^2)cos\theta + 4Fr^{0.33}sin\theta \quad (1)$$

where $H_s$is the maximum scour depth divided by mean-flow depth, H. The maximum scour is a function of the flow angle of attack (θ) and the Froude number. The equation employed in HEC-23 is intended to provide a first approximation of potential scour and is not expected to be predictive of actual scour in complex flows. This equation is based on work by Mussetter Engineering (2008) and its effectiveness has yet to be evaluated. Other references, such as the "Handbook of Geotechnical Investigation and Design Tables" (Look, 2007), suggest that the minimum embedment for retaining walls should be 20% of their height, without explicitly stating whether this guideline incorporates the effect of scouring or not. Due to this paucity of sound design tools, engineers have sought additional methodologies for the estimation of scour at retaining walls. For example, Carriaga (2000) and Davies and Carriaga (2001) describe a conservative scour estimation technique. According to this methodology, the total scour at the base of a retaining wall is estimated as the sum of a number of scour depths (local scour, long-

term degradation, bend scour, bedform trough, and general scour) multiplied by a safety factor of 1.3.

A.3 Field and laboratory investigations

Useful information about the scour phenomenon at the base of longitudinal structures can also be extracted from laboratory investigations and field observations. Maynord (1996) revisited a number of empirical equations for the prediction of scour at the toe of banks under the clear-water scour regime. Then, he furnished the following equation after regressing results from 215 measurements taken at various bends of the Mississippi River:

$$\frac{H_S}{H} = 1.8 - 0.051\left(\frac{R_c}{W}\right) + 0.0084\left(\frac{W}{H}\right) \quad (2)$$

Namely, the maximum scour depth (H_s) was obtained as a function of parameters such as the mean flow depth (H), the centerline radius of the meander bend (R_c), and the water surface width at the upstream end of the bend (W). Whereas the author of this work cautioned that this empirical equation might only be valid within specific bounds of bend curvature and channel aspect ratio, he did not inform about the nature of the embankments used (vertical or sloped). It is also worth noting that the coefficient of determination for the proposed equation was relatively low, namely r^2=0.49. Additionally, as it was pointed out in the discussion of the aforementioned article by Zimmerman (1997), this equation does not take into account critical parameters such as the local flow velocity and the diameter of the sediment present at the channel bed. In his closure, Maynord (1997) acknowledged the need for more elaborate, physics-based studies of the phenomenon that could provide more accurate descriptions and estimates of the scour compared to the purely empirical derivations. In a more recent study, Giró and Schleiss (2012) pursued an experimental investigation consisting of ten flume tests for a variety of flow rates and bed slopes. Emphasis was placed on retaining walls installed at meandering bends of the channel. Only measurements of the final geometry of the bed at predetermined locations were collected. This work highlights the development of two scour holes running parallel to the base of the walls. It was also reported that undulated retaining walls have a scour-reducing effect compared to smooth ones. Similarly, Martin-Vide (2010) carried out experiments to investigate the effect of the protrusion length of vertical longitudinal walls on the critical value of the flow intensity, which is responsible for the development of scour. Obtained data revealed a quadratic reduction of the critical flow intensity for increasing protrusion lengths. However, this finding was supported by only four experimental runs. In the same article, regression analysis was performed to derive a power law that described the temporal evolution of scour. For this formulation, knowledge of the equilibrium scour depth and the time necessary to achieve equilibrium conditions were required. As it was discussed by the author, equilibrium conditions could not be achieved for 75% of the experiments, even though the duration of every experiment lasted up to two weeks.

Other researchers have investigated scouring at long guide walls. These structures are primarily used as countermeasures for bridge abutment scour and as a means to protect bridge embankments. The rationale behind their use is to gradually change the direction of the approach flow, so that intense scouring due to constriction effects is avoided. The geometry of guide walls and the way they interact with water and soil could be considered similar to those of retaining walls. Fathi et al. (2011) reported that long guide walls reduce scouring close to abutments more effectively compared to short walls. The selected shape of the wall is also of importance (straight, elliptical, circular). The scour mechanism was speculated to be similar to that observed around unprotected piers and abutments. Namely, the turbulent horseshoe vortex system

(consisting of primary and secondary vortices) was identified as being responsible for the local increase of shear stresses that cause the dislodgement of sediments. The same researchers also provided evidence to support the logarithmic development of scour depth in time. Li et al. (2006) also investigated the effectiveness of guide walls in reducing abutment scour. They proposed that rock walls comprised of several non-affixed stones are more cost-effective compared to solid (monolithic) walls, because they require less material to achieve the same level of scour reduction. Most probably this can be attributed to the flexibility of the former type of wall to adapt to the dynamic nature of the water-soil interface. Protrusion of the edge of the wall into the main channel was found to have a detrimental effect, because it triggered additional scour at the base of the guide walls.

To evaluate a method to mitigate scour at retaining walls, Martin-Vide and his co-workers (2010) investigated the effectiveness of riprap. Stones were installed around a smooth vertical wall located at the outer bend of an open channel. The reported scour reduction was up to 79%. This value referred to a case where an apron of riprap was installed at the top of the un-scoured bed. Two layers of stones comprised the apron. Coarser material was superimposed on finer stones (half the diameter of the coarser stones) to emulate the behavior of a filter. Overall, riprap protected temporarily the junction region between the streambed and the wall, forcing the thalweg of the channel to migrate away from the outer bend. Eventually, the apron was deformed and subsided along the slope of the scoured bed. This rendered the toe of the wall vulnerable to future flood episodes. Another major finding demonstrated that the performance of riprap improved when stones adapt to the scoured geometry, so the authors advised against filling riprap voids with concrete. It is worth mentioning though, that no information was provided about the uncertainty and the repeatability of the results of this study. Roca et al. (2007) and Roca et al. (2009) carried out experiments in a meandering channel having vertical walls and horizontal foundations. They suggested that the depth and width of exposed horizontal foundations can affect the equilibrium scour depth. Specifically, they showed that an optimally designed horizontal foundation can result in 40% reduction of scour compared to walls without horizontal foundations. This finding requires further investigation because it is against a common design principle, namely that the foundation of an in-stream structure should not be exposed to the flow. For these experiments, topographic maps of the equilibrium state of the bed and time-averaged measurements of the flow topology are presented in Roca et al. (2007) and Roca et al. (2009), respectively.

In-stream structures have also been investigated to mitigate scour at the base of longitudinal structures such as embankments. Johnson et al. (2001) investigated the efficiency of rock vanes as a scour countermeasure, for the protection of an embankment. The author conducted tests over numerous flow conditions, with a range of submergence heights relative to the channel bank. The rock vanes were installed at a variety of angles, within $25^o - 45^o$. The vanes consistently separated the flow, decreasing the velocity at the vicinity of the channel bank while redirecting the high velocity thread. As a result, significant scouring was observed at the center of the channel. Papanicolaou et al. (2004) investigated the use of barbs for the mitigation of streambank erosion. They studied the effects of barb geometry on the flow and the bed morphology, using large-scale particle image velocimetry (LSPIV). They demonstrated that the use of a single barb resulted to increased uniform backwater flow, and slower velocities at the streambank. On the other hand, the use of multiple barbs showed more substantial results including the increase of the protection regions downstream of the barbs and the decrease of the average free-surface velocity by 30% at the channel banks. Papanicolaou et al. (2004) concluded that optimum channel bank protection was achieved using multiple barbs with a span between downstream barbs to protrusion length of barb ratio of 13:1.

A.4 Case studies

Literature references about the field installation of retaining walls provide insight about the state-of-practice and performance of these structures with respect to scouring. Anderson and Williams (2002) report the collapse and reconstruction of a retaining wall at Zion National Park (Utah). Scour caused by recursive floods of relatively low intensity was identified as the reason for the damage. Nevertheless, they did not perform any scour analysis for the design of the new wall. This might be indicative of the complexity of such a task. They merely selected the arbitrary value of 3.6 m as the maximum potential scour. They used this number as an input to a slope stability analysis model based on the limit equilibrium method. On another forensic-type of report for the case of a failed retaining wall, McKelvey (2011) recognized that "a scour analysis was neglected during the design". Nevertheless, he did not provide any recommendations regarding what needs to be done to avoid similar type of failures in the future. Finally, Kearney and Gloonan (2005) agreed that a rigorous scour analysis was needed to determine scour at the base of Mechanically Stabilized Earth walls installed close to the Indian River inlet bridge at Sussex County (DE). Instead, they made the assumption that the aforementioned scour is equal to constriction scour occurring at the cross-section of interest.

A.5 Conclusions

The major findings of this literature review effort are summarized as follows: (1) available design tools for the estimation of scour at retaining walls are limited and of questionable predictive ability; (2) laboratory investigations of the phenomenon have yet to benefit from experiments that utilize state-of-the-art instrumentation; (3) There is a direct need to develop reliable computational tools for the prediction of this type of scouring (no such model seems to be currently available); and (4) the study of cases with failed retaining walls revealed that some engineers are reluctant, or rather do not have the proper tools, to incorporate a rigorous scour analysis within their designs.

A.6 References

Anderson, S., and Williams, J. (2002). "Road Stabilization, Reconstruction, and Maintenance with a Combined Mechanically Stabilized Earth and Secant Pile Wall: Zion National Park, Utah." Transportation Research Record: Journal of the Transportation Research Board, 1808(-1), 76-83.

Carriaga, C.C. (2000). "Scour Evaluation Program for Toe-Down Depth Assessment." Building Partnerships, 1-10.

Davies, R., and Carriaga, C.C. (2001). "Scour Evaluation Procedure for Determining Toe-Down Depths of Hydraulic Structures." Bridging the Gap, 1-9.

Fathi, A., Zarrati, A.R., and Salamatian, S.A. (2011). "Scour depth at bridge abutments protected with a guide wall." Can. J. Civil Eng., 38(12), 1347-1354.

Federal Highway Administration (2009). "Bridge Scour and Stream Instability Countermeasures: Experience, Selection, and Design Guidance." Hydraulic Engineering Circular 23, Federal Highway Administration, Washington D.C., 256.

Giró, A.V., and Schleiss, A.J. (2012). "Bank protection at the outer side of curved channels by an undulated macrorough concrete wall." Proc., 4th IAHR International Symposium on Hydraulic Structures.

Huang, C.C., and Chen, Y.S. (2012). "Behavior of reinforced structures under simulated toe scouring". Geosynth. Int., 19(4), 272-283

Johnson, P.A., Hey, R.D., Tessier, M., Rosgen, D.L. “Use of vanes for control of scour at vertical wall abutments.” J. Hydraul. Eng., 127(9), 1-5.
Kearney, P.G., and Gloonan, J.F. (2005). "Scour analysis evaluation for the proposed Indian River inlet bridge at Sussex County, Delaware." Duffield Associates Inc., 10.
Li, H., Barkdoll, B., Kuhnle, R., and Alonso, C. (2006). "Parallel Walls as an Abutment Scour Countermeasure." J. Hydraul. Eng., 132(5), 510-520.
Look, B.G. (2007). "Retaining walls." Handbook of Geotechnical Investigation and Design Tables, Taylor & Francis, 251-263.
Martin-Vide, J.P. (2010). "Local Scour in a Protruding Wall on a River Bank." J. Hydraul. Res., 45(5), 710-714.
Martin-Vide, J.P., Roca, M., and Alvarado-Ancieta, C.A. (2010). "Bend scour protection using riprap." Proceedings of the Institution of Civil Engineers - Water Management, 163(WM10), 489–497.
Maynord S.T. (1997). "Toe-Scour Estimation in Stabilized Bendways." J. Hydraul. Eng., 122(8), 460-464.
Maynord, S.T. (1997). "Closure: Toe-Scour Estimation in Stabilized Bendways." J. Hydraul. Eng., 123(11), 1048-1050.
McKelvey, J.A. (2011). "Lessons Learned from Failures: The Wall of Shame." Geo-Frontiers 2011, 3235-3244.
Melville, B.W. and Coleman, S.E. (2000). “Bridge Scour.” Water Resources Publications, LLC, Highlands Randch Co.
Mussetter Engineering. (2008). "Sediment and Erosion Design Guide." Southern Sadoval County Arroyo Flood Control Authority, A3.49-A3.57.
Papanicolaou, A.N., Kjos, L. J., Fox, J. F. “Investigation of Flow and Local Scour Characteristics around Partially Submerged Permeable WSDOT Barb.” Washington State Transportation Center, 3-8, 10, 18, 43.
Roca, M., Blanckaert, K., and Martin-Vide, J.P. (2009). “Reduction of Bend Scour by an Outer Bank Footing: Flow Field and Turbulence.” J. Hydraul. Eng., 135(5), 361-368
Roca, M., Martin-Vide, J.P., and Blanckaert, K. (2007). “Reduction of Bend Scour by an Outer Bank Footing: Footing Design and Bed Topography.” J. Hydraul. Eng., 133(2), 139-147
Zimmermann, C. (1997). "Discussion: Toe-Scour Estimation in Stabilized Bendways." J. Hydraul. Eng., 123(11), 1047-1050.

Appendix B

Practitioner survey

B.1 Survey design

A survey was prepared and input was sought from engineers and practitioners. The focus of this survey was to obtain information on longitudinal in-stream structures and potential scour-related problems. Possible responders were identified from all the State Departments of Transportation (DOTs), a few private companies and several state and federal organizations, such as the US Forest Service (USFS), Departments of Natural Resources (DNRs), Departments of Environmental Quality/Protection (DEQs/DEPs), the US Geological Survey (USGS) and the US Army Corps of Engineers (USACE). Additional contact information was provided by a few responders.

The main goals of the survey can be summarized as follows: (1) categorization of commonly used longitudinal structures; (2) identification of design guidelines that are currently used and evaluation of their effectiveness; (3) estimation of the frequency of structure damages or failures, due to the scouring of the streambed; (4) development of a database with stream and structure characteristics of various projects, to facilitate the design of the experiments; (5) categorization of commonly used scour-countermeasures and evaluation of their effectiveness; and (6) detection of experienced practitioners that could provide feedback at various stages of this project.

An initial version of the survey was sent for review to the NCHRP panel. Based on the feedback we received, the survey was significantly revised. The purpose of these revisions was twofold: 1) to enhance the clarity of the questions, and 2) to increase the participation and quality/extend of responses. Most of the incorporated revisions involved the reformulation of several questions and the reduction of the overall size of the survey. Specifically, several questions that were not directly related to the scope of this project were removed (e.g. repair frequency and maintenance cost). Finally, the structure of the survey was modified. The final version includes two main sections. The first section solicits general information about the experience of the responders with longitudinal in-stream structures, the evaluation of existing design guidelines and the effectiveness of the most commonly used scour countermeasures. In the second section, the responders were asked to provide a detailed description of one or two longitudinal structures. In general, the inquired information included the characteristics of the structure and the stream, and the susceptibility of the structure to scour-induced damage. Finally, the responders were asked to grant their permission for further contact and to provide the contact information of other experienced engineers and practitioners who could contribute to this effort. It was estimated that the first part of the survey could be completed within 5-10 minutes, while the second part required 20-60 minutes, depending on the degree of detail included in the responses.

The survey was designed online using SurveyMonkey® and was distributed to the possible responders via e-mail. A brief description of NCHRP 24-36 and the scope of the survey were included in the cover letter that was e-mailed to the possible responders. The survey was open for 6 months, in which period the participants could access incomplete responses and make additions or corrections. Reminders were sent 3 weeks after the initial request to persons that had not accessed the survey. Also, reminders were sent to responders that had partially completed the survey without submitting it, a month after their last access. The response data was monitored

frequently to search for incomplete responses, collect additional contact information and address comments and recommendations. The distributed survey and the cover letter have been included at the end of this Appendix.

B.2 Survey results

B.2.1 Distribution of responses

Responders to this survey consisted of engineers and practitioners from 29 states. As shown in Table 1, the distribution ranged from Washington D.C. to California. The population of the survey responders include: State DOTs (32), Unreported Affiliation (9), Private Industry (2), State DNRs (4), USFS (2), USACE (1) and Academia (2). The research team contacted each of the 50 US DOTs to identify the most experienced individuals in this field. Further, the survey populated 52 responses from the 110 originally sent invitations.

Table 1: Distribution of Survey Responders by State.

Responder Geographic Distribution	
Arizona (1)	New Jersey (2)
California (3)	New York (2)
Connecticut (1)	North Carolina (1)
DC (3)	North Dakota (1)
Hawaii (1)	Ohio (1)
Indiana (2)	Oklahoma (1)
Iowa (1)	Pennsylvania (1)
Kentucky (1)	South Carolina (1)
Louisiana (1)	South Dakota (1)
Massachusetts (1)	Texas (1)
Minnesota (2)	Vermont (1)
Mississippi (1)	Virginia (1)
Montana (1)	Wisconsin (1)
Nebraska (2)	Wyoming (1)
Nevada (2)	

Practitioners were asked for their reporting location. Based on the project details shared in Section 1, 11 out of 25 USGS-defined physiographical provinces were represented. The various physiographic provinces in the US are shown in Figure 1. The largest amount of experience was reported for the Central Lowland province (130 projects). In comparison, a smaller number of structures were reported for the remaining provinces: Great Plains Province (65), Appalachian Plateaus Province (50), Northern Rocky Mountains (50), Valley and Ridge Province (25), Middle Rocky Mountains (24), Pacific Border Province (10) Coastal Plains (5), New England Province (4), Basin and Range Province (3), Blue Ridge Province (2).

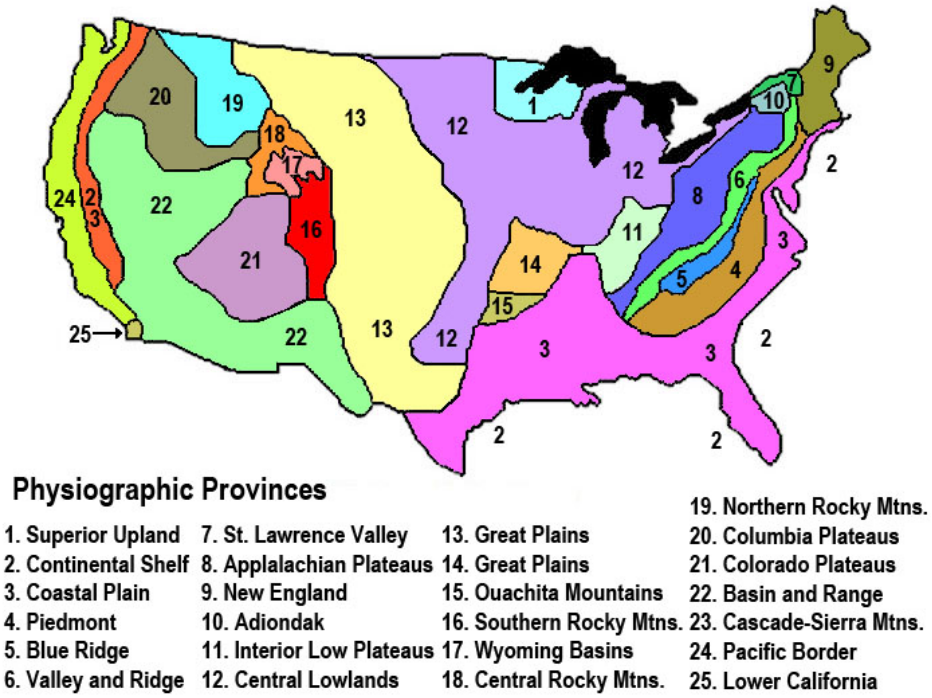

Figure 1: USGS Physiographic Provinces of the United States (Stoffer (2012).

B.2.2 Types of existing structures

In total, 18 types of longitudinal structures were shared and their distribution is displayed in Figure 2. Retaining walls were the most commonly reported structure (37%), and the one that most consistently experienced scour. Overwelmingly, 75% of these reported longitudinal structures were vertical structures. Longitudinal structure experience was not uniformly distributed throughout the country. Of the reported locations, 88% of Central Lowland reported using rip rap as well as alternate structures such as gabions and dikes. On the contrary, provinces with smaller response rates, such as the Appalachian Plateaus Province (75 %) and the Valley And Ridge Province (66%), overwelmingly reported experience with just retaining walls. Additionally, many responses received from some of the other lower reporting provinces had little variation and the majority of experiences were with retaining walls. Figure 2 validates the fact that there are significant variations of longitudional structure experience, directly attributing to the type of countermeasure installed.

B.2.3 Purpose of longitudinal structures

Longitudional structures serve various purposes including controlling flow, protecting exposed embankments, wall abutments, and bridge abutments as well as preventing bank erosion. Based on practitioner experience, 42% of survey responders reported that longitudional structures are most commonly used to protect the bank against erosion. Most projects detailed implementing these structures for mutliple purposes including protecting embankments. Unsurpsisingly, structures designated as having the primary purpose of protecting against bank erosion were found also to be vertical structures (60%).

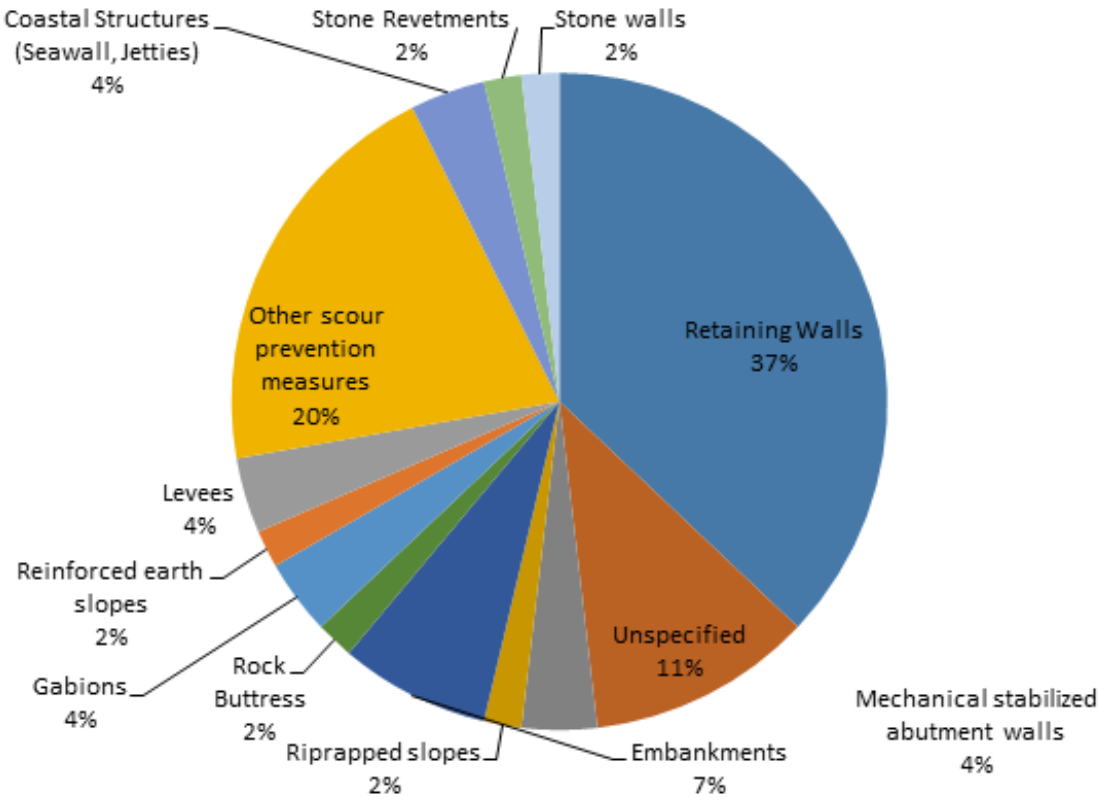

Figure 2: Distribution of the types of longitudinal structures reported in the practitioner survey.

B.2.4 Evaluation of existing guidelines

Practitioners were additionally asked to identify the scour prediction guideline they most commonly use. Coastal Plains was the most responsive province, with the widest distribution of scour prediction guidelines. In this region, 42% of the participants reported using HEC-23 and 28% other guidelines that were not specified. Overall the most widely used scour prediction guideline throughout the provinces is HEC-23 (72%), but it was consistently reported to be used in conjunction with an additional method. Other reported guidelines include local design techniques, namely HEC-18, HEC-11 and EM 1110-2-1601. Only 3 of 29 responders find the current available guidelines adequate. Several remarks were regularly made about the generality of the HEC-23 guideline and the need for an updated methodology. One responder even added that HEC-23 is not used for the design of a retaining wall, but only for channel revetment design. Wall design was therefore dictated by soil conditions, channel design efficiency and the stability of nearby structure's foundations. Many participants additionally commented that they often guess how to predict the scour magnitude rather than following the current inadequate guidelines. In regards to foundation depth design, 83% confirmed using HEC-23 as well as a supplemental method. These supplemental methods were specified to be Gessler's Method, HEC-RAS and local methods, supporting the belief that HEC-23 is inadequate for full design of these structures.

Further, characteristics of structures and scour depth did not lead to many clear trends. More than 7 of the 10 reported foundation depths were less than 10 feet, which did not correlate to the length of the structures. The flow angles of attack of these structures were fairly consistent. Shown in Table 2, 78% of flow angles of attack ranged between 0^{o} to 45^{o}. However no correlation could be made between the angles and reported scour depths.

B.3 Scour project sites

Following the initial general section of the survey, detailed information on site specific projects were provided in the second section. Project details were obtained through the regular survey and a supplemental survey for more experienced individuals. In total, 12 site specific projects from different physiographical regions were reported. As described in Table 2, longitudinal structures constructed from gabions and rip rap were used as a bank stabilization technique. The scour depth development at these structures encompasses a vast range from 0-24 ft. It is noteworthy that even though countermeasures were employed at 75% of these structures, 90% of them still reported scour development. This suggests that the overall effectiveness is contingent on site specific characteristics such as flow conditions, bed composition and position of structure.

Five out of twelve reported structures were extremely vulnerable to scour and were undermined after a flood event. One of the structures that experienced scour was discovered after a dam failure that occurred half a mile upstream of the structure site. Both pier footings of the retaining wall, designed to protect the bridge abutments, were exposed. Additionally, in another reported project in Bernardston, MA (near Route I-91), and bridge piers were unstable due to heavy rains and a dam breach that flooded the river and the neighboring floodplains. River bank and bottom soils were eroded, exposing older piers from a previous bridge. This previous bridge was said to having being wiped out during the flood of 1955. This area was determined to be extremely vulnerable to scour. As a result, geotextile filter fabric and rock filled gabions were placed around the current piers for scour protection. In three of the structures countermeasures were employed for protection; however excessive scour still developed at the toe of the structure. Practitioners commonly answered “not certain” in response to countermeasure effectiveness for situations where countermeasures were employed and scour was developed. Significant deposition at the vicinity of the structure is common among structures that successfully protected adjacent infrastructure.

In addition, the majority of responders from Section 1 of the survey (71%) reported using some type of countermeasures. Riprap revetment was the most widely reported countermeasure; however, the use of the other countermeasures did not exhibit any trends throughout the country. Results exemplify local trends; for example, 70% of the countermeasures used in the Central Lowlands were in-stream structures. However, in the Coastal Plains with a similar response number, responders reported using rip rap in over 75% of the projects. Nevertheless, the perceived performance of scour countermeasures in these regions was much higher than other regions. This suggests that a relationship may exist between local trends and overall countermeasure usage. The types of countermeasures are listed in Table 3. Rip rap was the only type of countermeasure employed in each represented physiographic province, while other countermeasures were geographically diverse and used based on local experience. Countermeasure effectiveness is diverse depending on the local stream conditions and geomorphic regions. As a result, local trends for implementing these countermeasures developed. Additionally, the variety countermeasures employed may also attribute to local engineering design methods.

One practitioner correlated the countermeasure effectiveness to the level of armoring of the stream. As confirmed by survey results, 71% of projects employing more than one countermeasure were deemed successful.

Figure 3 displays the distribution of projects for the provinces providing statistics, in respect to the occurrence of scour and the employment of a countermeasure. The Pacific Border Province reported 10 projects with longitudinal structure and countermeasures were installed in eight of them. While scour development was observed in all 8 of these project sites, in 4 of them the countermeasures were deemed successful in providing protection against scour. It is noteworthy that for the Central Lowland, where 130 longitudinal structures were reported, countermeasures were employed in less than half (58), which is much less than the overall percentage of countermeasure employment (71%).

As mentioned above, projects with a large geographic distribution were reported. The Appalachian Plateaus Province experienced a large amount of scour development in 18 out of 50 projects. Consistently, to mediate the scour, stone fill, concrete walls, rip rap and adjusted footing elevation were used. The use of these countermeasures was deemed to be successful. In total, 23 project sites were specified to be directly damaged due to scour, even though 191 of the 368 projects installed countermeasures as protection. Compared to the other provinces, the Pacific Border Province (8) had the most damaged structures compared to the small number of structures (10) (Figure 4). In the Pacific Border Province project sites, located in California, grouted rip rap was ineffectively employed to protect against scour. From Figure 3 and Figure 4 it is concluded that the frequency of scour damage can be associated with the usage of certain countermeasures.

Table 2. Types of employed counter-measures.

Countermeasures Reported
Universal
Rip Rap
Local
Armor Slopes
Articulated Blocks
Bendway Weir
Concrete Lining
Concrete Walls
Erosion Control Blankets
Extend Foundation (Piles)
Gabions
Imbricated Rip Rap
Jacks
Permeable Dikes
Reinforced Mattresses
Sheet Piling
Stone fill
Stone Reventment
Stream barbs
Vegetation

Table 3. Results Summary of Longitudinal Structure Survey

					Structure Characteristics					Channel Characteristics					
Structure Type	Project Goal	Scour Depth Observed	Damage During Severe Flood Event	Countermeasure Installed	Height (ft)	Length (ft)	Flow angle of attack	Foundation Depth (ft)	Structure Slope		Soil Composition			Position of Structure	Guidelines
Sheet Piles with patterns	Protect bridge abutments Protect embankments	6 ft	No	Rip Rap	30	300	20	75	1%			Gravel		Both banks within a meander bend	HEC-23
Rip Rap	Protect embankments	22- 24 ft	N/A	Rip Rap	23	850	30	5	2h:1v& 1.5h:1v	Silt	Sand	Gravel		The outer bank of a meander bend	HEC-23
Rough Concrete wall	and bank erosion Prevent bank erosion	0 ft	No	Rip Rap/Vanes	8	1200	20	8		0	Sand	Gravel	Cobbles	The outer bank of a meander bend	
Pile Core Spurs	Prevent bank erosion	5ft	No	Rip Rap	20	50	45	40		Silt	Sand	Gravel		One bank of a straight channel reach	
Imbricated Rip Rap	Protect embankments	N/A	Yes	Rip Rap										N/A	HEC-23
Sloping Rip Rap/Vegetation	and bank erosion Prevent bank erosion	1'	Yes	Vanes	5	120	100	3	4h:1v	Silt	Sand			Both banks within a meander bend	
Rip Rap	Prevent bank erosion	0 ft	No	None	5	50	90	5	3h:1v					The outer bank of a meander bend	HEC-23
Smooth Concrete Wall	and protect bridge abutments Prevent bank erosion	8ft	Yes	Rip Rap	15	90	20	4		0		Gravel		The outer bank of a meander bend	
Gabions	and protect bridge abutments Protect embankments	.67 ft	Yes	None	10	380	5		30°	Silt	Sand	Gravel		Both banks within a meander bend	HEC-23
Gabions	and bank erosion Protect embankments	2 ft	N/C	Boulders	460	11.7	0	3-7		0	Sand	Gravel	Cobbles	Both banks within a meander bend	N/A
Gabions	and bank erosion	5-6 ft	N/C	Boulders	265	9.3-11	0	3-7		0	Sand	Gravel	Cobbles	Both banks within a meander bend	N/A
Gabions	Prevent bank erosion	N/A	Yes	Rip Rap							Sand	Gravel		One bank of a straight channel reach	EM1110-2-1601

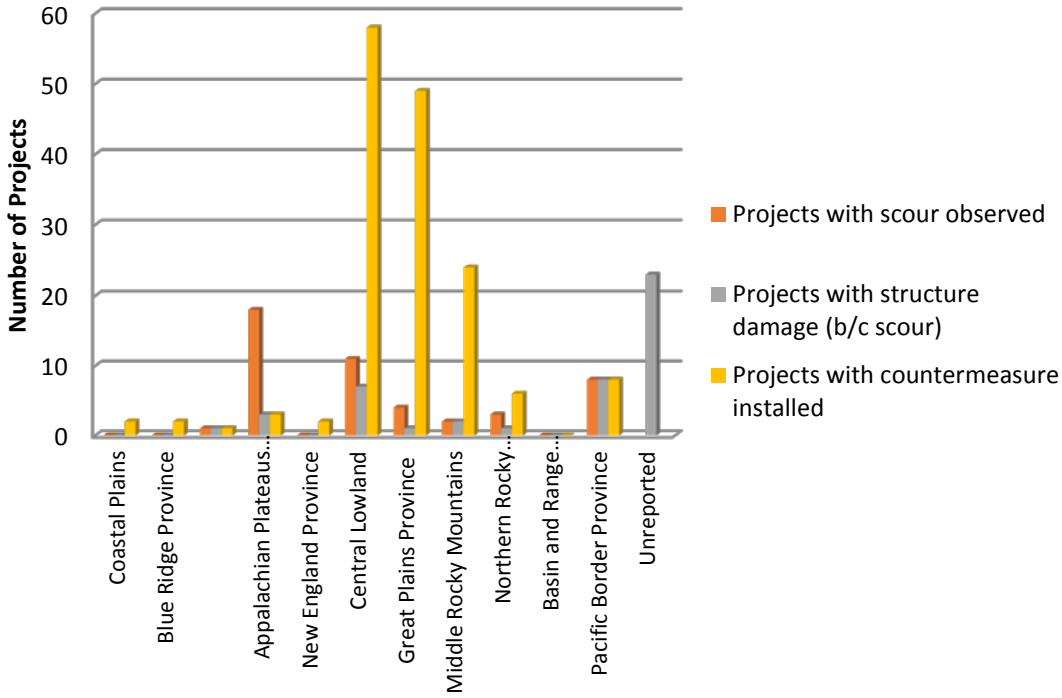

Figure 3. Distribution of reported projects, countermeasures and scour for physiographic regions.

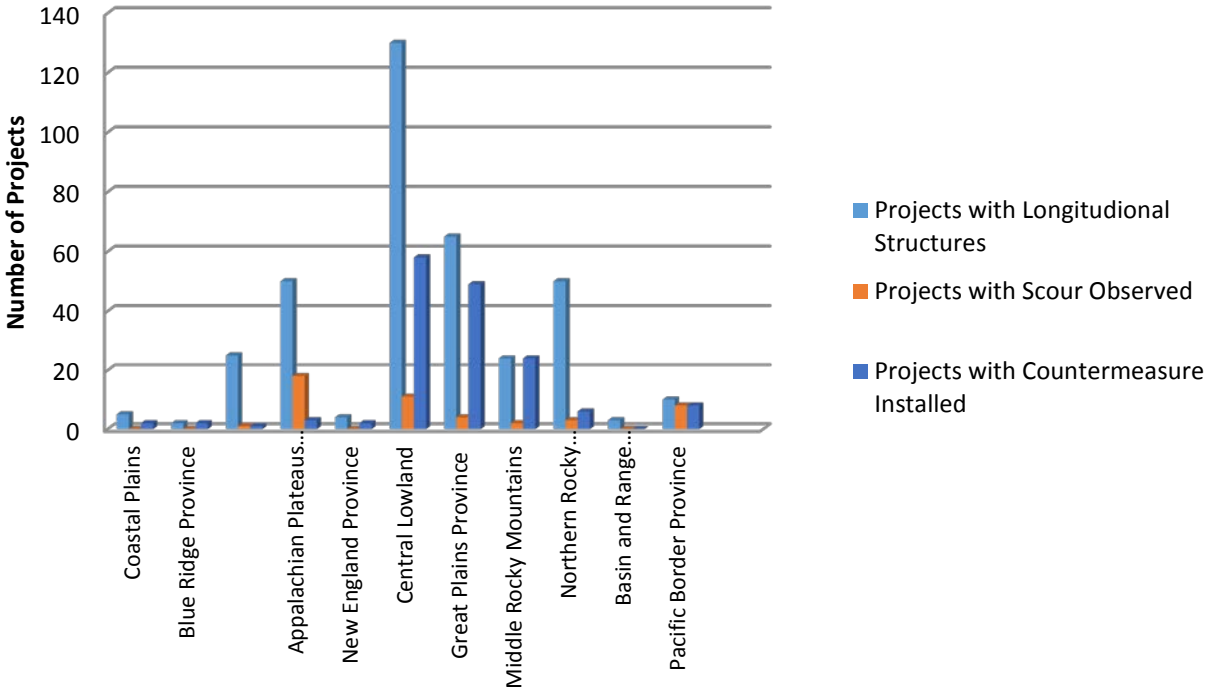

Figure 4. Distribution of reported projects, structure damage and countermeasures installed.

B.4 Personal communication feedback and DOT project data

The outreach to the DOT engineers is beyond the effort for the survey that was promised for the Phase I of this project. However, in an effort to gain more information about the currently employed design practices and learn more about the results of monitoring efforts of installed retaining structures, phone interviews with seven DOT members were conducted. In total sixteen experienced practitioners were contacted to participate in the phone interview. These interviews contributed to the development of the updated Phase II work plan. Additional project documents are being acquired from three responders, but due to the prolonged approval process for the districts of two responders, these documents could not be properly analyzed for Phase I.

B.5 Deficiencies of existing guidelines

The phone interviews provided a better understanding of the current design practices and the limitations of the existing guidelines as identified by the practitioners. The interviews were conducted with officials from the following states: Arizona, Massachusetts, Montana, Pennsylvania (2), Wisconsin, and Wyoming. Each shared their experiences and expertise on typical conditions and parameters associated with longitudinal structure scour. Three of the seven interviewees negatively commented on HEC-23 guidelines, especially emphasizing the inability to account for the variation of the different soil conditions. Several practitioners elaborated on multiple projects with different soil compositions. Scour development rates as well as the resulting shape of the scour hole varied for each project. One experienced practitioner reported in the survey and in the phone interview the need to revise current design procedure assumptions of the soil characteristics in HEC-23. Three responders additionally remarked that many previous projects did not exclusively contain cohesive soil and as a result an investigation into the assumptions of HEC-23 is needed.

Investigation into the development of scour resulting from disturbed soil was suggested by one official. The practitioner felt that HEC-23 catered to compact soils, which commonly underestimated the scour prediction. For example, in Phoenix, Arizona a partially dry water way, experienced several large flood events. The stream area was mined for many years before it was made illegal. After large flood events, the loose soil from the years of mining did not offer any resistance to local erosion. As a result, pronounced scour developed along a protective structure adjacent to a bridge crossing. Countermeasures employed at the structure together with reduction in mining activities are expected to reduce the scour development at this site.

Interviewees reported to rely on previous experience and local trends to find solutions against scour development. Several practitioners mentioned a high variability of geomorphic and stream conditions in project sites monitored by the same DOT district. Therefore, one official suggested incorporating more geomorphic parameters in the prediction of the scour depth.

B.6 Parameters associated with significant scour depths

Phone interviews validated the survey results, mainly that scour is consistently developed on the bendway of streams and outer banks of meandering rivers. Most practitioners described these meandering waterways to be medium to large in size, and most of them were monitored. Overall, each interviewee had been involved in multiple projects that experienced scour development. Stream migration contributed to scour development at a few project sites. One representative stated that the local DOT was unsure on how to prevent scour due to stream

migration, since their mitigation techniques lack substantial design backing. These approaches were described to be "trial and error based". Furthermore, the same representative stated his opinion that scour depth is correlated to the degree of armoring at a river. Additionally, this very experienced DOT official described several project sites, where the variety and quantity of in-stream countermeasures also increased the stability of the river.

DOT responders identified bankfull flows as the most damaging stream conditions, as far as scour is concerned. More specifically, four of them remarked that countermeasures were severely damaged or washed away following bankfull conditions. The majority of scour development seemed to commonly occur in unarmored streams with long term elevated base flow, close to or at the bankfull stage. In a described project from Missouri, a stream, normally not prone to scour, recently experienced many long term bankfull conditions. As a result, a scour hole was developed at the base of a retaining wall.

B.7 Research and improvement

Phone interviewees were asked what parameters they believed to contribute to longitudinal structure scour. A brief background on Phase II was given to provide a better understanding about the goals of this project. Responders shared suggestions about the characteristics that should be investigated in Phase II. Generally, responders agreed that the effects of the structure's material and roughness should be tested. A practitioner described a past project where the face of an older existing smooth structure was roughened to alter the flow. Based on this experienced, he described altering the roughness as a cost effective approach for older structures with scour problems. Unfortunately, this method could not be thoroughly tested, and was only used on older structures in this district. The employment of this countermeasure is limited since this DOT office is required to design based on proven successful local methods. These officials confirm the research plan included in the original proposal. Phase II specifies three types of wall roughness (low, medium, and high), which will tested with three flow rates (low, medium, high). The effect of the flow rate was also identified as a focal point by a DOT official with previous academic experience. As mentioned, many project sites in the Basin and Range provinces have different stream characteristics compare to a province such as the Coastal Plains. Many streams remain dry or low flowing until a large precipitation event. On the contrary, the Coastal Plains region experiences moderate and steady flow most of the time. Scour development therefore occurs over a different timeline. The initial proposal aimed to investigate the effect of the flow rate on the scour development.

B.8 Use of countermeasures

Countermeasures were installed at all the project locations described by the interviewed practitioners. Reinstating the trend observed in the survey responses, rip rap was consistently used at each project site. Several other countermeasures were used in combination with rip rap including gabions, sheet piles, and vanes. However, the effectiveness of each countermeasure varied geographically, as confirmed by the survey results. For example, the Arizona DOT interviewee described using rip rap and vanes in a low flowing and partially dry waterway. After receiving a significant amount of precipitation, this waterway became bankfull and fast moving, washing away both countermeasures. Even upon reinstallation, and redesigning using a more conservative method than HEC-23, these same countermeasures were damaged and soon washed away. As a result the DOT turned to a more costly approach, a sheet pile wall. Many DOT officials stray away from this option due to the cost, environmental impacts and construction depth. The sheet pile wall has successfully protected the retaining wall since installation.

B.9 Example projects

An example case of unstable longitudinal structures is a retaining wall in Uvalde County, TX that was damaged five years ago due to excessive scour. This retaining wall was undermined due to fast scour development and failing rip rap. The retaining wall was vertically positioned in the Nueces River, a medium size river that consistently approaches bankfull conditions after receiving large amounts of precipitation over short duration. Scour development occurred over several flood events within a few years, period of time, jeopardizing the stability of the structure before appropriate countermeasures could be installed. As a result, articulated concrete blocks are now used at the site. The final installation and design of the blocks is shown in the photograph of the Nueces River, Fig. 5. This costly alternative has been more successful than the previously used rip rap, with only minor damages. Figure 6 shows bankfull river conditions, under which the scour development is more pronounced.

Figure 5. Texicon articulated blocks installed along the Nueces River.

A small number of survey participants (17%) agreed that structures are commonly undermined during or after flood events. A project site in northeast Pennsylvania was nearly undermined from a large flood event. The Spruce Street project (Scranton, Pennsylvania) was not undermined, but left unstable after experiencing major scour development of 8-12 feet. The exposed piles and foundation led to structure instability (Figure 7). Serving as protection to embankments, this structure experienced multiple flood events. To address this problem, instead of employing a physical countermeasure, the existing retaining wall foundation was lowered five feet and partially grouted rock lining was added to prevent further erosion. This approach resulted in the stabilization of the scour growth in this area.

In the same area, another project site experienced retaining wall instability. Foundation exposure resulted from continued scour development over several years, caused by lateral stream migration. During this time, a building was

Figure 6. Bankfull flow conditions at the Nueces River, using the updated countermeasures.

constructed upstream of this site and altered the flow dynamics of the stream. Also, exposed railroad piles near the retaining wall contributed to the scouring problem. It is also noteworthy that as a result of the excess scour and retaining wall instability, a dam that was located upstream and the exposed piles will be removed. In general, many of these shared projects suggest that scour development consistently occurs adjacent to bridge or wall abutments. Consistently these structures accumulate debris or other forms of obstruction that alter the natural flow and trigger scour development. In many of the older structures, which experience scour over long periods, stream modifications and stream migration occur upstream of the problematic area.

Longitudinal structure scour is a reoccurring issue in Massachusetts. However, it is often not documented or monitored since the local longitudinal structures are not frequently inspected, compared to bridges. Massachusetts DOT shared several projects and procedures for the mitigation of longitudinal structure scour. From a Massachusetts DOT interviewee's experience, these walls normally remain unmonitored unless located next to larger bridges (over 30 foot span) that need inspections. In Ashfield, Massachusetts an unmonitored 80 year old retaining wall was undermined due to scour developing incrementally over decades. With 6 feet of scour in total, and a 4-foot thick exposed foundation, the wall was said to be fully undermined due to scour, since there was no confirmation of outward wall rotation adjacent to the footing. Scour rate at the toe was estimated as 0.9 inches per year. The project report details a down and inward flow to be the cause of scour, mobilizing the smaller cobble sediment away from the foundation toe. No changes in watershed land use upstream were reported, thus the scour development is predicted to remain constant for the following years. Several mitigation alternatives were suggested for this project. The most cost effective approach, rip rap and grout bags installation, was deemed to potentially secure the structure. Another alternative involved the construction of a new wall. Concerns for this option included cost, environmental impacts and construction duration.

Figure 7. Spruce Street (Scranton, PA) exposed pile and foundation.

Reports confirmed that the cheaper, practical options such as countermeasures are the most viable solution to this problem. Each interviewee described their local method of cost benefit analysis for deciding the proper countermeasure selection. Many officials expressed their hesitation to apply a more expensive countermeasure, when cheaper countermeasures such as rip rap are easier to install, since they don't have foundations and they require a simpler design. These economical countermeasures, shown in Table 2, prevented scour in only 2 of the 12 reported projects.

B.10 Conclusion

The major findings of the survey are summarized as follows: (1) Current methods to design longitudinal structures and evaluate scour are sparse, general, and untested; (2) Practitioners reported longitudinal structure failure due to excessive scour; (3) Scour countermeasure use was based on practitioner preference based on experience; (4) Current longitudinal structure guidelines were considered inadequate by practitioners because they were a) too general, and b) do not include soil conditions; (5) HEC-23 was the most used design methodology, often combined with a supplemental method (Gessler's, HEC-RAS, and local methods); (6) Longitudinal structure effectiveness is dependent on site-specific characteristics; (7) Floods with frequent return intervals ("bankfull") were identified as the most damaging in terms of scour; and (8) Practitioners recommended research that incorporates longitudinal structure roughness, bed materials and a focus on vertical walls.

B.11 References

Anderson, S., and Williams, J. (2002). "Road Stabilization, Reconstruction, and Maintenance with a Combined Mechanically Stabilized Earth and Secant Pile Wall: Zion National Park, Utah." Transportation Research Record: Journal of the Transportation Research Board, 1808(-1), 76-83.

Bennett, J. P. (2001). "User's Guide for Mixed-Size Sediment Transport Model for Networks of One-Dimensional Open Channels." U.S. Geological Survey, 1-2, 16-20.

Carriaga, C.C. (2000). "Scour Evaluation Program for Toe-Down Depth Assessment." Building Partnerships, 1-10.

Davies, R., and Carriaga, C.C. (2001). "Scour Evaluation Procedure for Determining Toe-Down Depths of Hydraulic Structures." Bridging the Gap, 1-9.

Fathi, A., Zarrati, A.R., and Salamatian, S.A. (2011). "Scour depth at bridge abutments protected with a guide wall." Can. J. Civil Eng., 38(12), 1347-1354.

Federal Highway Administration (2009). "Bridge Scour and Stream Instability Countermeasures: Experience, Selection, and Design Guidance." Hydraulic Engineering Circular 23, Federal Highway Administration, Washington D.C., 256.

Giró, A.V., and Schleiss, A.J. (2012). "Bank protection at the outer side of curved channels by an undulated macrorough concrete wall." Proc., 4th IAHR International Symposium on Hydraulic Structures.

Huang, C.C., and Chen, Y.S. (2012). "Behavior of reinforced structures under simulated toe scouring". Geosynth. Int., 19(4), 272-283

Johnson, P.A., Hey, R.D., Tessier, M., Rosgen, D.L. "Use of vanes for control of scour at vertical wall abutments." J. Hydraul. Eng., 127(9), 1-5.

Kearney, P.G., and Gloonan, J.F. (2005). "Scour analysis evaluation for the proposed Indian River inlet bridge at Sussex County, Delaware." Duffield Associates Inc., 10.

Li, H., Barkdoll, B., Kuhnle, R., and Alonso, C. (2006). "Parallel Walls as an Abutment Scour Countermeasure." J. Hydraul. Eng., 132(5), 510-520.

Look, B.G. (2007). "Retaining walls." Handbook of Geotechnical Investigation and Design Tables, Taylor & Francis, 251-263.

Martin-Vide, J.P. (2010). "Local Scour in a Protruding Wall on a River Bank." J. Hydraul. Res., 45(5), 710-714.

Martin-Vide, J.P., Roca, M., and Alvarado-Ancieta, C.A. (2010). "Bend scour protection using riprap." Proceedings of the Institution of Civil Engineers - Water Management, 163(WM10), 489–497.

Maynord S.T. (1997). "Toe-Scour Estimation in Stabilized Bendways." J. Hydraul. Eng., 122(8), 460-464.

Maynord, S.T. (1997). "Closure: Toe-Scour Estimation in Stabilized Bendways." J. Hydraul. Eng., 123(11), 1048-1050.

McKelvey, J.A. (2011). "Lessons Learned from Failures: The Wall of Shame." Geo-Frontiers 2011, 3235-3244.

Melville, B.W. and Coleman, S.E. (2000). “Bridge Scour.” Water Resources Publications, LLC, Highlands Randch Co.
Roca, M., Blanckaert, K., and Martin-Vide, J.P. (2009). “Reduction of Bend Scour by an Outer Bank Footing: Flow Field and Turbulence.” J. Hydraul. Eng., 135(5), 361-368
Roca, M., Martin-Vide, J.P., and Blanckaert, K. (2007). “Reduction of Bend Scour by an Outer Bank Footing: Footing Design and Bed Topography.” J. Hydraul. Eng., 133(2), 139-147
Papanicolaou, A.N., Kjos, L. J., Fox, J. F. “Investigation of Flow and Local Scour Characteristics around Partially Submerged Permeable WSDOT Barb.” Washington State Transportation Center, 3-8, 10, 18, 43.
Stoffer, Phil. “Geographic Provinces of the United States.” 2012. Geology Cafe. 21 December 2013. <http://www.geologycafe.com/physiographic/>
Mussetter Engineering. (2008). "Sediment and Erosion Design Guide." Southern Sadoval County Arroyo Flood Control Authority, A3.49-A3.57.
Zimmermann, C. (1997). "Discussion: Toe-Scour Estimation in Stabilized Bendways." J. Hydraul. Eng., 123(11), 1047-1050.

B. 12 distributed survey and cover letter

Dear ,
We would like to request your assistance with a research study on longitudinal in-stream structures (e.g. embankments, retaining walls, mechanically stabilized earth, guide walls, etc.).

The goal of this National Cooperative Highway Research Program study (NCHRP Project 24-36) is to predict the scour depth at the base of existing longitudinal structures and develop new design procedures to mitigate scour problems. A survey of all 50 state Departments of Transportation (DOTs), Departments of Natural Resources (DNRs), other state or federal organizations and engineering firms is being conducted. The results of this survey will be combined with a literature review of existing work, laboratory and field measurements, and a numerical model to develop design guidelines. These guidelines will be publicly available from the Transportation Research Board.

A very important part of this research is to document the experience of engineers and practitioners and create a database with quantitative information about existing longitudinal structures. The survey that you are asked to complete is a vital part in our efforts to:

-Classify existing design methods and evaluate their performance.
-Estimate the number of structure failures that are attributed to scour.
-Identify potential field monitoring sites.
-Design laboratory experiments and carry out numerical simulations.
Please visit the following link to complete the survey:
https://www.surveymonkey.com/s/NCHRP_1

The survey includes an introductory part inquiring your general experience on longitudinal structures and a more detailed site-specific part that can be completed for up to 2 projects that you have been involved in. Please note that you can visit this link many times before you submit the survey and that your responses will be saved (if the survey is accessed from the same computer).

Thank you for your participation. Please do not hesitate to contact us at polyb86@vt.edu (Pol Bouratsis) if you have questions or would like to provide additional recommendations. For more information on NCHRP 24-36, refer to the following link:

http://apps.trb.org/cmsfeed/TRBNetProjectDisplay.asp?ProjectID=3186

Sincerely,

Dr. Fotis Sotiropoulos
Dr. Panos Diplas
Dr. Jessica Kozarek
Dr. Ali Khosronejad
Dr. Clinton Dancey
Pol Bouratsis
Nikos Apsilidis

1. Contact information

Name:

Organization:

Position:

E-mail:

Phone number:

*2. Do you have experience with longitudinal structures (embankments) on channels or floodways?

- [ ] No
- [ ] Retaining walls
- [ ] Other longitudinal structures

Please explain

3. What scour prediction guidelines do you use most often to design longitudinal structures?

- [ ] HEC-23
- [ ] None

Other (please explain)

4. Do you find the present design guidelines for the prediction/prevention of scour at the base of longitudinal structures to be adequate?

- ◯ Strongly Agree
- ◯ Agree
- ◯ Not Certain
- ◯ Disagree
- ◯ Strongly Disagree

***5. Have you used scour countermeasures for the protection of a longitudinal structure?**

- ◯ Yes
- ◯ No

6. Please specify the types of countermeasures you have used.

Countermeasure-A	
Countermeasure-B	
Countermeasure-C	
Countermeasure-D	
Countermeasure-E	

7. Evaluate the average performance of every scour countermeasure you have used, in terms of scour reduction/prevention.

	Effective	Not certain	Ineffective
Countermeasure-A	◯	◯	◯
Countermeasure-B	◯	◯	◯
Countermeasure-C	◯	◯	◯
Countermeasure-D	◯	◯	◯
Countermeasure-E	◯	◯	◯

8. Answer the following questions considering the typical performance of longitudinal structures.

	Strongly Disagree	Disagree	Not Certain	Agree	Strongly Agree
Structures successfully halt further bank erosion	◯	◯	◯	◯	◯
Structures result in excessive scour at the toe of the structure	◯	◯	◯	◯	◯
Structures are commonly undermined during/after flood events	◯	◯	◯	◯	◯
Structures result in sediment deposition at the project site	◯	◯	◯	◯	◯
Structures successfully protect infrastructure	◯	◯	◯	◯	◯

9. Answer the following question regarding your experience with longitudinal structures.

Approximately how many projects have you been involved in that have used a longitudinal structure, of any type?	
For how many projects was excessive scour observed?	
For how many projects was the structure damaged because of scour?	
For how many projects was a scour countermeasure installed?	
For how many projects did the scour countermeasure successfully protect the structure?	

***10. Would you be willing to complete an additional survey that inquires information about site-specific details?**

- ◯ Yes
- ◯ No

Please complete the following survey for up to two projects. Please give priority to projects for which scour at the base of the structure has been observed.

11. Specify the location of the structure.

Country	
State	
Near City	
Name of the Stream	
Other Description	

12. In what year was the project completed?

13. What was the purpose of the structure? Select all that apply.

- [ ] Protect bridge abutments
- [ ] Protect embankments
- [ ] Prevent bank erosion

Other (please specify)

14. Was the structure:

- ◯ Vertical
- ◯ Sloping

15. Describe the type of the structure, using the images on the right.

- ◯ i. Smooth concrete wall
- ◯ ii. Artificially-roughened concrete wall
- ◯ iii. Cobbles and vegetation
- ◯ iv. Rip-rap
- ◯ v. Gabions
- ◯ vi. Sand bags
- ◯ vii. Tires

Other (please specify)

i. Smooth concrete wall

ii. Artificially-roughened concrete wall

iii. Cobbles and vegetation

iv. Rip-rap

v. Gabions

vi. Sand bags

vii. Tires

16. Describe the type of the structure, using the images on the right.

- ◯ i. Smooth concrete wall
- ◯ ii. Artificially-roughened concrete wall
- ◯ iii. Sheet piles with patterns
- ◯ iv. Gabions (vertically-installed rip-rap)
- ◯ v. Sand bags
- ◯ vi. Organic (woody) materials with vertical holders
- ◯ vii. Tires

Other (please specify)

i. Smooth concrete wall

ii. Artificially-roughened concrete wall

iii. Sheet piles with patterns

iv. Gabions (vertically-installed rip-rap)

v. Sand bags

vi. Organic (woody) materials with vertical holders

vii. Tires

17. Was a scour prediction analysis carried out prior or after the construction of the structure?

- ◯ Yes
- ◯ No

18. What guidelines were used for the selection of the foundation depth?

- ◯ HEC-23
- ◯ None

Other (please specify)

19. How frequently has the project been monitored?

- ◯ Never
- ◯ Every 2 years or longer
- ◯ Every 1 year
- ◯ More than once a year

20. What is the design flood return period for this site?

21. Has the structure experienced a design flood event?

- ◯ Yes
- ◯ No
- ◯ Not certain

22. Has significant scour been observed in the vicinity of the structure?

- ◯ Yes
- ◯ No

23. Can you provide an estimate of the maximum scour depth that has been observed?

24. Has significant deposition been observed in the vicinity of the structure?

- ◯ Yes
- ◯ No

25. Has the structure been damaged or failed due to the undermining of its foundation?

- ◯ Yes
- ◯ No

26. Did the damage occur during a severe flood event?

- ◯ Yes
- ◯ No
- ◯ Not certain

27. Have there been used any countermeasures for the mitigation of scour? Select all that apply.

- [ ] Rip-rap
- [ ] Vanes
- [ ] None

Other (please specify)

28. Were the scour countermeasures successful?

- ◯ Strongly Agree
- ◯ Agree
- ◯ Disagree
- ◯ Strongly Disagree

29. Has the structure been damaged or failed due to a reason other than scour?

- ◯ No
- ◯ Yes

Please specify

30. Evaluate the estimated repair needed after flood events.

- ◯ None
- ◯ Minor repair
- ◯ Moderate repair
- ◯ Major repair
- ◯ Replacement

31. Where was the structure positioned?

- ◯ One bank of a straight channel reach
- ◯ The outer bank of a meander bend
- ◯ The inner bank of a meander bend
- ◯ Both banks within a straight reach
- ◯ Both banks within a meander bend

32. Please describe the characteristics of the structure (approximate values will suffice).

Height:	
Length:	
Material:	
Flow's angle of attack:	
Foundation's depth:	
Structure's slope:	

33. What was the channel bed/bank's soil composition? Select all that apply :

- ☐ Clay
- ☐ Silt
- ☐ Sand
- ☐ Gravel
- ☐ Cobbles

34. What were the channel's dimensions where the structure was installed (approximate values will suffice)?

Depth:	
Width:	
Radius of curvature (if in a meander bend):	
Slope:	

35. The current NCHRP project (No. 24-36) is looking for field sites to monitor scour at the base of longitudinal structures. Would you recommend this site for monitoring?

- ◯ Yes
- ◯ No

***36. Would you be willing to complete this survey for an additional project?**

- ◯ Yes
- ◯ No
- ◯ Not now. Send me a reminder in a few days.

Copy of page:

Please answer the following questions for the additional project.

37. Specify the location of the structure.

Country	
State	
Near City	
Name of the Stream	
Other Description	

38. In what year was the project completed?

39. What was the purpose of the structure? Select all that apply.

- [ ] Protect bridge abutments
- [ ] Protect embankments
- [ ] Prevent bank erosion

Other (please specify)

40. Was the structure:

- ◯ Vertical
- ◯ Sloping

Copy of page:

41. Describe the type of the structure, using the images on the right.

- ◯ i. Smooth concrete wall
- ◯ ii. Artificially-roughened concrete wall
- ◯ iii. Cobbles and vegetation
- ◯ iv. Rip-rap
- ◯ v. Gabions
- ◯ vi. Sand bags
- ◯ vii. Tires

Other (please specify)

i. Smooth concrete wall

ii. Artificially-roughened concrete wall

iii. Cobbles and vegetation

iv. Rip-rap

v. Gabions

vi. Sand bags

vii. Tires

Copy of page:

42. Describe the type of the structure, using the images on the right.

- ◯ i. Smooth concrete wall
- ◯ ii. Artificially-roughened concrete wall
- ◯ iii. Sheet piles with patterns
- ◯ iv. Gabions (vertically-installed rip-rap)
- ◯ v. Sand bags
- ◯ vi. Organic (woody) materials with vertical holders
- ◯ vii. Tires

Other (please specify)

i. Smooth concrete wall

ii. Artificially-roughened concrete wall

iii. Sheet piles with patterns

iv. Gabions (vertically-installed rip-rap)

v. Sand bags

vi. Organic (woody) materials with vertical holders

vii. Tires

Copy of page:

43. Was a scour prediction analysis carried out prior or after the construction of the structure?

- ◯ Yes
- ◯ No

44. What guidelines were used for the selection of the foundation depth?

- ◯ HEC-23
- ◯ None

Other (please specify)

Copy of page:

45. How frequently has the project been monitored?

- ◯ Never
- ◯ Every 2 years or longer
- ◯ Every 1 year
- ◯ More than once a year

46. What is the design flood return period for this site?

47. Has the structure experienced a design flood event?

- ◯ Yes
- ◯ No
- ◯ Not certain

48. Has significant scour been observed in the vicinity of the structure?

- ◯ Yes
- ◯ No

49. Can you provide an estimate of the maximum scour depth that has been observed?

50. Has significant deposition been observed in the vicinity of the structure?

- ◯ Yes
- ◯ No

51. Has the structure been damaged or failed due to the undermining of its foundation?

- ◯ Yes
- ◯ No

52. Did the damage occur during a severe flood event?

- ◯ Yes
- ◯ No
- ◯ Not certain

Copy of page:

53. Have there been used any countermeasures for the mitigation of scour? Select all that apply.

- [ ] Rip-rap
- [ ] Vanes
- [ ] None

Other (please specify)

54. Were the scour countermeasures successful?

- ◯ Strongly Agree
- ◯ Agree
- ◯ Disagree
- ◯ Strongly Disagree

Copy of page:

55. Has the structure been damaged or failed due to a reason other than scour?

- ◯ No
- ◯ Yes

Please specify

56. Evaluate the estimated repair needed after flood events.

- ◯ None
- ◯ Minor repair
- ◯ Moderate repair
- ◯ Major repair
- ◯ Replacement

Copy of page:

57. Where was the structure positioned?

- ◯ One bank of a straight channel reach
- ◯ The outer bank of a meander bend
- ◯ The inner bank of a meander bend
- ◯ Both banks within a straight reach
- ◯ Both banks within a meander bend

58. Please describe the characteristics of the structure (approximate values will suffice).

Height:	
Length:	
Material:	
Flow's angle of attack:	
Foundation's depth:	
Structure's slope:	

59. What was the channel bed/bank's soil composition? Select all that apply :

- ☐ Clay
- ☐ Silt
- ☐ Sand
- ☐ Gravel
- ☐ Cobbles

60. What were the channel's dimensions where the structure was installed (approximate values will suffice)?

Depth:	
Width:	
Radius of curvature (if in a meander bend):	
Slope:	

61. Would you recommend this site for NCHRP monitoring?

- ◯ Yes
- ◯ No

62. Are you aware of (other) sites with longitudinal structures that have experienced problems because of scour? Please specify.

63. May we contact you for further details?

- ◯ Yes
- ◯ No

64. Could you provide us with the contact information of engineers or practitioners within your organization that may have experience with longitudinal structures?

Name:	
Organization:	
E-mail:	
Phone number:	

Thank you very much for your participation! Please do not hesitate to contact us if you have questions or would like to provide additional recommendations.

Appendix C

Large-scale physical experiments

C.1 Experimental setup

Large-scale experiments to quantify scour at the base of longitudinal structures were conducted in the Outdoor StreamLab (OSL) at St. Anthony Falls Laboratory of the University of Minnesota. The goal of these experiments was to examine the effect of wall angle (approach angle) and wall roughness on scour at the base of a vertical longitudinal wall in a meandering channel. The OSL is a field-scale experimental channel with the ability to independently control flow and sediment feed (Fig. 1). This provides the opportunity to examine flow and sediment transport phenomena under well controlled conditions but with channel dimensions and other characteristics resembling those typically encountered in the field. The experimental test section was within the middle meander bend of the channel with a median bed grain size of 0.7 mm and a sinuosity of 1.3.

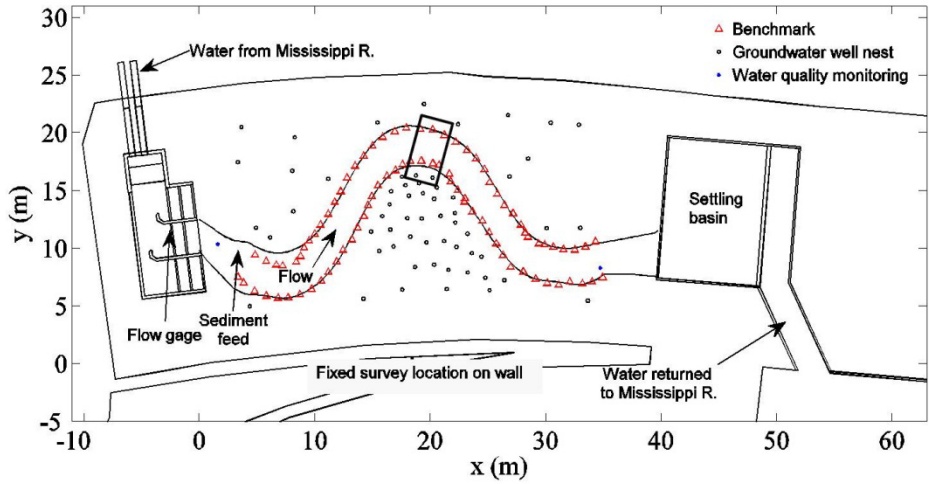

Figure 1. Schematic of Outdoor StreamLab (OSL) from top view. The topography cart was placed at the black rectangle and surveyed into the OSL coordinate system.

A total of five experimental runs were conducted in the OSL (Table 1).The first experimental run documented flow and bed topography prior to the installation of a longitudinal wall structure (baseline case). Two different wall roughness characteristics were used in the OSL experiments (Table 1).Walls were installed with two different approach angles (Table 1; Figure 3) in the same approximate location. Each wall was installed at least 20 cm below the depth of maximum scour prior to wall installation and was carefully checked to ensure it was vertical. The wall location was surveyed to verify as built dimensions. Experimental runs included rough and smooth walls

at two different approach angles. The smooth wall (Figure 3) was constructed of smooth plastic and the rough wall (Figure 4) was modified with pea gravel (~ 1 cm).
Bathymetry and velocity measurements were obtained within the vicinity of the longitudinal wall structure in the middle bend of the experimental stream. We utilized a high-resolution data acquisition (DAQ) carriage specifically designed for use in the OSL, which enables the precise positioning of instrumentation in all three dimensions (Figure 2). An ultrasonic transducer was used to record water surface elevations, combined with subaqueous bed topography from sonar. ADV records were obtained using a 3-D Nortek Vectrino (Nortek) probe mounted in a downward-looking configuration; records were 1.5 minutes long and obtained at 100 Hz and were post-processed to remove velocity spikes (Parsheh 2010).Water discharge and sediment feed measurements were monitored at the OSL inlet. Each experiment started with a flat bed (raked and set to a specific elevation; Figure 5). Cross-sectional topography upstream and downstream of the topography cart was monitored approximately every hour with a point gauge mounted on horizontal metal cross-sections.

Table 1. Longitudinal wall scour experiments conducted in the OSL at SAFL.

Run #	**Flow Rate (L/s)**	**Sediment Feed Rate (kg/min)**	**Roughness**	**Angle**	**Measurements**
BL	285±5	6.7±0.4	N/a	N/a - baseline	Initial topography, ADV cross sections, scour development, final topography
W1	283±5	6.7±0.4	smooth	angle 1: 140^{o} to approach flow	Initial topography, ADV cross sections, scour development, final topography
W2	285±1	6.7±0.4	smooth	angle 2: 130^{o} to approach flow	Initial topography, ADV cross sections, scour development, final topography
W3	281±2	6.7±0.4	rough	angle 2: 130^{o} to approach flow	Initial topography, ADV cross sections, scour development, final topography
W4	282±3	6.7±0.4	rough	angle 1: 140^{o} to approach flow	Initial topography, ADV cross sections, scour development, final topography

Figure 2. Smooth wall installed in the OSL just downstream of the meander apex.

Figure 3. Rough wall installed in the OSL just downstream of the meander apex.

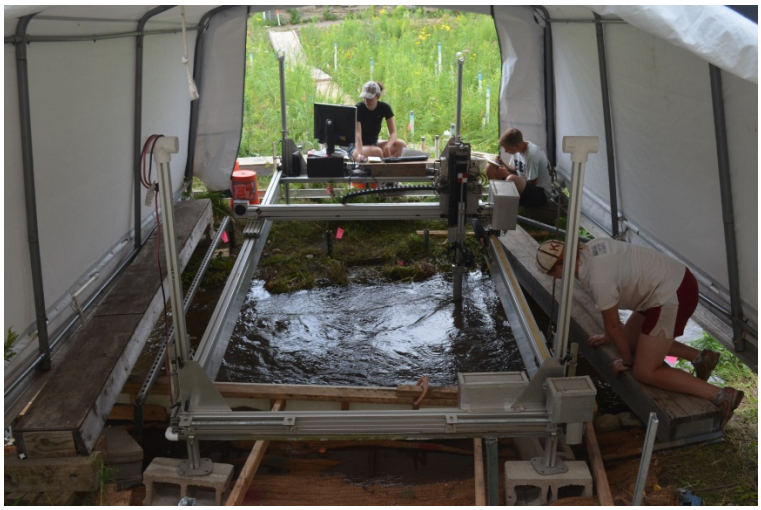

Figure 4. Collecting bed (sonar) and water surface (ultrasonic transducer) data using a computer controlled cart.

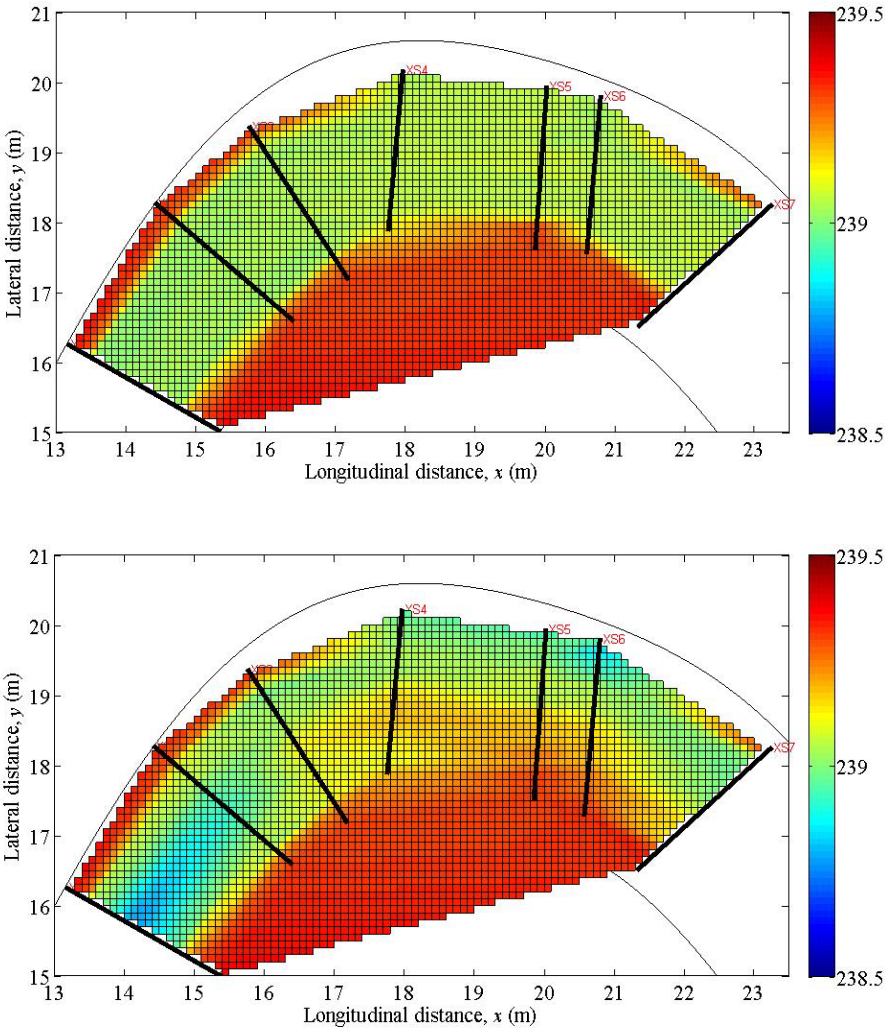

Figure 5. Permanent transects surrounding the cart location were used to verify that each experiment started with a flat bed (top) and monitor maximum scour along the wall (bottom). These data are from the W1: smooth wall, angle 1 run.

C.2 Experimental results for longitudinal wall experiments

C.2.1 Effect of wall angle on scour

The final quasi-equilibrium bar topography was similar in all five runs (including baseline) as illustrated by topographic transects extracted from the cart data in Fig. 6. For the most upstream transect (US) and the middle transect (MID), the bar top is wider and the bar shoulder is steeper with a wall in place. For the most downstream transect (DS) the bar top was lower and the shoulder was shallower with a wall in place. Within the window scanned by the cart sonar, there were no discernable differences on bar morphology based on wall angle or wall roughness (Fig. 7).

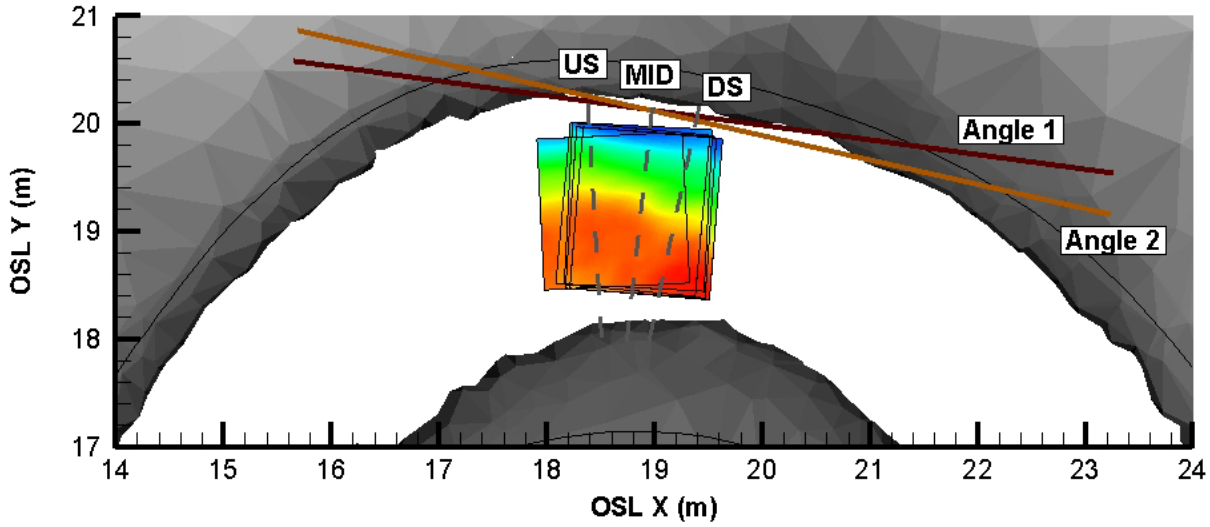

Figure 6. Location of three transects (US, MID, and DS) overlaying the cart scan data in the OSL. The boxes are locations of cart scans and the black line roughly indicates the outer limits of the OSL channel. Wall 1 and 4 were installed at Angle 1 and Walls 2 and 3 were installed at Angle 2.

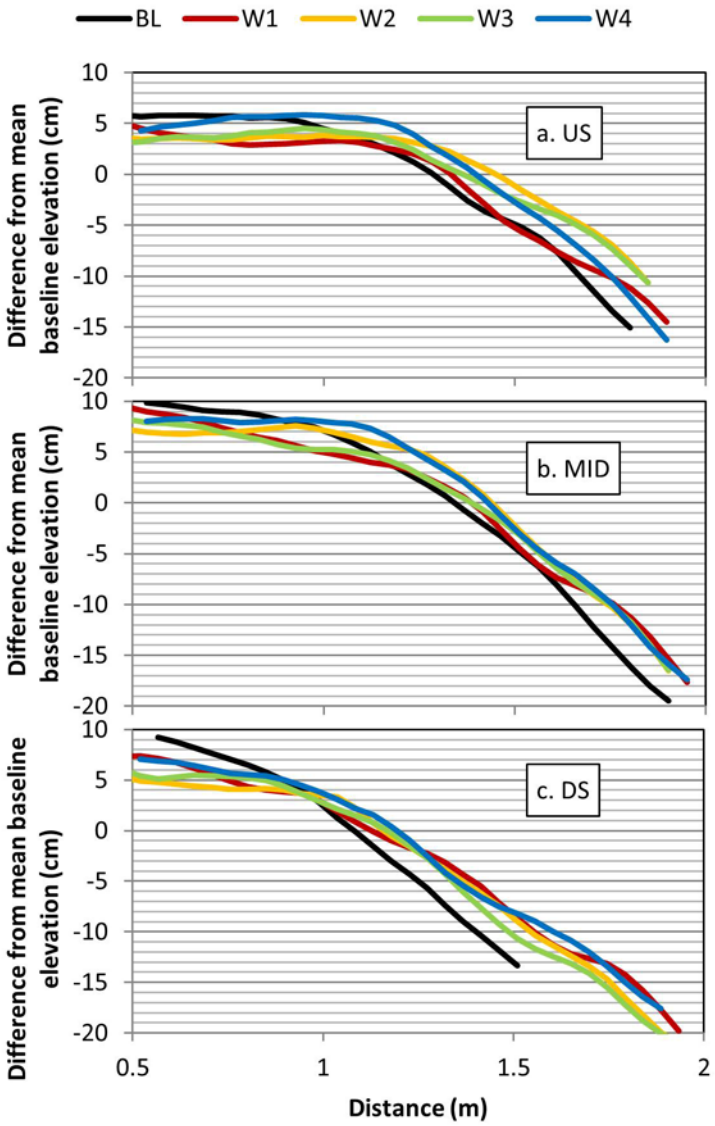

Figure 7. Bed topography from the cart data for three transects shown in Figure 6. BL is baseline, Wall 1 (W1)=smooth, angle 1; Wall 2 (W2)=smooth, angle 2; Wall3 (W3)=rough, angle 2; Wall 4 (W4)=rough, angle 1. Elevations were calculated as difference from the mean BL elevation from each cross-section.

C.2.2 Flow field and scour

Differences between the baseline flow fields (no wall) and the four wall scenarios were minor. Fig. 8 illustrates the flow paths through the test meander in the OSL with natural banks (before wall installation) overlaid over the quasi-equilibrium topographic scan. Strong helical flow patterns are seen starting at the second cross section.

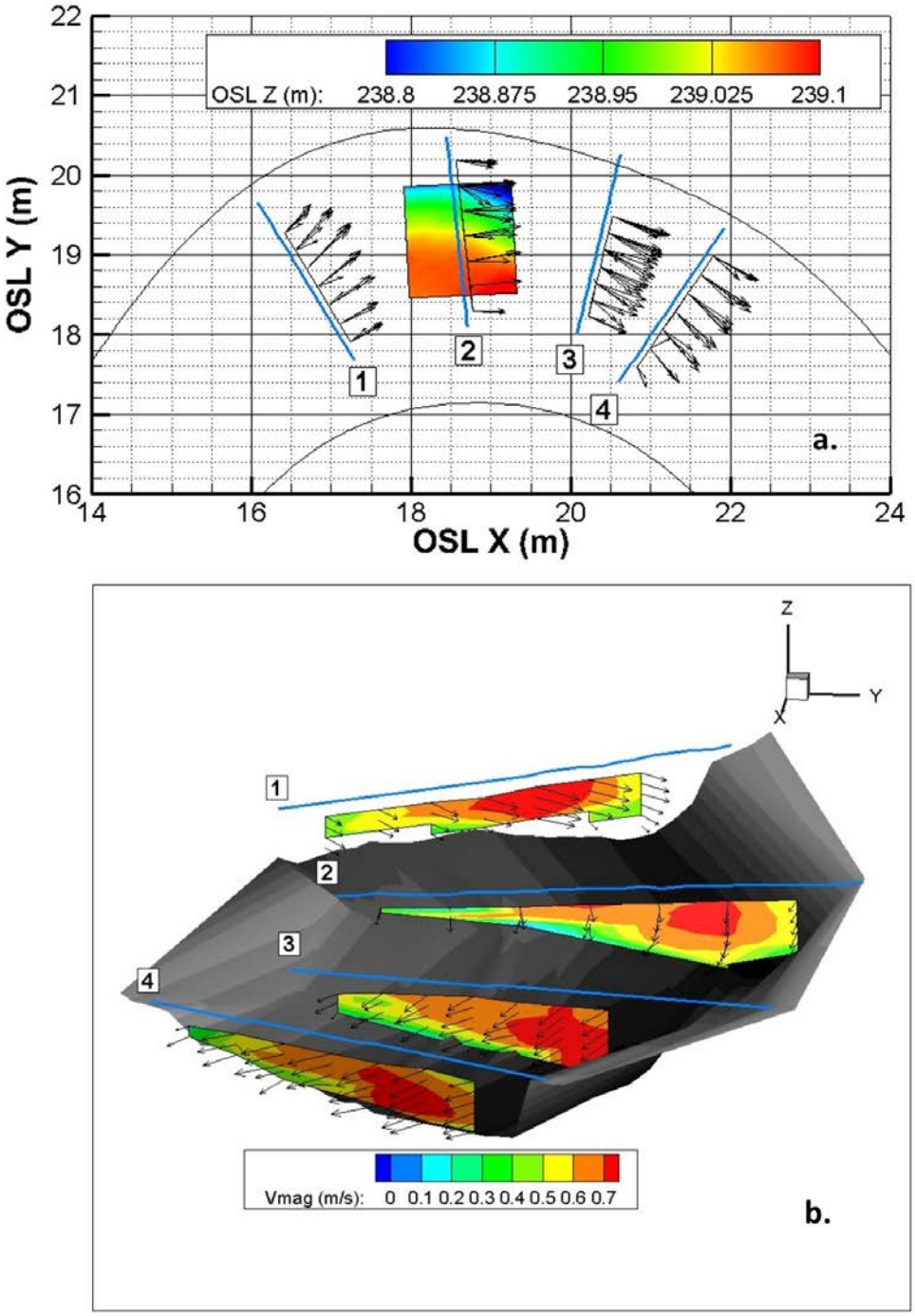

Figure 8. a.) Plan view of flow around the OSL meander during bankfull flow with natural banks, and b.) velocity magnitude (m/s) in the middle portion of the meander.

The installation of a wall seems to interrupt these patterns (Fig. 9 and Fig. 10) with the strongest cross currents occurring after main flow intercepts the wall (at cross section 3 for angle 1 (walls

1 and 4) and at cross section 2 for angle 2 (walls 2 and 3)). The location of maximum scour (orange dots in Fig. 9) indicates that the wall angle had a much larger impact on maximum scour in the meandering experiment than the wall roughness. Angle 1 was approximately 140^o relative to the approach flow from cross-section 1; angle 2 was approximately 130^o relative to the approach flow from cross-section one. The location of maximum scour moved downstream with the larger approach angle. All wall scenarios had scour greater than the baseline case (Table 2). There were no discernable differences between wall angle and roughness with the depth of maximum scour, but there was a small effect of roughness on the scour immediately adjacent to the wall where the rougher walls (wall 3 and 4) had smaller scour immediately adjacent to the wall.

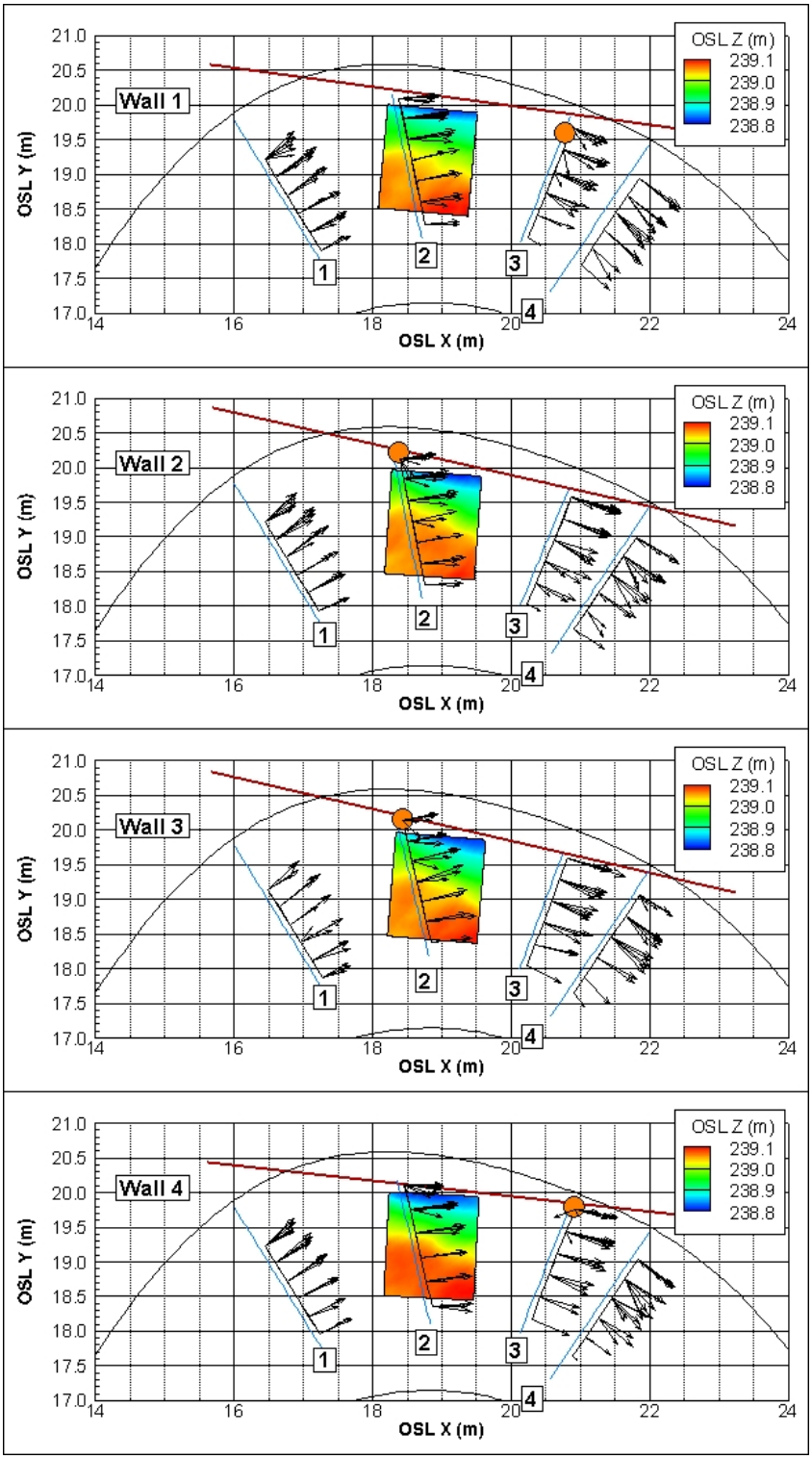

Figure 9. Plan view of velocity patterns for each wall experiment overlaying final quasi-equilibrium bed topography as recorded by the DAQ cart. Orange dot illustrates the location of maximum scour. Wall characteristics are shown in Table 1.

Table 2. Location of minimum elevation (maximum scour) for each OSL experiment. The difference is the difference between the flat bed elevation (238.96 m) and the scoured elevation. (NR = not recorded).

	OSLX (m)	OSLY (m)	OSLZ (m above sea level)	Difference (m)	Max Scour along wall (m)
Baseline	19.26	19.82	238.78	0.17	-
Wall1	20.78	19.61	238.77	0.19	NR
Wall2	18.38	20.22	238.74	0.22	0.22
Wall3	18.43	20.16	238.78	0.18	0.18
Wall4	20.91	19.80	238.73	0.23	0.18

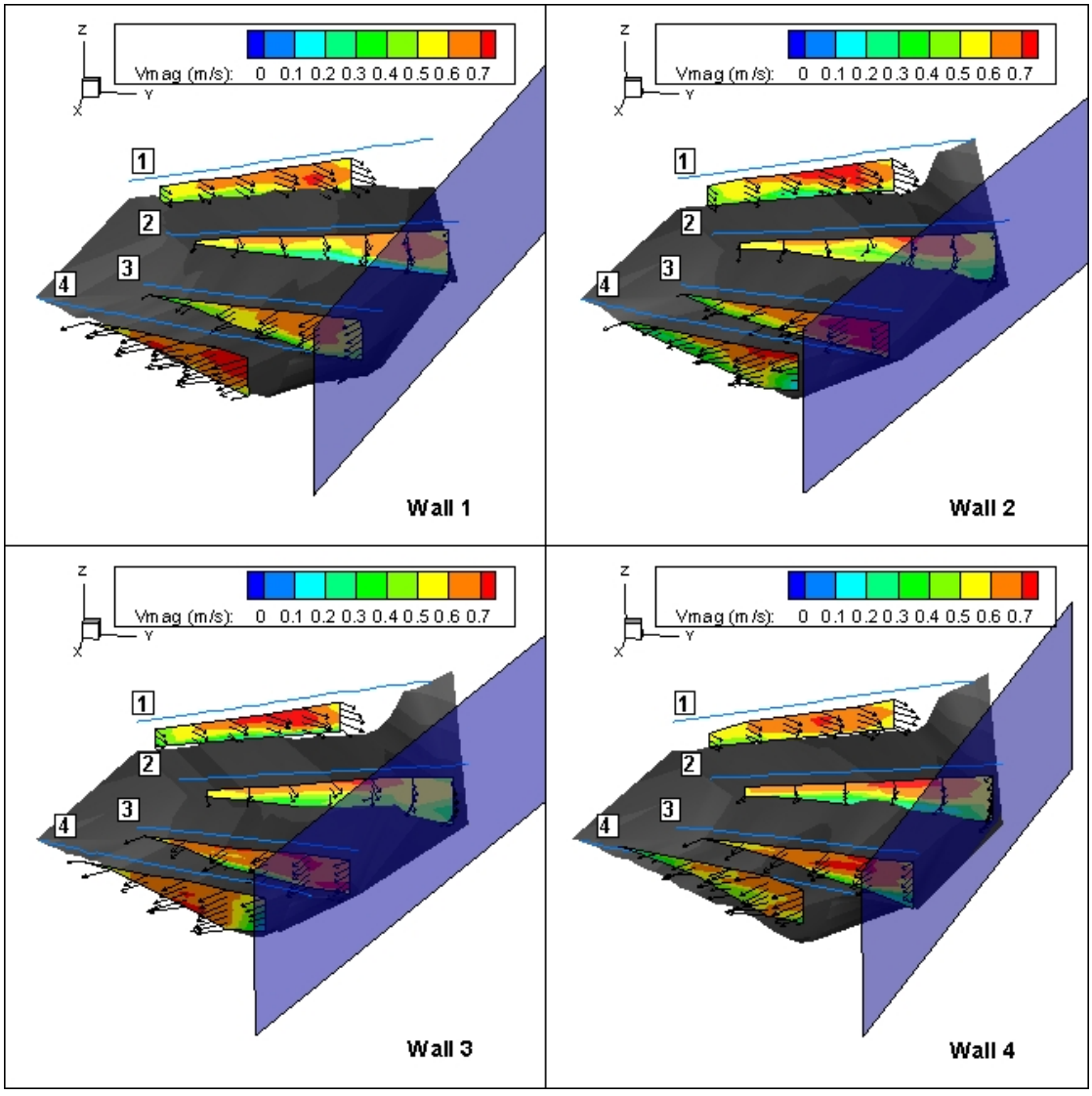

Figure 10. Velocity magnitude (m/s) in the middle portion of the meander.

C.3 Summary of large-scale experiments

The data collected from the OSL were used to validate the computational model used to calculate scour in different river systems to expand the dataset to develop predictive equations for the calculation of scour at the base of a longitudinal wall. Taken alone, these data imply that in natural systems, wall roughness has little to no effect on maximum scour depth or location (likely due to the roughness of the channel and vegetated banks).Wall angle relative to the approach flow also has little effect on the scour depth (although the presence of a wall did increase scour relative to the baseline case). Wall angle relative to the approach flow had the largest impact on the scour location; the larger angle (between approach flow and wall) resulted in scour shifted downstream and away from the wall. The smaller angle resulted in scour immediately adjacent to the wall.

Appendix D

Small-scale physical modeling

D.1 Experimental Setup

The small-scale physical modeling experiments, designed to quantify scour at the base of longitudinal retaining walls, were performed in the state-of-the-art flume facility at Lehigh University. The flume is 15-m long, 1.2-m wide and 0.6-m deep. It has a tilting capability (up to a maximum slope of 5%) and can recirculate both water and sediment.

The design of the experimental setup (Figure D1) reflects the general characteristics of retaining wall structures that have been observed in the field, including those in Dunmore and Scranton, PA (with and without apparent scour problems) (Figure D2). The latter ones were identified by PennDOT District 4 engineers, who accompanied us to a visit at the corresponding field sites. In most sites, the transition from natural channel banks (with 28-35 degrees of slope although some sites with bedrock bank can have near-vertical slope) to the vertical retaining wall appeared to be abrupt (Figure D2 (A), (C)). Some of the transitions have rock riprap and/or planted vegetation between the natural channel banks and the retaining wall location (e.g., Figure D2 (B)). Similarly, abrupt transitions from a sloping channel bank to a vertical retaining wall were observed at many field sites around the U.S. that were identified through the use of the search engine Google. These findings helped with the initial design of the modeled retaining wall and its vicinity in the Lehigh flume. However, it should be mentioned here that the Lehigh experiments were not intended to model one or more specific field sites. Instead, the objective was to study the phenomenon in broader terms and examine the role of a number of flow parameters and stream characteristics on scour near a retaining wall. Such an approach is well suited for developing design criteria that will lead to reduced scour problems in the vicinity of these structures. The background work mentioned above, extensive review of the available literature on scour related phenomena, and a significant number of preliminary experiments guided the selection of the key parameters that were considered during the experimental work at Lehigh.

The retaining wall used in the laboratory experiments was 1 m long and it was located 10 m downstream of the channel entrance (Figure D1). The upstream channel section was sufficiently long to allow the flow to become fully developed before entering the retaining wall area. It was built from Plexiglas to allow for the recording of the erosional process and provide overall visual access to the area of interest. Besides the Plexiglas wall with smooth surface, the case of a retaining wall having a rough surface was considered as well. The 10-m upstream section and 4-m section downstream of the wall (A-A’ and C-C’, respectively, in Figure D1) had a channel bank with a constant angle. This angle was adjusted to cover a wide range of field conditions.

More specifically, multiple experiments were performed with each of the following bank angles: 28, 35, 45, 70, and 80 degrees.

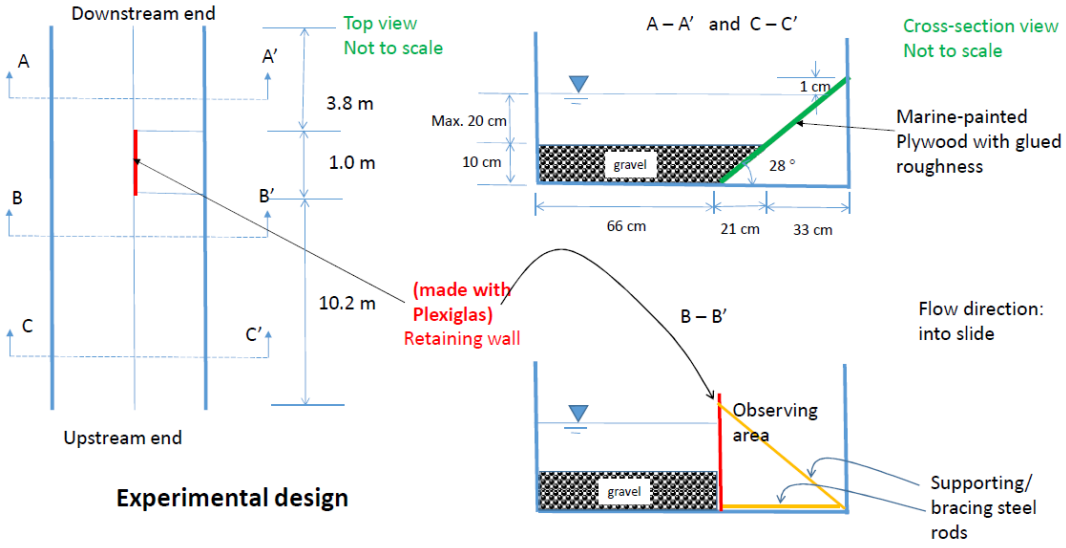

Figure D1. Design for the small-scale physical modeling experiments at Lehigh.

Figure D2. Complementary field observations by Lehigh group in Dunmore and Scranton, PA, with PennDOT.

A concerted effort was made to reproduce in the laboratory the characteristics of the transition between the channel bank and the retaining wall typically encountered in the field. As a result, the abrupt transition between the bank and the retaining wall, at both the upstream and downstream sides of the structure, were employed in this set of runs (Figure D3). This abrupt contraction design is expected to contribute to the local scour in a significant way. Consistent with field observations, the channel bank in the flume has an angle of 28 – 80 degrees. Figure D3 shows the setup for run G-1 (with gravel-bank angle of 28 degrees and 15% contraction) which is designated as baseline case scenario.

Figure D3. The flume setup at Lehigh showing the transition from the channel bank to the 1-m long retaining wall (made of Plexiglas) for run G-1. Looking downstream.

We used sub-rounded gravel with d_{10} = 2 mm, d_{35} = 3.1 mm, d_{50} = 3.6 mm, and d_{90} = 6.0 mm (where d_x is the sediment size for which x% of the material is finer by weight) as bed material in most runs. The sediment was purchased from a local supplier, who quarried the material from a fluvial deposit. In summary, the criteria used for the design of the laboratory experiments were as follows. 1) Consider clear-water scour conditions. 2) Keep the free stream flow Froude number at or below 0.5 ($Fr = U/\sqrt{gH}$, where H is flow depth, U is depth-averaged flow velocity and g is gravitational acceleration) to reproduce conditions that are typical of streams with retaining wall structures. 3) Limit the degree of contraction of the channel cross-section in the retaining wall section to less than 20%. This will minimize potential blockage effects and their impact on scour characteristics. Therefore, the laboratory experiments will be representative of prototype conditions, where this contraction is typically low. 4) Employ a two-pronged approach regarding the experiments. Use one set of more detailed experiments to examine the role of various parameters, including bank angle, wall roughness, and presence of an armor layer, on scour hole development in the vicinity of a retaining wall (see Table D1). Carry out an additional, larger but not as detailed set of experiments for the purpose of augmenting the data base under a wide range of experimental conditions, which, in turn, will facilitate the development of a more reliable empirical formula for estimating maximum scour depth at the

leading edge of a retaining wall (see Table D2). This part is implemented here in the same fashion as other types of scour data reported in the literature, such as those near embankments or bridge abutments (i.e., HEC-18 or HEC-23 reports). For the most part, these constitute an extension of runs G1 and G5, meaning there were no armored bed, bank vegetation, cohesive bed, or rough wall conditions considered during the additional runs.

To satisfy the first criterion, the flow parameters for each experiment were selected in such a way that near threshold of motion conditions were present in the upstream section of the flume. For the Table D1 experiments, this selection was mainly guided by the critical value of the Shields stress parameter ($\tau_* = HS/Rd_{50}$, where H is flow depth, S is channel bed slope, and $R = \frac{\rho_s - \rho}{\rho}$ is submerged specific density; where ρ_s is the density of sediment and ρ is the density of water). A fairly narrow range of critical Shields stress values ($\tau_{cr}^* \approx 0.05$-0.08) was employed for these experiments.

This selection for the remaining, less detailed experiments, was guided by both the Shields criterion and visual inspection of sporadic particle movement. The present methodology was motivated by the fact that initiation of motion is highly sensitive to a number of parameters, including the effect of water induced grain movement on particle arrangement and degree of bed surface coarsening. The resulting variability in the Shields stress value characterizing near threshold conditions was evident in many of our experiments. This approach represents a range of flow conditions that is wider than critical and thus it can increase the scatter in the collected scour data.

The Froude criterion was met in all but 5 of the experiments. The highest overall Froude number was 0.56. The third criterion is satisfied in all experiments. The highest degree of contraction for our experiments was 15% and occurred for the case of a bank angle of 28°. A total number of 75 experiments were performed in the laboratory flume (Tables D1 and D2) in an effort to satisfy part four. Sixteen of them belonged to the set of more detailed experiments (Table D1).

Table D1. Experimental matrix for small-scale experiments.

Run#	Retaining wall & Bank slope	Transition	Wall surface roughness	Sediment type
G1	**Baseline case scenario** (contraction of 15% & bank angle of **28°**); three sub-runs (G1-a to G1-c)	Abrupt	Smooth (Plexiglas)	gravel (d_{50} = 3.6 mm)
G2	Same as baseline case (bank angle of 28°); four sub-runs (G2-a to G2-d)	Abrupt	**Rough** (using coarse sandpaper, d = 0.6 mm, and glued bed-gravel on sheet)	gravel
G3-tree	Same as baseline case (bank angle of **28°**); two sub-runs (G3-a & G3-b)	Abrupt / **trees**	Smooth	gravel
G4-armor	Same as baseline case (bank angle of **28°**)	Abrupt	Smooth	**Armored** gravel bed
G5	Bank slope of **35°** **(**contraction of 13%**)**	Abrupt	Smooth	gravel
G6	Bank slope of **45° (**contraction of 10%**)**	Abrupt	Smooth	gravel
G7	Bank slope of **70° & 80°** **(**contraction of 5% & 2.5%**)**	Abrupt	Smooth	gravel
C1	Same as baseline case (bank slope of **28°**)	Abrupt	Smooth	**Cohesive** bed
G8	Same as baseline case (bank slope of **28°**)	**Gradual**	Smooth	gravel

Table D2. Additional experimental runs to assist in the development of an empirical formula for estimating the maximum scour depth (H_s) in the vicinity of a retaining wall. Five runs from Table D1 have been included here (see below). The run time for each experiment ranged from 1.5 to 4.0 hours, until the bed morphology reached a quasi-equilibrium condition.

Run #	d_{50}, mm	θ, deg	S, %	H, m	Q_w, l/s	U, m/s	τ*	F_r	F_{rd}	H_s, m
1	3.6	28	0.09	0.21	107	0.5	0.03	0.35	2.65	0.1
2	3.6	28	0.09	0.182	76	0.41	0.03	0.31	2.18	0.06
3	3.6	28	0.4	0.136	68	0.51	0.09	0.44	2.72	0.05
4	3.6	28	0.4	0.15	86	0.58	0.1	0.48	3.08	0.088
5	3.6	28	0.02	0.193	71	0.36	0.01	0.26	1.91	0.04
6	3.6	28	0.25	0.182	90	0.48	0.08	0.36	2.58	0.07
7 (G1-c)	3.6	28	0.25	0.17	80	0.47	0.07	0.36	2.48	0.042
8 (G1-a)	3.6	28	0.25	0.17	80	0.47	0.07	0.36	2.48	0.053
9	3.6	28	0.09	0.178	65	0.36	0.03	0.27	1.91	0.035
10	3.6	28	0.15	0.188	78	0.4	0.05	0.3	2.15	0.058
11	3.6	28	0.15	0.172	62	0.36	0.04	0.27	1.9	0.025
12	3.6	28	0.25	0.163	66	0.4	0.07	0.32	2.15	0.043
13	7.6	28	0.09	0.198	88	0.43	0.01	0.31	1.59	0.027
14	7.6	28	0.09	0.21	106	0.49	0.02	0.34	1.8	0.047
15	7.6	28	0.25	0.17	80	0.47	0.03	0.36	1.71	0.015
16	7.6	28	0.25	0.19	103	0.53	0.04	0.39	1.94	0.05
17	7.6	28	0.4	0.136	67	0.5	0.04	0.44	1.85	0.015
18	7.6	28	0.4	0.15	85	0.57	0.05	0.47	2.09	0.02
19	7.6	28	0.4	0.165	102	0.62	0.05	0.48	2.25	0.048
20	7.6	28	0.325	0.161	85	0.53	0.04	0.42	1.93	0.032
21	7.6	28	0.325	0.179	106	0.58	0.05	0.44	2.13	0.043
22	7.6	28	0.325	0.194	127	0.64	0.05	0.46	2.34	0.1
23	7.6	28	0.25	0.204	123	0.59	0.04	0.42	2.15	0.059
24	5.5	28	0.09	0.182	75	0.4	0.02	0.3	1.74	0.023
25	5.5	28	0.09	0.198	88	0.43	0.02	0.31	1.87	0.045
26	5.5	28	0.09	0.21	106	0.49	0.02	0.34	2.12	0.075
27	5.5	28	0.25	0.17	80	0.47	0.05	0.36	2.01	0.03
28	5.5	28	0.25	0.195	106	0.53	0.05	0.38	2.28	0.078
29	5.5	28	0.15	0.188	78	0.4	0.03	0.3	1.74	0.03
30	5.5	28	0.325	0.161	83	0.51	0.06	0.41	2.22	0.043
31	5.5	28	0.325	0.179	105	0.58	0.06	0.43	2.48	0.078
32	5.5	28	0.4	0.136	67	0.5	0.06	0.44	2.17	0.02
33	5.5	28	0.4	0.15	85	0.57	0.07	0.47	2.46	0.045
34	5.5	28	0.4	0.165	102	0.62	0.07	0.48	2.65	0.08

Table D2 (continued)

Run#	d_{50}, mm	θ, deg	S, %	H, m	Q_w, l/s	U, m/s	τ*	F_r	F_{rd}	H_s, m
35 (G5)	3.6	35	0.25	0.17	80	0.48	0.07	0.38	2.58	0.019
36	3.6	35	0.4	0.15	85	0.59	0.1	0.49	3.15	0.025
37	3.6	35	0.4	0.165	102	0.64	0.11	0.5	3.4	0.04
38	3.6	35	0.15	0.194	93	0.48	0.05	0.35	2.58	0.02
39	3.6	35	0.15	0.198	110	0.56	0.05	0.4	2.95	0.035
40	3.6	35	0.09	0.215	107	0.5	0.03	0.34	2.64	0.018
41	3.6	35	0.25	0.195	107	0.55	0.08	0.4	2.95	0.033
42	7.6	35	0.25	0.19	127	0.68	0.04	0.5	2.48	0.015
43	7.6	35	0.4	0.165	103	0.64	0.05	0.51	2.36	0.015
44	7.6	35	0.325	0.194	127	0.66	0.05	0.48	2.42	0.022
45	7.6	35	0.4	0.177	127	0.73	0.06	0.56	2.69	0.025
46	5.5	35	0.25	0.188	123	0.66	0.05	0.49	2.86	0.043
47	5.5	35	0.09	0.21	106	0.5	0.02	0.35	2.17	0.022
48	5.5	35	0.325	0.179	105	0.6	0.06	0.45	2.58	0.033
49	5.5	35	0.15	0.21	119	0.57	0.03	0.39	2.44	0.038
50	5.5	35	0.4	0.16	93	0.6	0.07	0.48	2.59	0.015
51	5.5	35	0.4	0.177	126	0.73	0.08	0.55	3.14	0.04
52	3.6	45	0.25	0.2	93	0.49	0.08	0.35	2.6	0.033
53 (G6)	3.6	45	0.25	0.18	80	0.47	0.08	0.36	2.52	0.026
54	3.6	45	0.09	0.19	79	0.44	0.03	0.32	2.34	0.024
55	3.6	45	0.09	0.225	100	0.46	0.03	0.31	2.46	0.034
56	3.6	45	0.325	0.17	82	0.52	0.09	0.4	2.75	0.022
57	3.6	45	0.15	0.2	104	0.55	0.05	0.39	2.91	0.041
58	5.5	45	0.25	0.2	95	0.5	0.06	0.36	2.15	0.032
59	5.5	45	0.325	0.16	82	0.55	0.06	0.44	2.37	0.022
60	5.5	45	0.325	0.188	108	0.61	0.07	0.45	2.62	0.038
61	5.5	45	0.15	0.2	104	0.55	0.03	0.39	2.36	0.037
62	5.5	45	0.4	0.17	86	0.54	0.07	0.42	2.33	0.028
63	3.6	70	0.325	0.19	123	0.73	0.1	0.54	3.89	0.012
64	3.6	70	0.43	0.17	103	0.69	0.12	0.53	3.66	0.007

Note: θ is the bank slope angle, H is average water depth far upstream from the retaining wall, Q_w is water discharge, Fr is flow Froude number far upstream (= $U/\sqrt{gH}$), Fr_d is grain size Froude number (= $U/\sqrt{gd_{50}}$), and H_s is the maximum scour depth below the initial bed surface.

D.2 Results

D.2.1 Hydrodynamics near the retaining wall in the absence of bed material

Prior to pursuing experiments in the presence of an erodible boundary, a gravel bed in our case, it was deemed appropriate to collect water surface and velocity data during a reference run on a fixed, smooth channel bed devoid of any sediment. The intent of this run was to identify the flow patterns in the vicinity of the retaining wall under flow conditions resembling those employed during the regular experiments (Tables D1 and D2) but in the presence of a Plexiglas channel bottom. A comparison between the hydraulic-only run here and subsequent erosion experiments can shed some light regarding the role of the local scour in the intensity of local flow patterns and their potential in undermining the wall. For the reference run, the channel slope was set at 0.2% and water discharge at 45 l/s. This resulted in a flow depth of 11.0 cm and a Froude of 0.51.

Figure D4 provides a perspective of the flow behavior near the retaining wall, showing spatial changes of water surface or non-uniform flow. It is evident that there is local flow acceleration near the upstream face of the retaining wall and subsequent flow separation at the leading edge that can cause bed scour in the case of an erodible bed surface (Figure D4 (A)-(C)). A point gauge and an Acoustic Doppler Velocimeter (ADV) from Nortek USA were used to measure the water surface elevation and velocity field, respectively. With the help of Matlab®, the data were processed and plotted as shown in Figure D5. It is clear that in the immediate vicinity of the upstream portion of the retaining wall, the depth-averaged velocity is higher due to the local acceleration. The depth-averaged velocity was obtained by using the $4/10^{th}$ rule, which states that the velocity at the vertical distance of 40% of water depth from the bed is representative of the mean value.

Figure D6 shows the time-averaged velocity profiles in 4 locations (three of which are shown in Figure D5 (C)). Location 1 is far upstream from the retaining wall, location 2 is within the section of the retaining wall, and location 3 is 3.0 cm away from the retaining wall (Figure D5 (C)). The fourth profile measurements were located at a lateral distance of 6.0 cm away from the wall. Figure D6 illustrates the flow acceleration from location 1 to 2 due to contraction. In addition, the retaining wall and the local flow separation induces further acceleration near the leading edge (location 3) stronger than location 2, which is in the middle of the channel section. The flow adjustment at the downstream part, trailing edge, of the wall, due to local expansion and deceleration, is mild (Figs. 5(D), 6(B) and (C)).

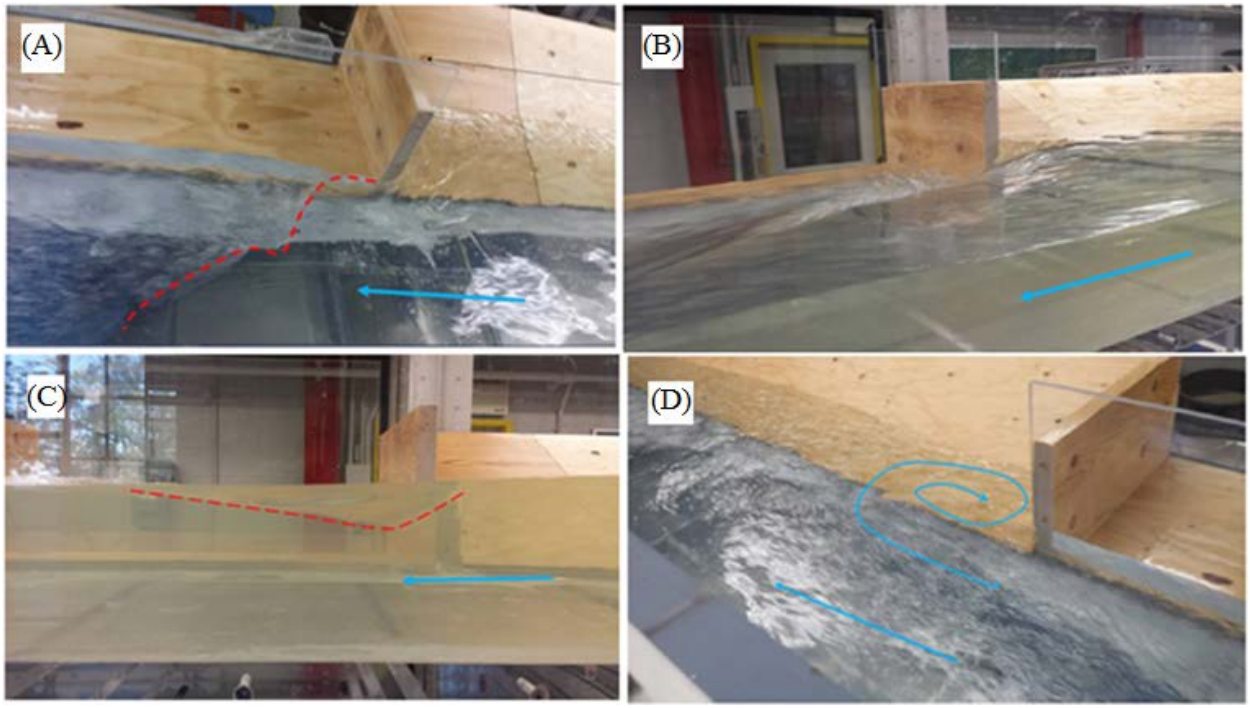

Figure D4. The non-uniform flow affected by the retaining wall; (A) an oblique top view showing local acceleration or water surface depression (dash line); (B) a lower angle of the jump in A); (C) a side view of the jump (dash line), and d) a circular vortex in the downstream area of the wall.

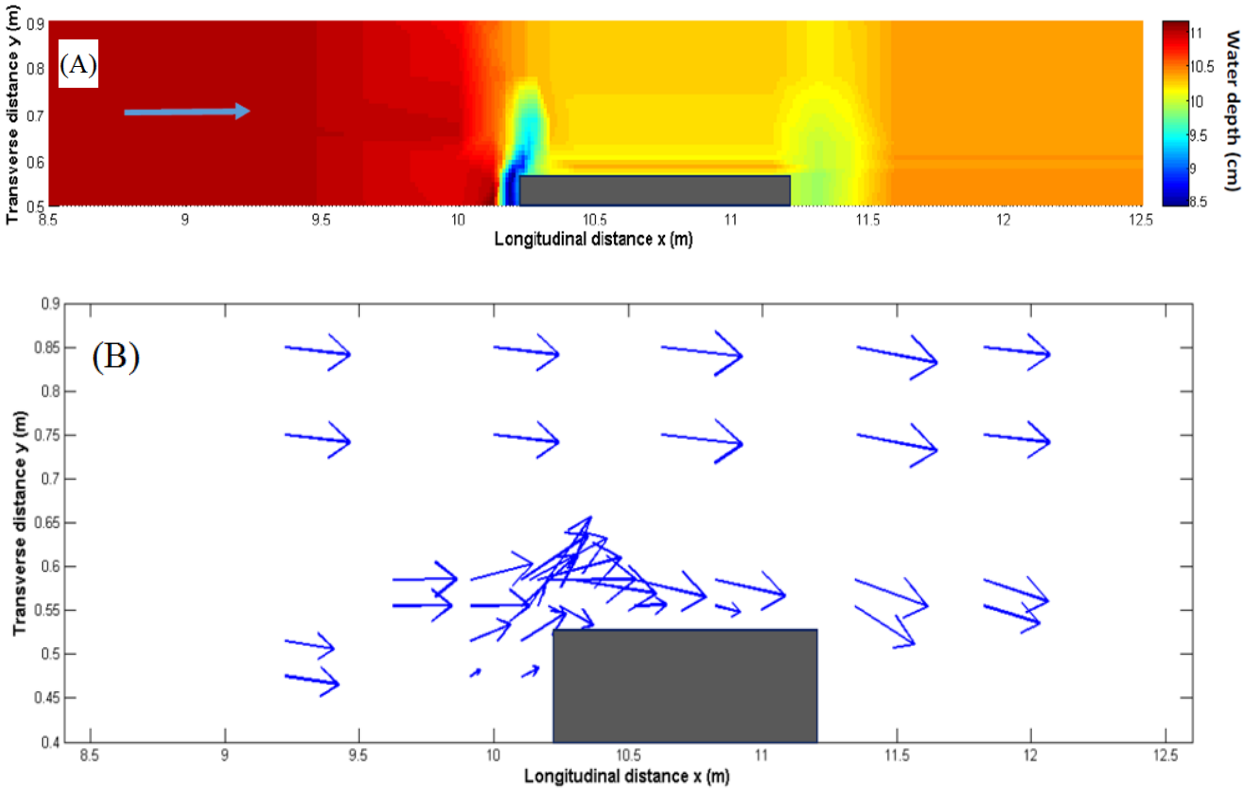

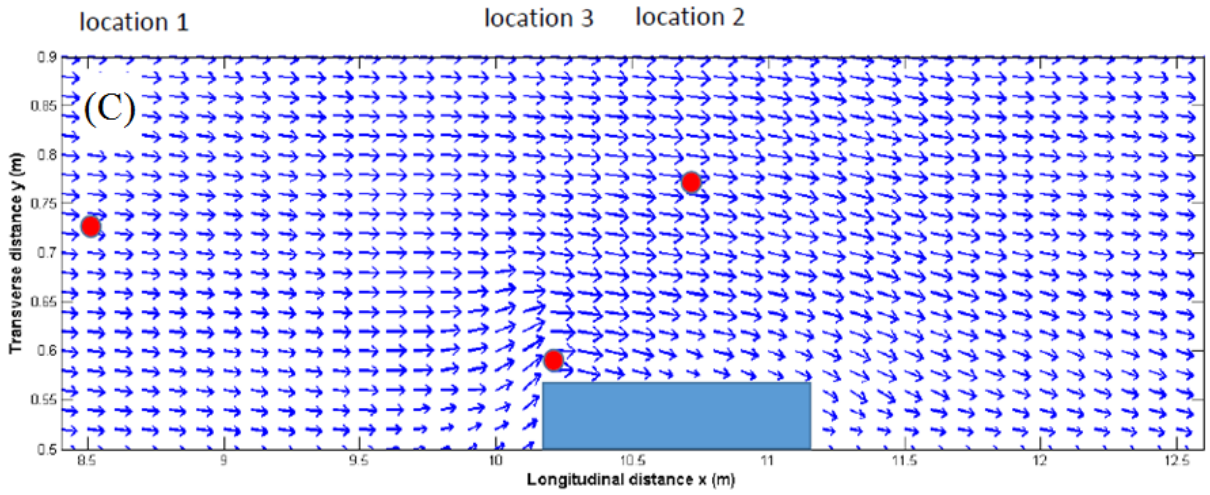

Figure D5. Flume measurements of (A) water surface elevation; (B) depth-averaged flow velocity as measured by the ADV; (C) depth-averaged flow velocity as interpolated in Matlab® into grids. The blue box is part of the retaining wall. Note that the ambient velocity (top part of Figure D5 (B) and centered left/right part of Figure D5 (C)) is 0.53 m/s for scale. Notice the higher velocity when the flow passes in front of the retaining wall. Red dots are locations of measurements for velocity profiles in Figure D6; see location numbers on top of the figure.

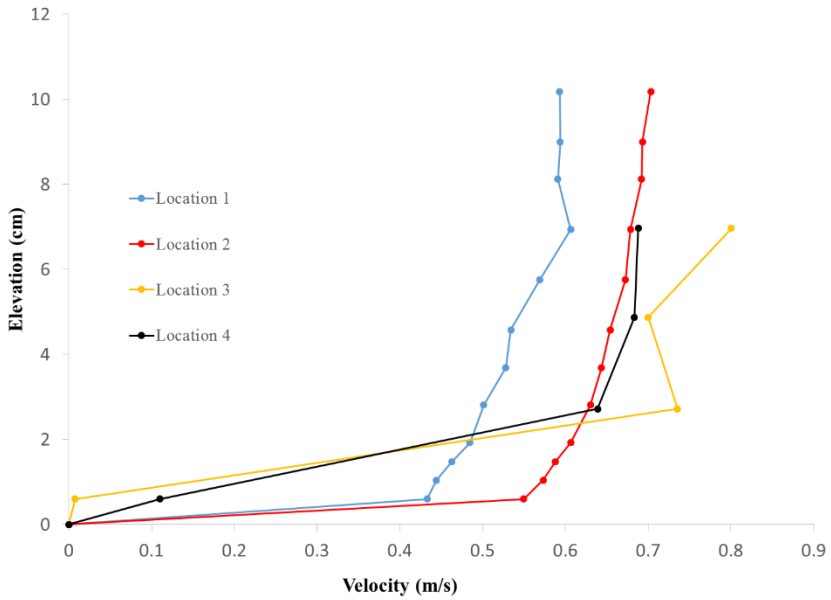

Figure D6. Time-averaged velocity profiles as measured by the ADV for 4 locations, shown in Figure D5 (C), for this case of Plexiglas bed. It shows clearly that velocity in locations 2&3 are higher than location 1 due to area contraction.

D.2.2 Results of erosional scour experiments

D.2.2.1 Run G-1: baseline case scenario

The G1 set of runs represents the baseline case scenario with gravel bank slope of 28 degrees and resulting area contraction of 15%; it is comprised of three sub-runs, G1-a to G1-c. The gravel bed material had a median diameter of 3.6 mm and a thickness of 10-cm. The channel bed slope was 0.25%.

Run G1-b was a replicate of G1-a and was intended to test the repeatability of the scour results. Both shared the exact same hydraulic conditions; a discharge of 80 l/s, flow depth of 17.0 cm, Froude number of 0.36, and $\tau_* = 0.07$. The maximum scour depths obtained for runs G1-a and G1-b were 5.3 and 5.8 cm, respectively, which are reasonably close (approximately within a grain size diameter) considering the uncertainty of depth measurement on loose gravel using a point gauge. Figure D7 shows the scour development near the retaining wall by looking through it. The grids of 5 × 5 cm have been drawn on the Plexiglas so that the topographic evolution of the scour and depositional areas near the wall can be observed and extracted. For this purpose, *x* and *y*-axes are defined at the upstream corner of the retaining wall. A 3-cm drop of the water surface near the leading edge of the retaining wall (Figure D7 (A)) is due to the local flow separation and associated vortex structure. Figure D7 (C) shows the temporal evolution of the bed topography adjacent to the retaining wall, including the maximum scour depth and deposition locations. As it can be seen there, most of the scour hole development occurred in the first 20 minutes, before it quickly reached a quasi-equilibrium state.

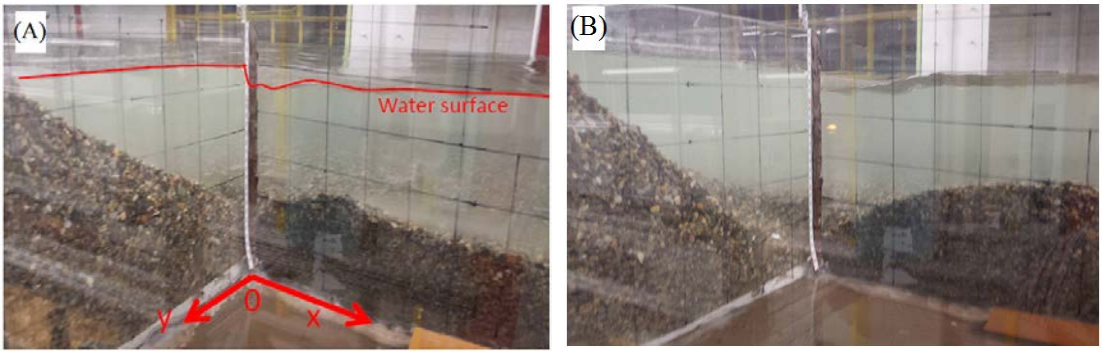

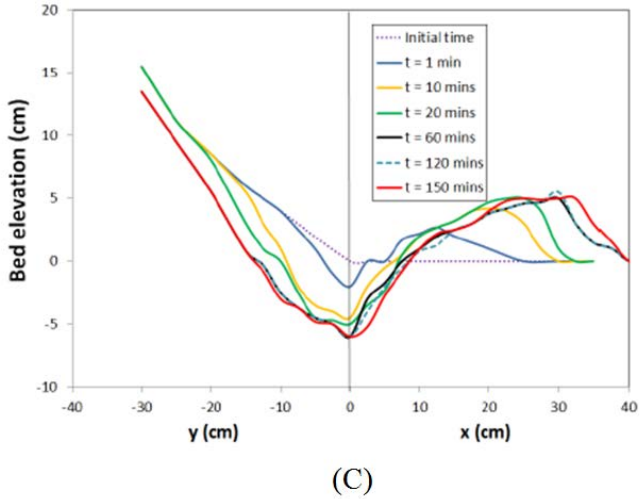

(C)

Figure D7. Scour development for run G1-a; (A) at time = 1 min; (B) at time = 1 hour; and (C) at multiple time records. The deepest scour depth is 5.3 cm. Note that the y and x axes are perpendicular to each other.

Run G1-c operated under the same hydraulic conditions as runs G1-a and G1-b, except for the adhesive material (3M® glue) that was lightly sprayed over a 30 cm long bank section located immediately upstream of the wall (Figure D8 (B)). This is to account in some way for the degree of cohesion that river banks in natural settings exhibit due to the presence of vegetation, tree roots, or clay material. Such cohesion is expected to reduce soil erosion and thus affect the morphological evolution of the bank near the retaining wall, which in turn can influence the local scour hole development. Comparing the results of erosion and deposition in Figure D8, it is evident that the adhesive material (shown in white color) holds the bank together better than the loose gravel (G1-b) case after 3 hours of run time. This results in a slightly lower maximum scour depth of 4.2 cm for run G1-c. Figure D9 shows the results of scour hole development over time for run G1-c. Substantial deposition is observed in both runs (G1-a and G1-c) immediately downstream of the scour hole (x = 10 - 40 cm) (Figures D7 (C) and 9(C)). This is probably due to flow reattachment and deceleration in that area. Because of various limitations of this approach, including the need for dry conditions and the incomplete representation of soil cohesion, the glue spraying approach was only used for a few runs. In the majority of the runs the non-cohesive gravel bank was used as the worst case scenario for determining the maximum scour in the vicinity of a retaining wall (Figure D8).

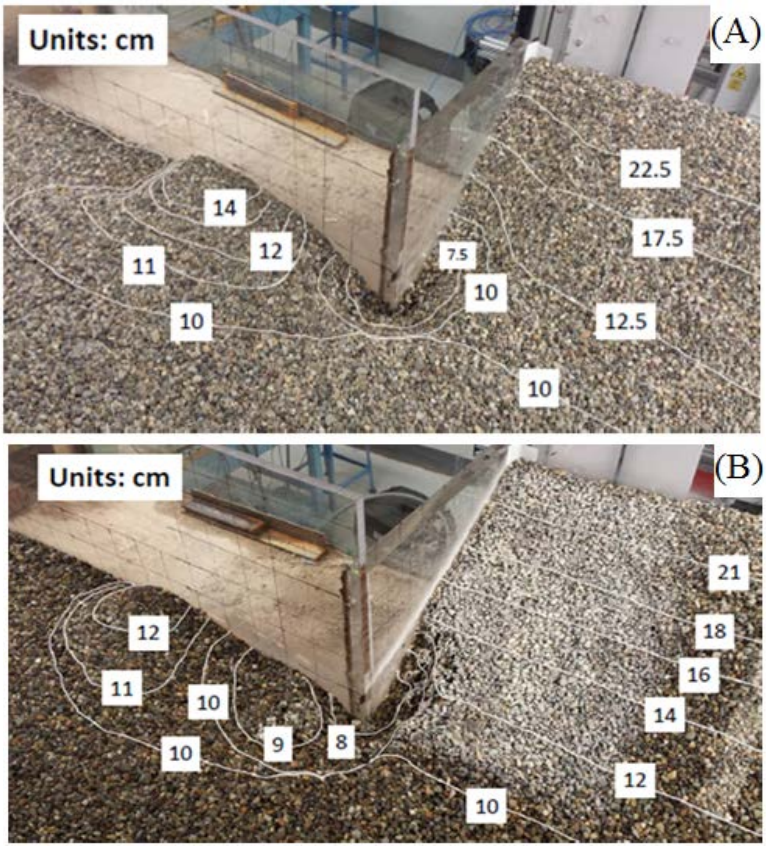

Figure D8. Topographic contours at the end of (A) G1-b (without cohesive glue spray on the bank); and (B) G1-c (with cohesive glue spray on the bank). The maximum scour depths are 5.8 cm and 4.2 cm, respectively. The adhesive material (white) was used to hold the bank.

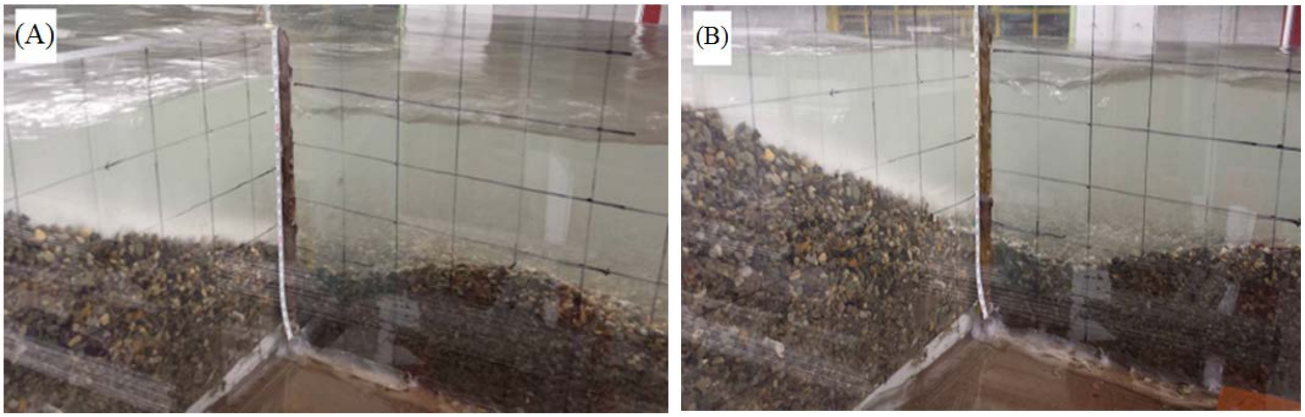

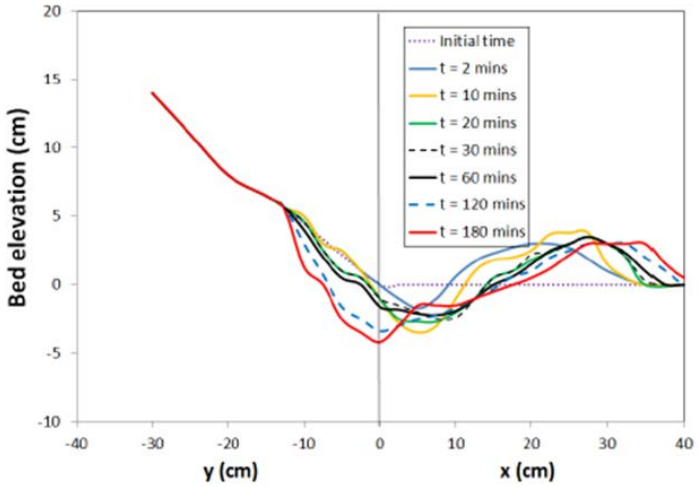

(C)

Figure D9. Scour development for run G1-c (with light adhesive glue on the bank); (A) at time = 2 min, (B) at time = 1 hour and (C) at multiple time records. The deepest scour depth is 4.2 cm.

We also employed a recently developed stereo-photogrammetry technique (Bouratsis et al., 2013) to monitor the scour hole development under hydraulic conditions similar to those of G1-b Two commercial waterproof Nikon cameras (Nikon 1 AW 1) were used to record the evolution of the scour and in-house developed software was employed for 3-D image reconstruction purposes. Figure D10 depicts the scour development over time, in terms of extend and depth. A 3-D representation of the bed topography after 60 min of run time is shown in Figure D11.

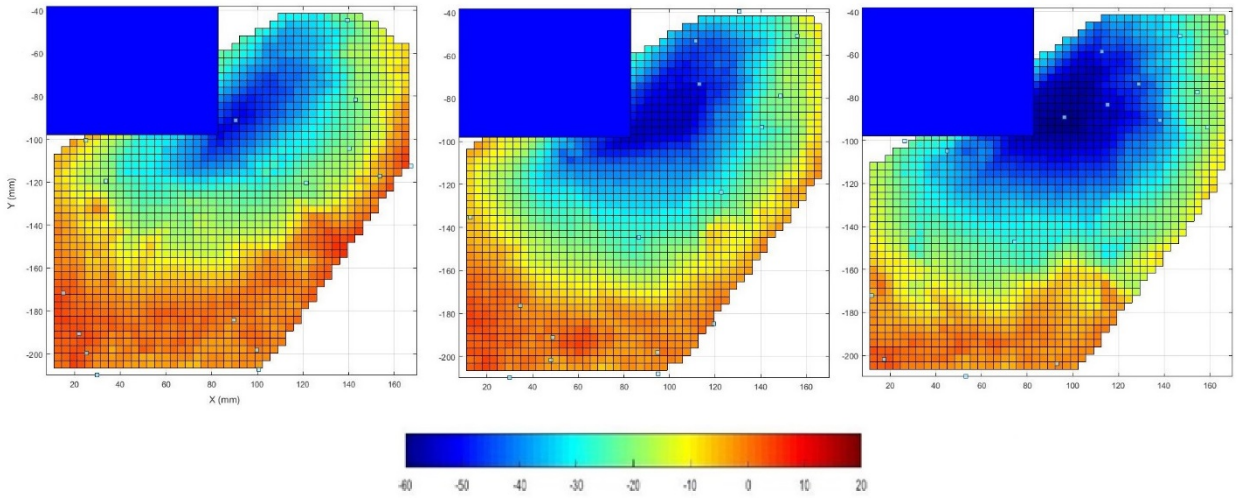

Figure D10. Instantaneous bed surface representation after time = 10 (left), 30 (middle), and 60 mins (right) from the initiation of scour. Flow from right to left.

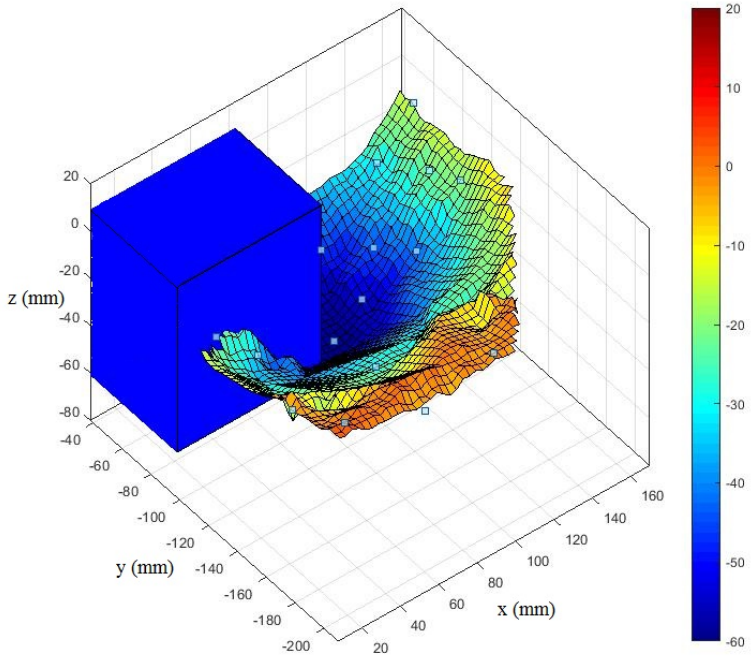

Figure D11. Three-dimensional representation of the bed in run G1-b after 60 minutes. Flow from right to left. The unit of elevation in color bar is in mm.

Velocity measurements obtained in case G1-c with an ADV, after the scour hole had reached a quasi-equilibrium condition, have been used to generate a depth-averaged velocity field map over a channel reach that includes the retaining wall section (Figure D12 (A)) and plot the vertical velocity profiles at three locations, one in the free stream area (location 1), a second near the mid-point of contraction area (location 2), and a third one near the leading edge of the wall (location 3) (Figure D12 (B)). A 38% increase in the depth-average velocity at location 2, within the retaining wall section, compared to the velocity at location 1, in the free stream region, is evident (0.62 vs 0.45 m/s). A qualitative comparison between the present velocity measurements and those obtained in section 2.1 (Figure D5; reference run, without any sediment) indicates an overall similarity of flow behavior. Differences though exist in the immediate vicinity of the leading edge of the retaining wall (see Figures D6 and 12 (B)). This is attributed to the scour hole presence in G1-c.

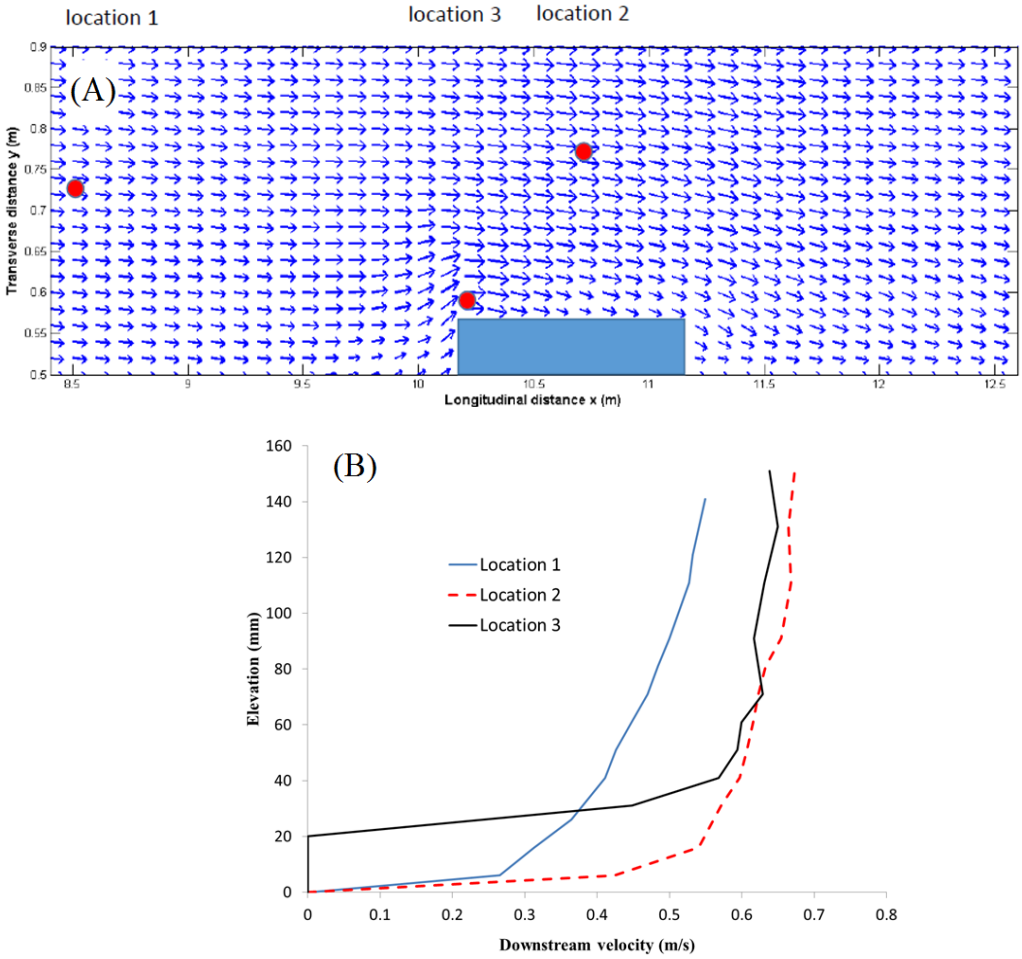

Figure D12. (A) Spatial distribution of the depth-averaged flow velocity for run G1. The arrow size in the upstream area (sufficiently far from the retaining wall) indicates a longitudinal velocity of 0.45 m/s. The red dots show locations of ADV measurements for the velocity

profiles. (B) Vertical velocity profiles at locations 1, 2, and 3 measured during run G1-c. The lower most of the profile for location 3 is 2 cm higher than the rest because of a chunky gravel deposit.

D.2.2.2 Run G-2: retaining wall with rough surface

In run G2, the surface of the retaining wall has been rendered rough through the use of either very coarse sandpaper or gravel glued on a plastic sheet covering the retaining wall surface (Figure D13). In the latter case, the gravel used were identical to the bed material (d_{50} = 3.6 mm). There are 4 sub-runs for these rough wall conditions. Runs G2-a and G2-b had sandpaper sheets pasted on the wall surface. The sandpaper is number 30 (standard) and has an equivalent sand grain size of 0.6 mm. However, the sandpaper sheets blocked the observation window for the view of the sediment deposition area; hence, only the erosional data or scour was observed and recorded (Figures D14 (A) and 15 (A)). Figure D14 compares the bed evolution for G2-a against the baseline case scenario (G1-a). Both runs share the exact same hydraulic conditions; a discharge of 80 l/s, slope of 0.25%, flow depth of 17.0 cm, flow Froude number of 0.36, and $\tau_* = 0.07$. Results show that in the case of a rough wall, the scour hole developed relatively slower and reached a shallower quasi-equilibrium depth. The maximum scour depth at t = 150 mins for run G2-a is 3.7 cm, compared with 5.3 cm for run G1-a (with smooth wall).

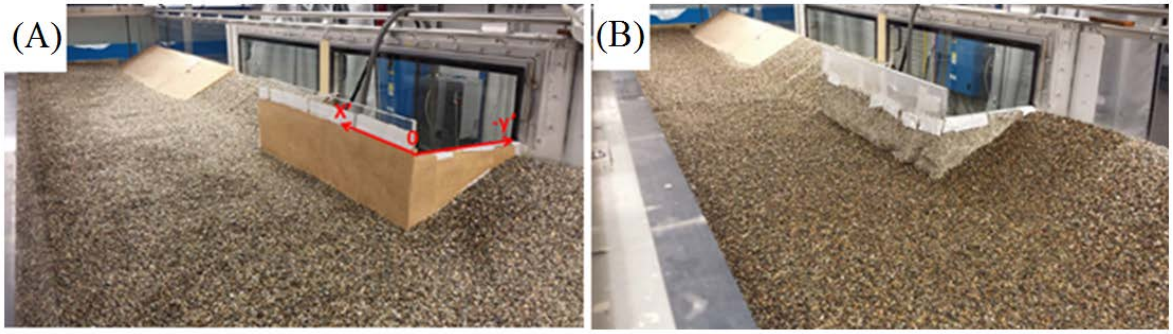

Figure D13. Run G2 showing rough-wall condition for the retaining wall; (A) sandpaper; and (B) glued gravel on plastic sheet. Note the x' and y' axes, used for plotting the results of bed surface evolution below. Contraction is about 15%. Looking downstream.

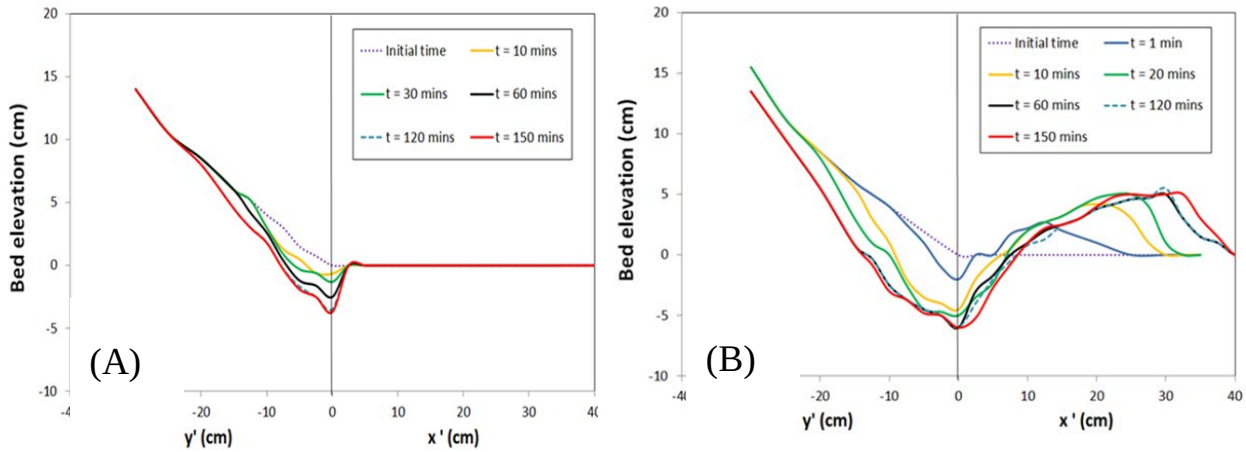

Figure D14. Bed surface evolution for (A) run G2-a; and (B) G1-a. The sandpaper wall leads to scour reduction. Deposition parts in Figure D14 (A) were not recorded because the observing wall window was blocked by the sandpaper sheet.

It should be noted that run G2-a was performed twice and achieved the same conclusion, a shallower scour on rougher wall. Run G2-b hence was performed to seek further insight; this run was different from G2-a in that the flow discharge was increased from 80 to 90 l/s. A special baseline run (called here G1-90), similar to the baseline run G1-a but with discharge of 90 l/s, was also performed for the purpose of comparing the results with run G2-b (Figure D15). Similar results have been found; the sandpaper-glued wall leads to moderate scour reduction. The maximum scour depth at t = 150 mins for run G2-b and run G1-90 is 5.6 cm and 7.0 cm, respectively.

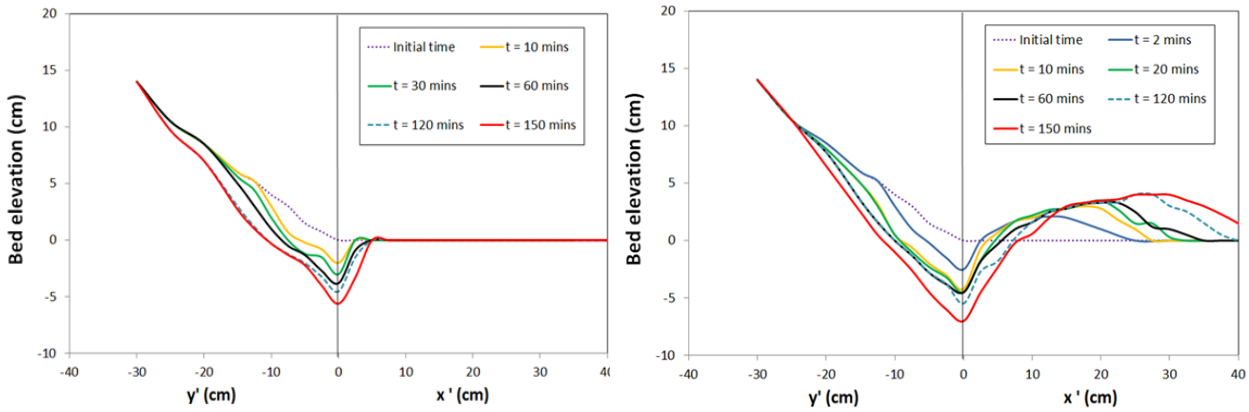

(A) (B)

Figure D15. Bed surface evolution for (A) run G2-b; and (B) special baseline run, G1-90. The sandpaper-glued wall leads to scour reduction.

Runs G2-c and G2-d had the same slope of 0.25% but different discharge, 80 and 90 l/s, respectively. In these two cases the retaining wall was covered with the gravel-glued sheet (Figure D13 (B)) Figures D16 and D17 compare the results of bed evolution with the corresponding baseline runs G1-a and G1-90. Results show that in the case of this rougher wall, the scour hole also developed relatively slower and reached even shallower quasi-equilibrium depth than that for the case of sandpaper (Figure D14 (A)). The maximum scour depth at t = 150 mins for run G2-c is 2.3 cm, compared with 5.3 cm for run G1-a. Likewise, the maximum scour depth at t = 150 mins for run G2-d is 4.7 cm, compared with 7.0 cm for run G1-90.

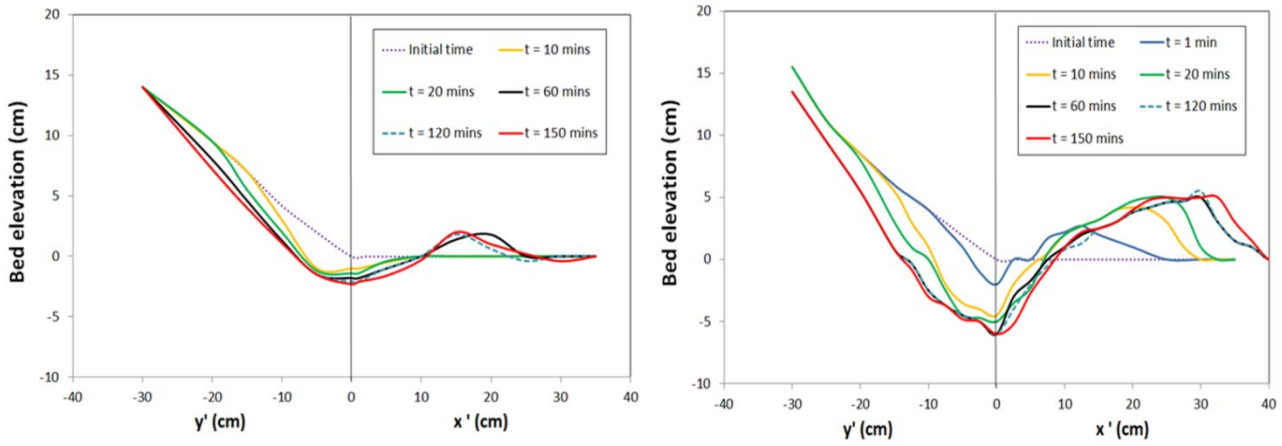

Figure D16. Bed surface evolution for (A) run G2-c; and (B) G1-a. The gravel-glued wall leads to considerably shallower scour.

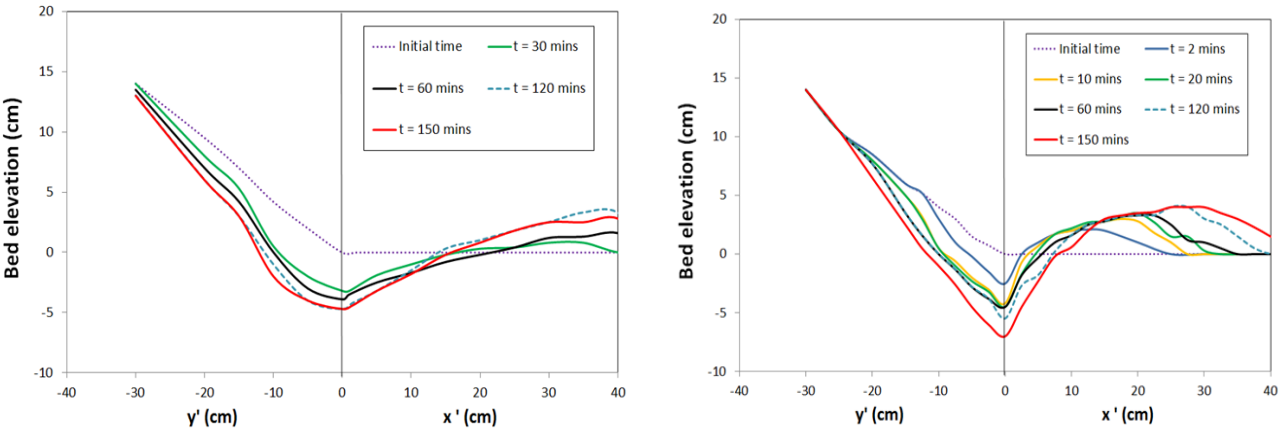

(A) (B)

Figure D17. Bed surface evolution for (A) run G2-d; and (B) G1-90. The gravel-glued wall leads to considerably scour reduction.

D.2.2.3 Run G-3: retaining wall with vegetated bank

Run G3 includes plastic models of vegetation, simulating similar conditions that we observed in the field, including Scranton, PA, and several other sites located through the Google search. Apparently, vegetation is used as a measure to protect the river bank in the area immediately upstream of the retaining wall (Figure D18 (A)). Our runs showed that trees could potentially reduce scour depth near the leading edge of the retaining wall by deflecting the high velocity

thread farther into the channel. Run G-3 has two sub-runs, G3-a and G3-b, based on the number of rows of the model trees placed on the bank (Figures D18 (B), (C)). The former had a single row with 6 trees, placed 10-cm apart, while the latter had 4 rows with similar arrangement of trees within each one of them. Both runs, G3-a and G3-b, had the exact same hydraulic conditions as the baseline case, run (G1-a).

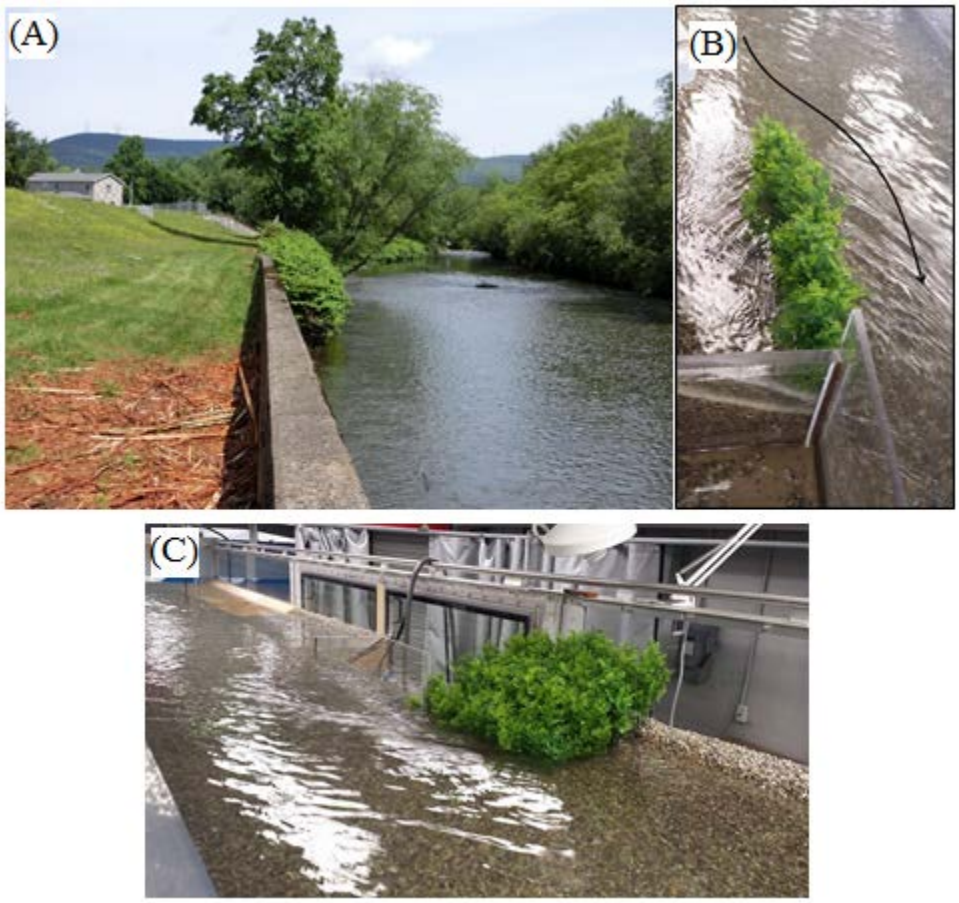

Figure D18. (A) The field condition in Scranton, PA, showing bushes and trees on the river bank before transitioning to the leading edge of the retaining wall. Flow direction is out of the page. (B) Our experimental run G3-a, testing the effect of bushes (single row). (C) Run G3-b, testing the effect of multiple rows of model trees on the bank.

The model trees were found to steer the flow away from the bank and the leading edge of the retaining wall, thus providing for a more gradual channel transition (Figure D18 (B)). Figure D19 shows the scour configuration near the upstream end of the retaining wall at the end of both runs, G3-a and G3-b, after 150 mins of run time. The maximum scour depth was 3.8 cm for run G3-a, compared to 5.3 cm in the baseline case, and zero for run G3-b. Surprisingly, no scour was observed for the multiple row vegetation case even when the discharge was increased to 90 l/s. A further increase in the water discharge (102 l/s) resulted in failure of the model trees.

Figure D20 illustrates the comparison of bed evolution between G3-a and the baseline case scenario G1-a. The scour and deposition for run G3-a are significantly smaller than the baseline run. The vegetation arrangement used in run G3 has the potential to strengthen the bank through the root system, displace the high velocity thread away from the bank and minimize the flow separation at the leading edge of the retaining wall. All three effects reduce bank erosion and local scour near the wall. The impact on the flow field, depth-averaged velocity, for the G3-a case is reflected in Figure D21. The design with multiple rows of trees or bushes on the bank (Figures D18 (C)) appears to be the most effective for minimizing erosional scour during floods. Possible uprooting of the vegetation during major floods is expected to adversely affect the local scour condition.

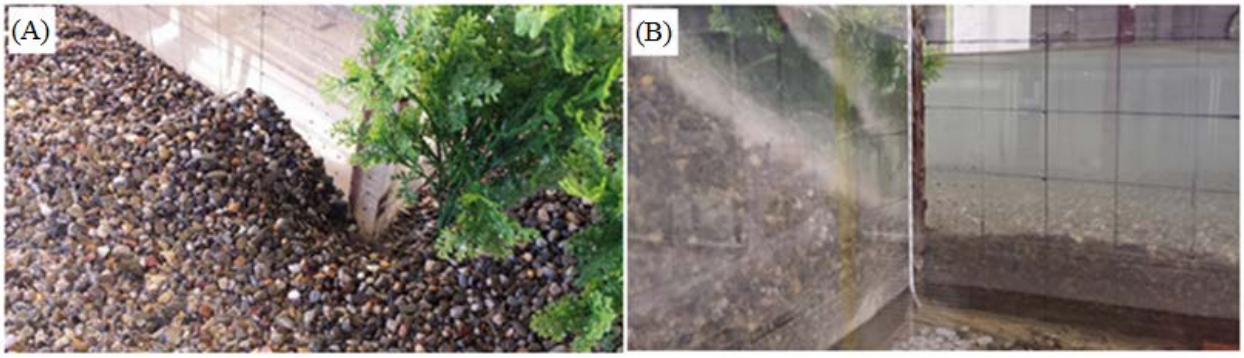

Figure D19. (A) Scour development at the leading edge of run G3-a after 150 mins; and (B) the zero-scour condition of run G3-b, taken behind the retaining wall.

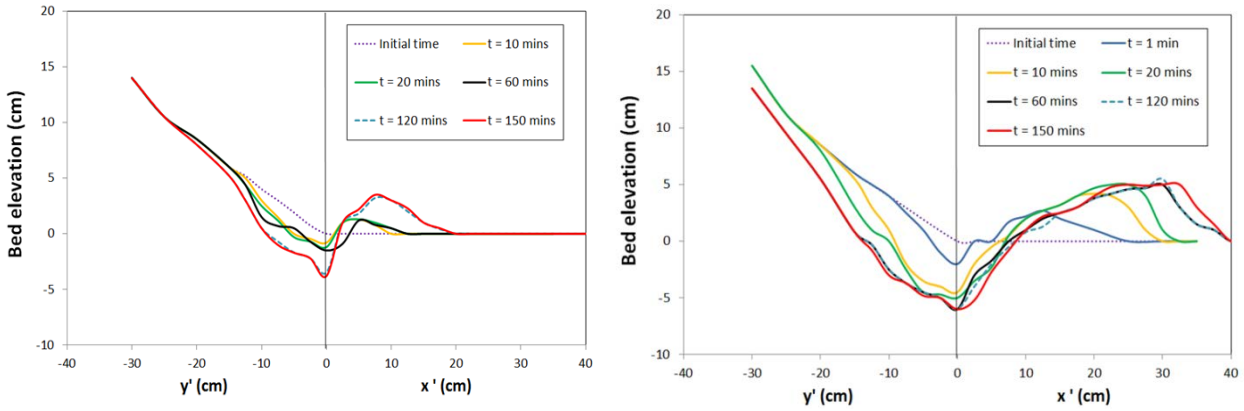

(A) (B)

Figure D20. Bed surface evolution for (A) run G3-a and (B) run G1-a (for comparison). It is clearly seen that vegetation can potentially reduce the erosional scour near the leading edge of the retaining wall.

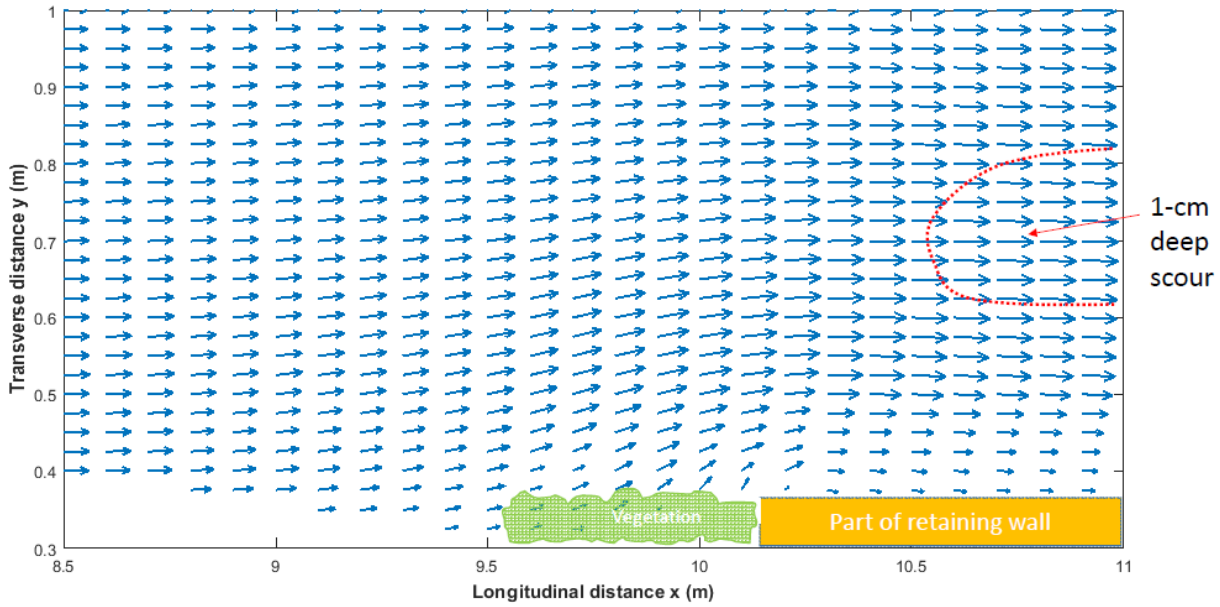

Figure D21. Depth-averaged flow velocity as interpolated in Matlab® into grids for run G3-a in the first hour of run time. Note that the ambient velocity upstream (left most) is 0.45 m/s for scale.

D.2.2.4 Run G-4: armor layer on the bed

In this section, we are reporting the experimental results for run G4, performed in the presence of an armored layer bed. The armor layer is two grain-size diameters thick ($2d_{50}$) of sediment with d_{50} of 5.5 mm and d_{90} of 7.0 mm, while the subsurface bed material is identical to the sediment that has been used in all previous runs (d_{50} of 3.6 mm and d_{90} of 6.0 mm). The channel bank near the retaining wall in run G4 was sprayed lightly with 3M® glue to preclude its collapse and potential influence on the scour development. Then, G1-c, the baseline run with cohesive spray on the bank, is used for comparison. Results show that as long as the flow is capable of mobilizing the material within the armor layer, its presence does not appear to have much impact on the maximum scour depth or even the entire evolution of scour. The maximum scour depth for run G4 is 5.0 cm compared with 4.2 cm in the case of G1-c (Figure D22). Another run for armor layer testing was conducted without the glue spray on the bank (not shown here). Similar results were found; no apparent difference in topographic evolution was observed compared to the corresponding baseline case scenario, G1-a, with no glued bank.

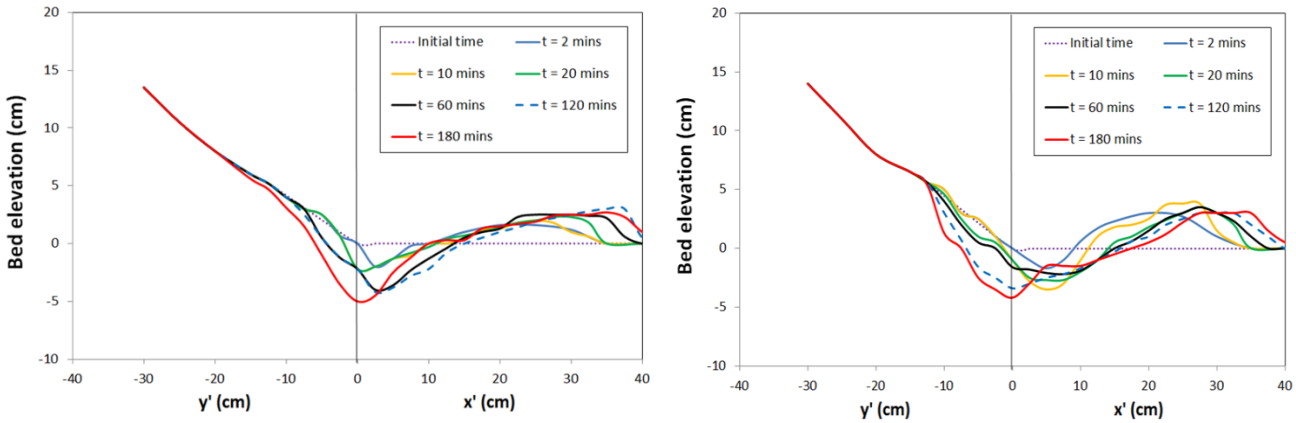

Figure D22. Bed surface evolution for (A) run G4 and (B) run G1-c (for comparison). The difference is insignificant.

D.2.2.5 Run G-5: Bank slope of 35 degrees

All of the results so far stated in previous sections have had bank slope of 28°. In this section, we are reporting the experimental results for run G-5, which has steeper channel-bank slope. The bank has an angle of 35°, which coincides with the angle of repose of the gravel used. Figure D23 illustrates the comparison of bed evolution between run G-5 and the baseline case scenario G1-a. The erosional scour and deposition for run G-5 are significantly lower than the baseline run, likely due to less contraction of the local area (from 15% to 13%). It proves that the abrupt contraction design at the leading edge of the retaining wall contributes to the local scour development in a significant way. The maximum scour depth for G-5 was 1.9 cm compared to 5.3 cm for G1-a. Sixteen more runs with this steeper channel-bank slope have been considered (Table D2) for the purpose of investigating further the role of bank slope on maximum scour depth. All these runs support the same conclusion; a steeper bank leads to shallower scour near the retaining wall.

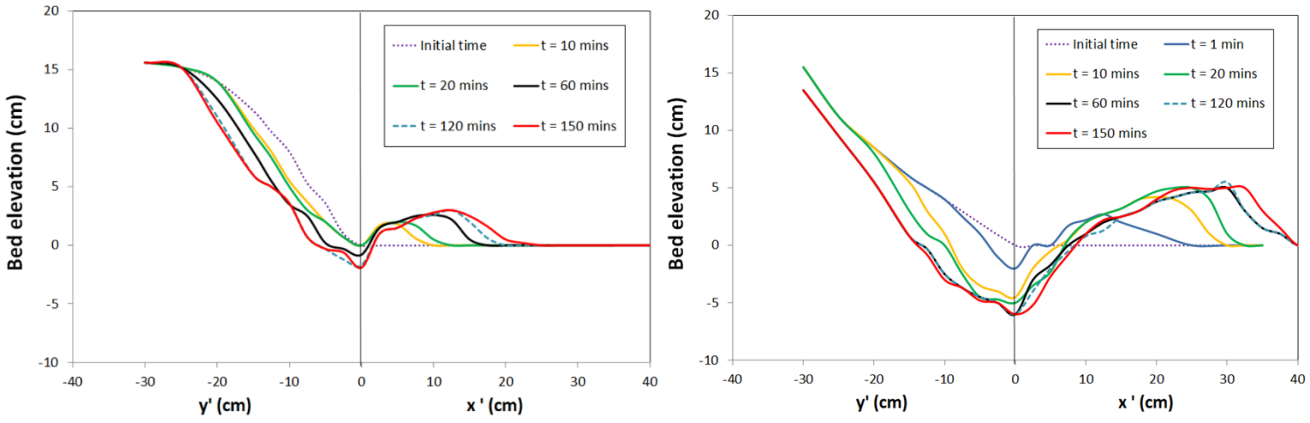

Figure D23. Bed surface evolution for (A) run G-5 and (B) run G1-a (for comparison). Steeper bank slope leads to shallower scour.

D.2.2.6 Run G-7: Bank slope of 70 and 80 degrees

Run G-6 is comprised of 11 sub-runs with bank slope of 45 degrees (see Table D2). The experimental results were intermediate, between those with bank slopes of 35 and 70 degrees. Here, we are reporting the experimental results for runs G-7a and G7-b, which had even steeper channel-bank slopes, namely 70 and 80 degrees. These steep slopes could simulate bedrock or strongly cohesive banks. In Scranton, PA, where we conducted a field survey, there are many locations where the river bank is bedrock (e.g., Figures D2 (C) and (D)). The steep bank slopes were built within the flume by using an additional wooden insert. Obviously, judging from previous runs the much smaller contraction area in these cases (Figures D24 (A) & (B)) should not be expected to cause significant erosion.

Starting with 80-degree bank slope (run G7-b; Figure D24 (B)), no scour was observed under hydraulic conditions similar to those in the baseline case scenario (run G1; S = 0.25%, Q_w = 80 l/s, H = 17 cm). The most extreme case considered here had a channel bed slope of 0.42% and discharge of 105 l/s (H = 17 cm). Though this run caused considerable movement of sediment within the flume and a water surface depression of 2 cm near the leading edge of the structure, it did not generate any scour in the vicinity of the retaining wall.

Run G7-a, with bank slope of 70° (Figure D24 (A)) was tested under the same hydraulic conditions as run G7-b. For S = 0.325% and Q_w = 120 l/s (water surface drop = 5 cm), maximum local scour of about 1.2 cm was developed at the completion of a 2-hr experiment

(Figure D24 (C)). For S = 0.42% and Q_w = 105 l/s (water surface drop = 3 cm), the corresponding maximum local scour for a 2-hr experiment was about 0.7 cm.

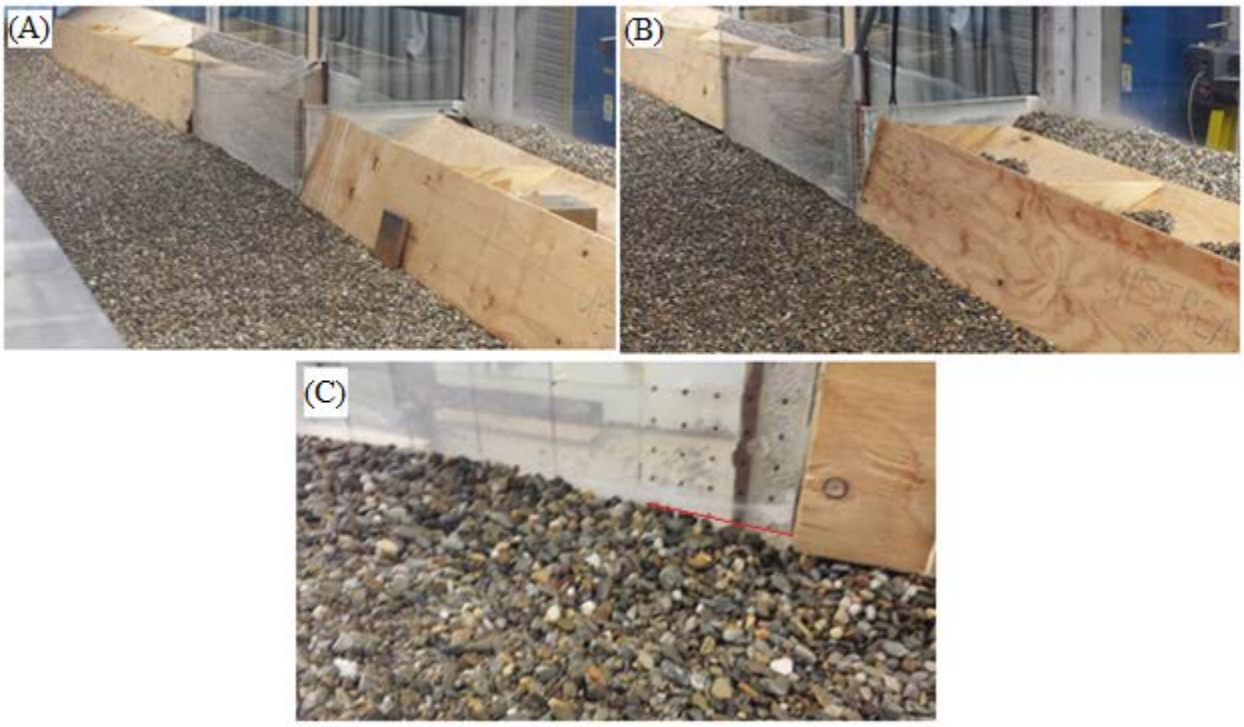

Figure D24. The bank conditions for (A) slope of 70°, and (B) slope of 80°. (C) A small amount of bed erosion (up to 1.2 cm deep) developed near the leading edge of the wall in the case of 70-degree bank slope (the red line shows the initial bed level).

D.3 Development of Empirical Relationship for Estimating Maximum Scour Depth

The results obtained from small-scale indoor experiments, listed in Table D2, were used to develop an empirical relationship for estimating the maximum scour depth in the vicinity of a retaining wall in a straight channel. It was found that in all experiments the maximum scour depth occurs near the leading edge of the wall, which is due to the abrupt contraction from the channel bank to the vertical wall (Figure D25). The abrupt contraction results in pronounced local flow separation and intense vorticity. The formulation presented here will provide practitioners with a scour evaluation methodology at the base of the leading edge of longitudinal walls, especially during flood conditions. The analysis below provides much improvement for the case of scour near the base of longitudinal retaining walls, currently not available in the literature.

Several formulas included in HEC-23 and HEC-18 reports for predicting scour in other types of structures have utilized some concept of dimensionless variables and power laws to achieve simple scaling analysis. Here we start from the Buckingham Pi theorem in order to achieve the most comprehensive analysis. Figure D25 shows a schematic of the area near the leading edge of the retaining wall in the flume experiments at Lehigh.

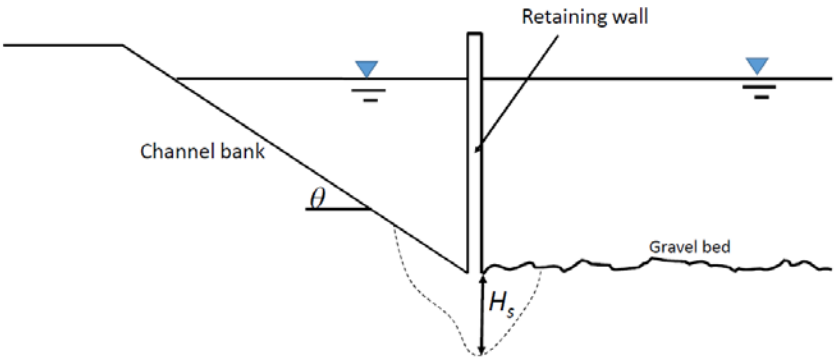

Figure D25. Schematic of cross-section at the transition from a sloping bank to rectangular section within the retaining wall area. Flow direction out of the paper.

Considering dimensional analysis, the maximum scour depth (H_s) can be written as a function of other independent dimensional variables. One possible set of such variables is included in equation (1):

$$H_s = \text{f}\,(H, d_{50}, U, \theta, g, \nu, R,) \tag{1}$$

Where ν is the kinematic viscosity of water. By selecting d_{50} and g as the repeating variables, and following standard dimensional analysis procedures, equation (1) can be recast in terms of dimensionless parameters in the following way:

$$\frac{H_s}{d_{50}} = f\left(\frac{H}{d_{50}}, Fr_d, \theta, Re_p, R\right) \tag{2}$$

Where Re_p is particle Reynolds number ($=\frac{Ud_{50}}{\nu}$) and $Fr_d = U/\sqrt{gd_{50}}$ is the "grain-size Froude number". Re_p is not as important for a fully rough boundary, where the friction factor (and critical Shields stress) becomes independent of particle Reynolds number. Additionally, for natural rivers, R is approximately constant. Therefore, equation (2) is reduced to:

$$\frac{H_s}{d_{50}} = f\left(\frac{H}{d_{50}}, Fr_d, \theta\right) \tag{3}$$

This analysis is limited to non-cohesive bed material. Using all 64 data points (Table D2) obtained from the experiments, and employing forward multiple regression analysis, the following expression is obtained:

$$\frac{H_s}{d_{50}} = 0.0178\left(\frac{H}{d_{50}}\right)^{1.24}\left(cot(\theta)\right)^{1.325} Fr_d^{1.108} \tag{4}$$

This equation has a goodness of fit r^2 = 0.63 and covers considerable range of bank slopes ($28° \leq \theta \leq 70°$), bed slopes ($0.09 \leq S \leq 0.6\%$), relative roughness values ($17.9 \leq \frac{H}{d_{50}} \leq 62.5$) and grain size Froude number ($1.59 \leq F_{rd} \leq 3.89$).

Figure D26 depicts the best-fit curve between the measured values of scour depth and the combination of independent variables with the exponents obtained from the multiple regression analysis. Analysis revealed that all the variables in the model were statistically significant, the p-value of the exponents were less than 0.005.

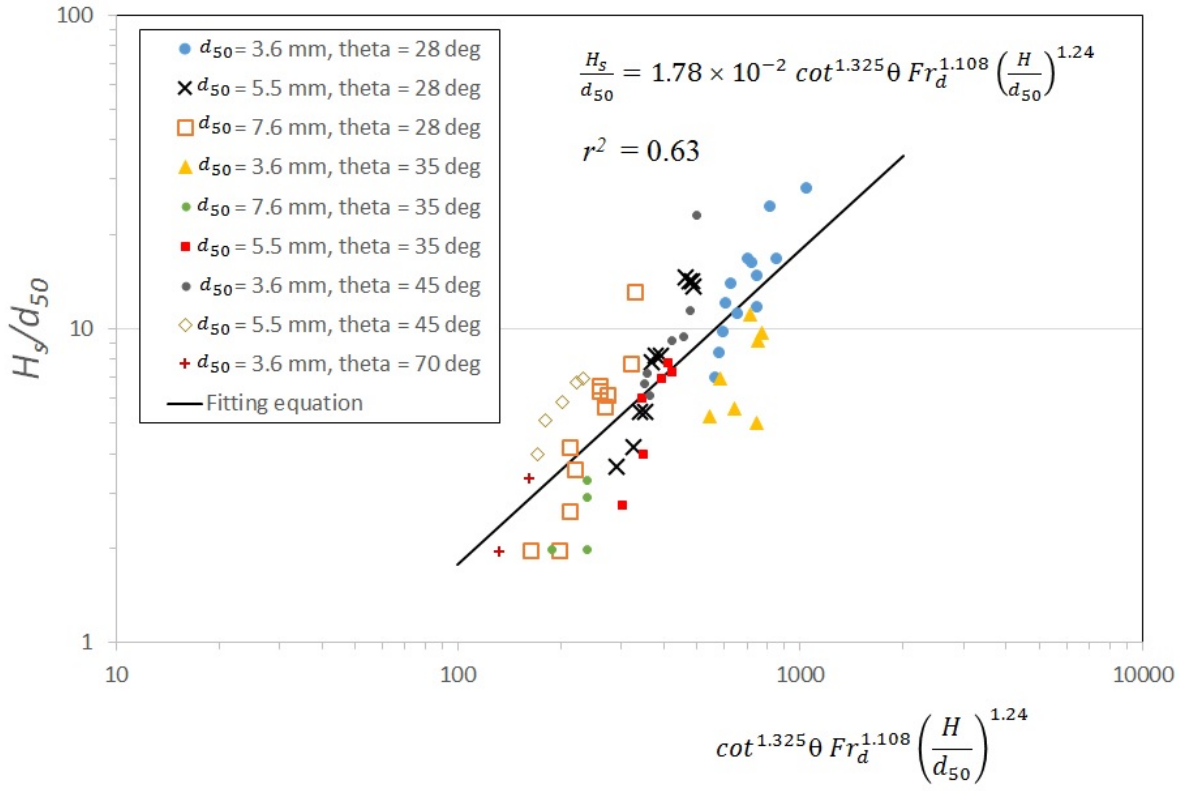

Figure D26. Regression equation to estimate maximum scour depth at the leading edge of the retaining wall.

Figure D27 shows a histogram of the residuals. The Kolmogorov-Smirnov and Shapiro-Wilk normality tests presented in Table D3 show that the residuals are normally distributed (significant values (sig.) are greater than 0.05). Therefore, the outcome of the regression analysis is valid and it can explain all the trends in the dataset.

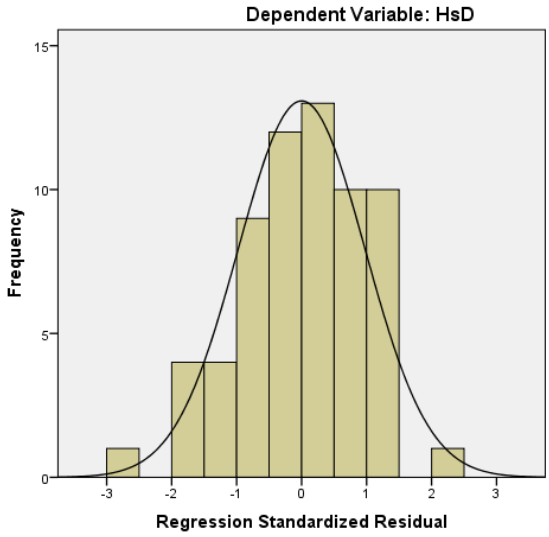

Figure D27. Histogram of the residuals in our analysis.

Table D3. Normality test results for the residuals.

	Kolmogorov-Smirnov[a]			Shapiro-Wilk		
	Statistic	df	Sig.	Statistic	df	Sig.
Unstandardized Residual	.096	64	.200*	.978	64	.303

*. This is a lower bound of the true significance.
[a]. Lilliefors Significance Correction

D.4. Discussion

In addition to the above report of experimental results in section 2, we performed supplementary runs using 1) a section of clay bed, and 2) gradual transition from the channel bank to the retaining wall (run C-1 and G-8 in Table D1, respectively). These experiments were performed in order to qualitatively investigate the development of scour on cohesive bed, and the effect of gradual transition between the bank and the wall rather than the abrupt transition as done in runs G-1 to G-7. These runs are preliminary and should not be viewed as conclusive. The observations mentioned below can assist the design of more detailed experiments in future studies.

For the clay bed, kaolinite (d_{50} = 2 µm) and silica sand (d_{50} = 0.2 mm) were mixed at a ratio of kaolinite to sand of 9:1. Quick direct shear test results revealed that the shear strength of the prepared sample, saturated and consolidated for 48 hours under its own weight, was 1.3 kPa. The baseline case scenario hydraulic condition, with S = 0.25% and Q_w = 80 l/s, generated a bed shear stress of 4.3 Pa and caused no bed scour or sediment suspension. A subsequent increase in bed slope and flow discharge to about 0.325% and 120 l/s, respectively, augmented the bed shear stress by 50% (6.5 Pa) and generated significant amount of suspended load. This is quite

different from the shear strength value (1.3 kPa) measured via the geotechnical method due to, among other things, the inherent difficulties in duplicating the laboratory flume soil conditions. Similar variability in critical shear stress values, of more than an order of magnitude, has been extensively reported in the literature for the case of cohesive soils [e.g., Parchure and Mehta, 1985; Williamson and Ockenden, 1996; Kamphuis and Hall, 1983; Mitchener and Torfs, 1996]. Local scour developed as well during this experiment, though at a slower pace compared to the prior runs with non-cohesive material (gravel). More specifically, while for the gravel bed case most of the local bed erosion occurred in the first 30 - 60 mins, here most of the scour near the leading edge of the wall occurred at time t = 1.0 to 3.5 hrs (Figure D28). During the next 2.5 hrs (t = 3.5 to 6.0 hrs), the near-wall bed topography reached quasi-equilibrium condition and the erosion expanded toward the channel center. The final maximum scour depth at the leading edge of the retaining wall was 3.0 cm. The bed topography at the completion of the experiment (t = 6.0 hrs) is shown in Figure D29.

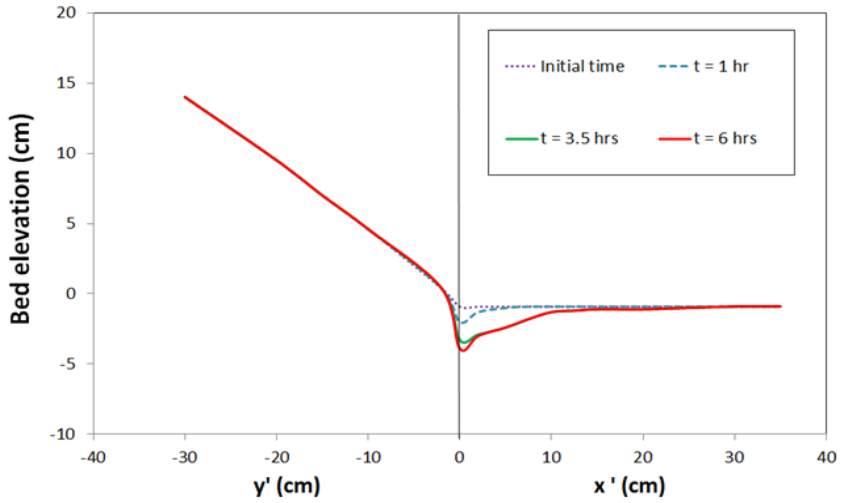

Figure D28. Bed surface evolution for the clay bed.

Figure D29. Erosional scour near the retaining wall after 6.0 hrs.

For the run with gradual transition (G8) or “berm”, a gradually transitional bank from 28 to 35 degree slope was built (Figure D30). The dimension of this berm is shown in Figure D30 (B). The experiment in this setting then was run with a hydraulic condition similar to the baseline scenario, S = 0.25% and Q_w = 80 l/s. No scour was observed in this experiment after an hour of run time. Similarly, no scour took place in two subsequent experiments when the flow discharge was increased to 90 l/s first and then to 100 l/s. A further increase in the discharge to 110 l/s caused to gradual collapse of the berm. This result emphasizes that the scour near the retaining wall is truly influenced by the contraction. The gradual transition may constitute a further improvement, compared to the abrupt contraction case.

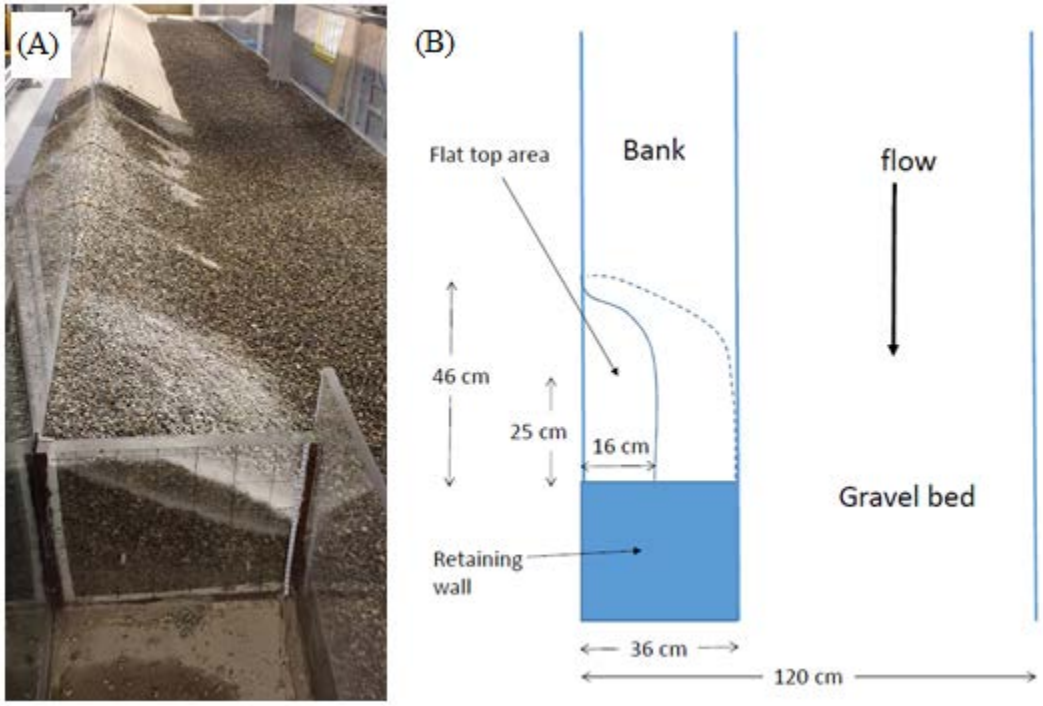

Figure D30. (A) Gradual transition of the bank, or berm, near the leading edge of the retaining wall. (B) Berm dimensions.

D.5. Conclusion

To investigate the clear-water scour mechanism at the base of longitudinal retaining walls, we conducted small-scale physical experiments using a tilting flume facility and appropriate instrumentation for measuring local flow velocity profiles and bed topography development. A total of 75 runs were performed. The maximum scour depth occurred at the leading edge of the retaining wall, where the local flow acceleration was strongest due to the transition from the sloping bank onto the vertical face of the wall. Results showed that rough-wall condition can potentially reduce erosional scour near the retaining wall. Moreover, runs with model vegetation

on the bank, in the vicinity of the upstream transition to the wall, suggested that the erosional scour is significantly reduced by the trees/bushes because they displace the high velocity thread away from the bank and minimize the flow separation and acceleration near the leading edge of the wall. Limited number of runs with armor bed indicated that, in our cases, armor-layer bed does not have noticeable influence on the scour mechanism. The variation of bank slope from 28° to 80° in multiple runs demonstrated that a steeper bank leads to shallower scour near the retaining wall. Dimensional analysis was used next to identify the important dimensionless parameters that influence the scour phenomenon and assist in the development of a suitable empirical relationship that best describes the trends exhibited by the experimental results shown in Table D2. A forward multiple regression analysis was carried out to obtain the relationship for estimating the maximum scour depth. Finally, the present experiments indicated that the flow adjustment at the downstream end, trailing edge of the structure, due to the abrupt expansion was relatively mild and thus it did not result in significant local erosion.

D.6 References:

Bouratsis, P. P., Diplas, P., Dancey, C. L., and Apsilidis, N. (2013). High-resolution 3-D monitoring of evolving sediment beds. Water Resources Research, vol. *49*(2), 977-992.

Kamphuis, J. W., and Hall, K. R. (1983). Cohesive material erosion by unidirectional current. Journal of Hydraulic Engineering, vol. 109(1), 49-61.

Mitchener, H., and Torfs, H. (1996). Erosion of mud/sand mixtures. Coastal engineering, vol. 29(1), 1-25.

Parchure, T. M., and Mehta, A. J. (1985). Erosion of soft cohesive sediment deposits. Journal of Hydraulic Engineering, vol. 111(10), 1308-1326.

State Departments of Transportation (2001). Evaluating Scour at Bridges, Hydraulic Engineering Circular No. 18 (HEC-18), Fourth edition, FHWA Publication Number: NHI-01-001.

State Departments of Transportation (2009). Bridge Scour and Stream Instability Countermeasures Experience, Selection, and Design Guidance, Hydraulic Engineering Circular No. 23 (HEC-23), Third edition, FHWA Publication Number: NHI-09-111.

Williamson, H., and Ockenden, M. (1996). ISIS: An Instrument for Measuring Erosion Shear Stress In Situ. Estuarine, Coastal and Shelf Science, vol. 42(1), 1-18.

Appendix E

Numerical model validation and simulation results

E.1 Model validation using large-scale experimental data of Outdoor StreamLab (OSL)

As mentioned in Appendix C, in summer 2014, a series of experiments were carried out in the OSL of St. Anthony Falls Laboratory at the University of Minnesota, during which the evolution of OSL's bed morphology under live-bed and bankfull flow conditions and various longitudinal wall configurations were investigated. The OSL under bankfull flow conditions has a mean flow depth and bulk velocity of ~0.3 m and ~0.32 m/s, respectively, which obtains $Re = 95 \times 10^3$. We use the acquired data of three of these large-scale experiments runs to validate the simulation results of the model (see Table 1 of Appendix C):

a) OSL with no longitudinal wall (baseline case): Run # BL;
b) OSL with the Wall 1 configuration: Run # W1
c) OSL with Wall 2 configuration: Run # W2

In all the cases the experiments in the OSL started from a flatbed condition. After approximately 7 to 8 hours when the bed morphology and scour pattern reached quasi-equilibrium the experimental team used a point gage to measure the *instantaneous* bed elevation of the OSL along 7 cross-sections in the test meander (pool zone) of the OSL. We note that these bed elevation measurements are instantaneous and that the passage of migrating dunes may have locally influence the measured topography.

The computational grid system used in these validation simulations of the OSL consist of ~9.9 million grid nodes, which is a 1201×201×41 grid system in streamwise, spanwise, and vertical directions, respectively. Given the vertical (~0.3 (m)), spanwise (~2.5 (m)), and longitudinal (~12 (m)) dimensions of the OSL, with such grid system we have a spatial step of about 0.01 m, which is fine enough to capture most of the energetic large scale vertical structures that contribute to the sediment dynamics within the channel.

E.1.1 Numerical simulation of the baseline (BL) case: OSL with no longitudinal wall

We used the measured bathymetry of the OSL along with its measured water surface, at quasi-equilibrium, to produce the computational mesh for the coupled modeling. In Fig. 1 we show the computational mesh used in this simulation. We carried out the simulation by coupling the large-eddy simulation with the bed morphodynamics module in which both the suspended load and bed load are taken into account.

In Fig. 2 we present instantaneous snapshots of the velocity and vorticity fields in the OSL at the free-surface. The bed morphology of the OSL in its pool zone is constantly evolving. In Fig. 3 (A) we plot the simulated and time-averaged bed bathymetry of the OSL (baseline case). We time-averaged the simulated bed elevation data to filter out the migrating dunes. This way we can compare the simulated bed profiles with measured values. To show the effect of migrating

bedforms on the time-averaged bed profiles we compute the *RMS* of the bed fluctuations. The simulated bed morphology in Fig. 3 (A) shows a general pattern of scour and deposition in a meander bend with point bar near the inner bend, while a deep scour region near the outer bend of the meander.

Before presenting the quantitative comparisons, we in Fig. 4, we show the initial bed profiles with which we started the simulations as well as the experimental campaign in the OSL. The 7 cross-sections in this figure are taken from the same cross-sections shown in Fig. 3. Finally, in Fig. 5 we show the comparison between measured and simulated bed elevations along the six cross-sections (Fig. 3). We note that a major discrepancy can be seen for the first two cross-sections (*OSL-BL-1* and *OSL-BL-2*). The reason for such discrepancies can be attributed to the fact that the inlet boundary condition at the beginning of the pool zone of the OSL was unknown. Instead we feed the sediment material at the free-surface at a location about 10 m upstream of the pool zone. The sediments are numerically traced and enter the pool zone. The process through which these bed load sediments enter the pool zone (where we start simulating the bed morphodynamics) is unknown and thus we do not prescribe a deterministic inlet boundary condition for the bedload sediment at the beginning of the pool zone. Such uncertainty in the inlet boundary condition for the bedload sediment significantly contributes to the discrepancy we see in Fig. 5 for the two first cross-sections.

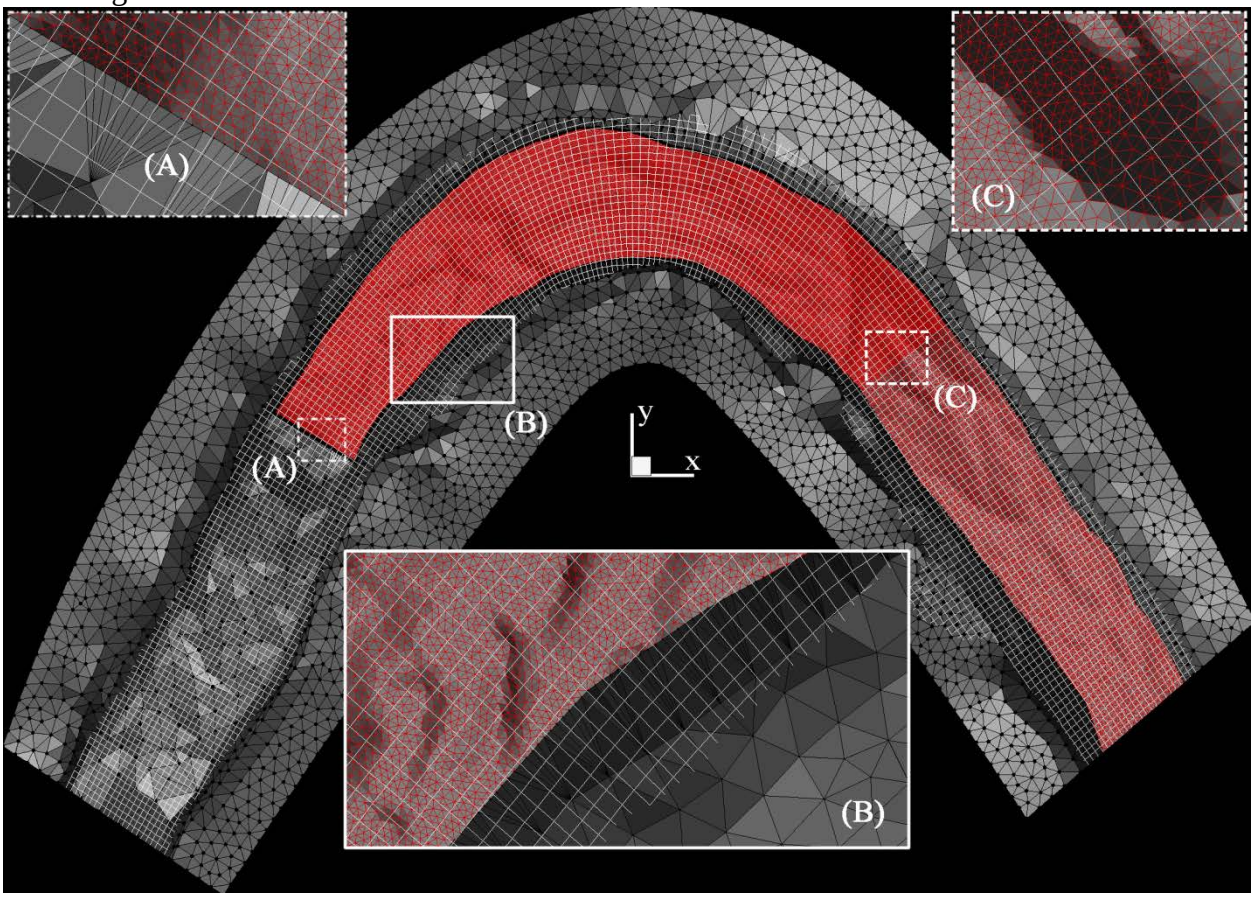

Figure 1. Computational mesh for the baseline case of the OSL. Bed morphodynamics is solved on the unstructured red triangular mesh, the white structured mesh is the background mesh on

which the flow field is solved. The white square background mesh is skipped by a factor of 5 for the sake of visual clarity. The black-dots are the points surveyed in the OSL to produce the geometry of the OSL. Flow is from left to right. The grid resolution is almost uniform in all directions and is about 1.5 cm.

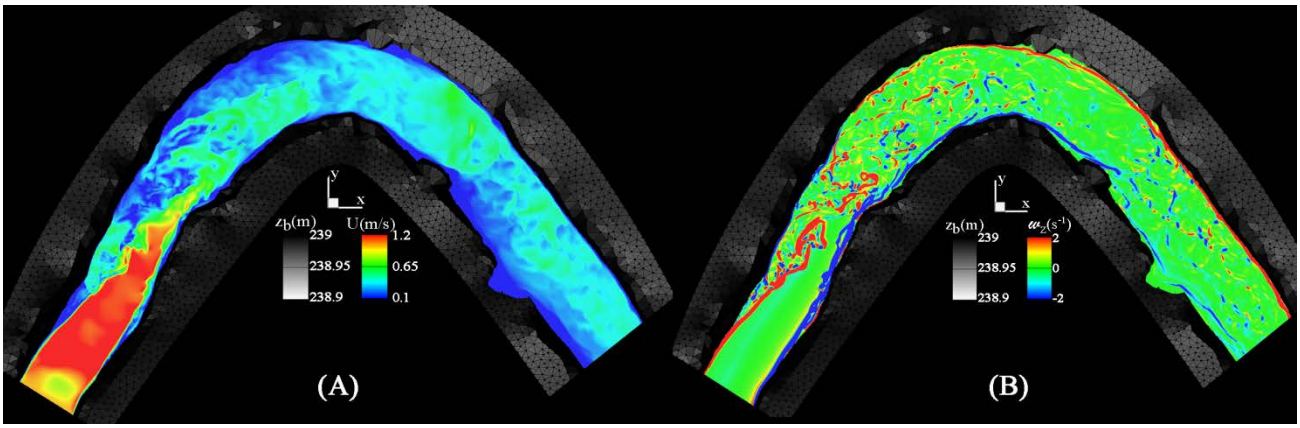

Figure 2. Simulated instantaneous velocity (A) and vorticity (B) fields for the baseline case of the OSL. (A) Contours of velocity magnitude at the free-surface. (B) Contours of out-of-plane vorticity at the free-surface. Flow is from left to right.

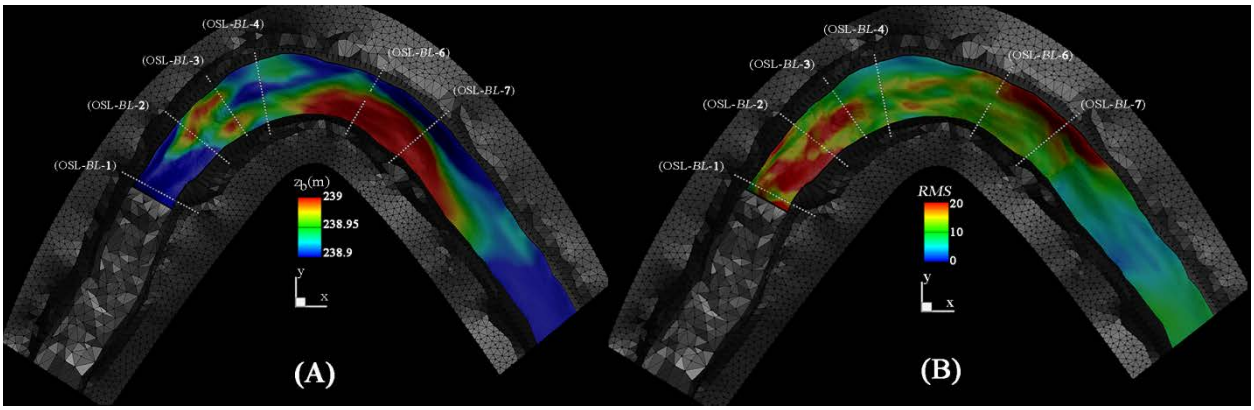

Figure 3. Simulated time-averaged bed elevation (A) and *RMS* percentage of the bed fluctuations for the baseline case of the OSL. The simulated and measured bed elevations will be quantitatively compared along the six cross sections shown in (A) and (B): "*OSL-BL-1*" to "*7*". "BL" stands for the baseline case. Flow is from left to right.

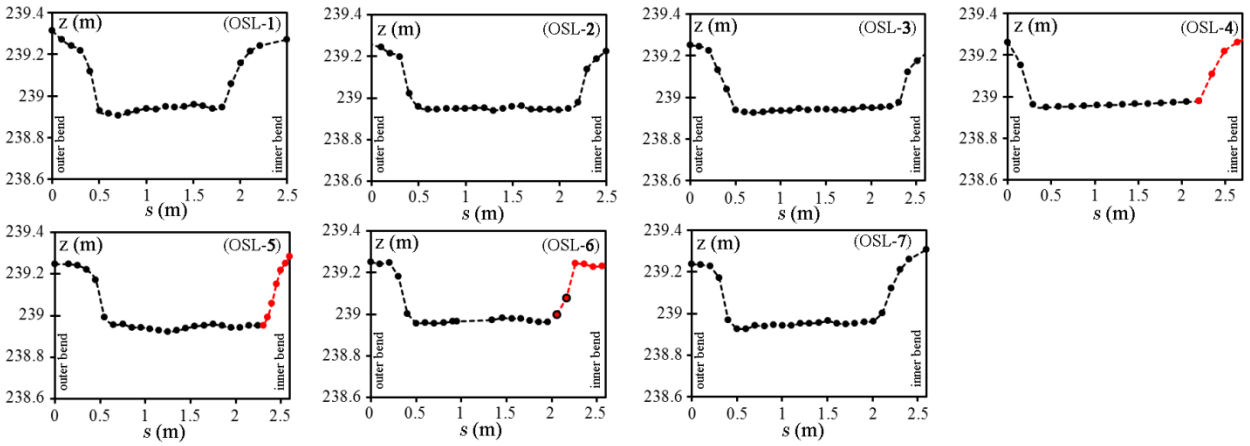

Figure 4: Initial bed elevations (flatbed profiles) at the beginning of the simulations and experiments (black dotted lines). The cross-sections are taken from OSL-1 to 7 in Fig. 3. Red dots and hollow black-circles in OSL-4, OSL-5 and OSL-6 correspond to other test cases (Wall 1 and Wall 2) which will be presented in next sections.

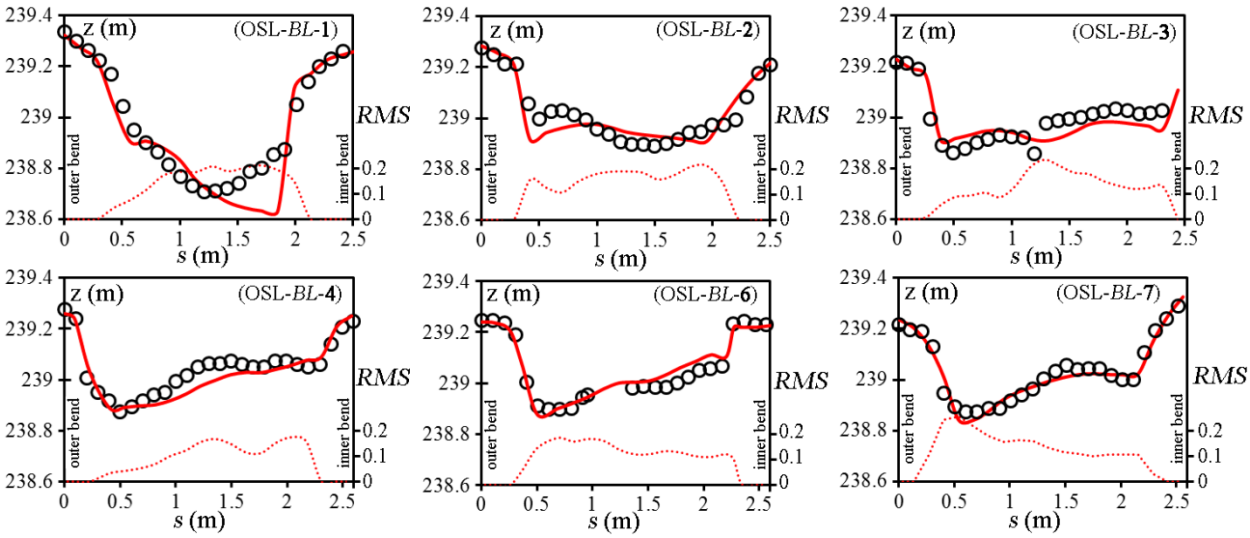

Figure 5. Simulated (time-averaged) (red lines) and measured (instantaneous) (black circles) bed elevations (z) along cross-sections OSL-BL-1 to 7 in Fig. 3. The vertical axis on the right represents the *RMS* of bed fluctuations (red dotted-line) for the simulated bed morphology and s (in m) is the vector along each cross-section. Note that since the stream banks are almost stationary, the *RMS* of fluctuation near the stream banks approaches zero. While in the mid-channel where migrating bedforms are present in the simulations the *RMS* value varies between 0 and 0.2.

At distances farther downstream of the inlet section where the dominant processes are the sediment transport due to the helical flows in the meander bend, the coupled flow-morphodynamics model has done a better job and predicted bed profiles are in great agreement with the measured ones. We note, however, that some of the discrepancies between the measured

and computed values can be attributed to the transient nature of the measurements and passage of migrating bedforms, which in times can lead to higher or lower bed elevations. But overall the agreement between the measurements and simulated results is reasonably good with a mean error of 9 percent.

E.1.2 Numerical simulation of the W1 test case: OSL with a longitudinal wall 1

For this test case, a longitudinal wall was installed in the OSL and after flattening the bed bathymetry the bankfull flow experiment was run until the bed bathymetry reached its quasi-equilibrium. At this point, the instantaneous bed profiles along seven cross-sections *OSL-W1-1* to *7* (Fig. 8) were measured.

We used the surveyed geometry of the OSL in this case to produce the computational mesh (see Fig. 6) and simulated the coupled flow and bed morphodynamics of the test case. We plot in Fig. 7 the instantaneous velocity and vorticity fields of the *OSL-W1* test case at the free-surface. The simulated bed morphodynamics for this test case is also shown in Fig. 8 where we plot a snapshot of the simulated bed morphology (Fig. 8 (A)) along with the time-averaged bed bathymetry (Fig. 8 (B)). The simulated bedforms migrate and thus the bed bathymetry continuously evolves. The time-averaged bed elevations are computed to produce a bed bathymetry that can be better compared with the measured bed profiles.

Like the baseline case in the previous section, we note that the initial bed profiles with which we started the simulations as well as the experimental campaign in the OSL are shown in Fig. 4. In Fig. 9 we compare the simulated and measured bed profiles along the seven cross-sections shown in Fig. 8. Similar to the baseline case, we observe a major discrepancy between measured and simulated bed profiles for the first two cross-sections (*OSL-W1-1* and *OSL-W1-2*). The reason for such discrepancies can be attributed to the uncertainty in the inlet boundary condition for the bed load sediment transport at the interface between the riffle and pool zones of the OSL. Given the fact that the measured bed profiles in Fig. 9 are instantaneous while the simulated results are time-averaged, the agreement observed in Fig. 9 for the cross-sections *OSL-W1-3* to *7* is reasonably good and the mean error percentage is about 10 percent. Additionally, as one can see in this figure, the generic scour and deposition areas are well predicted.

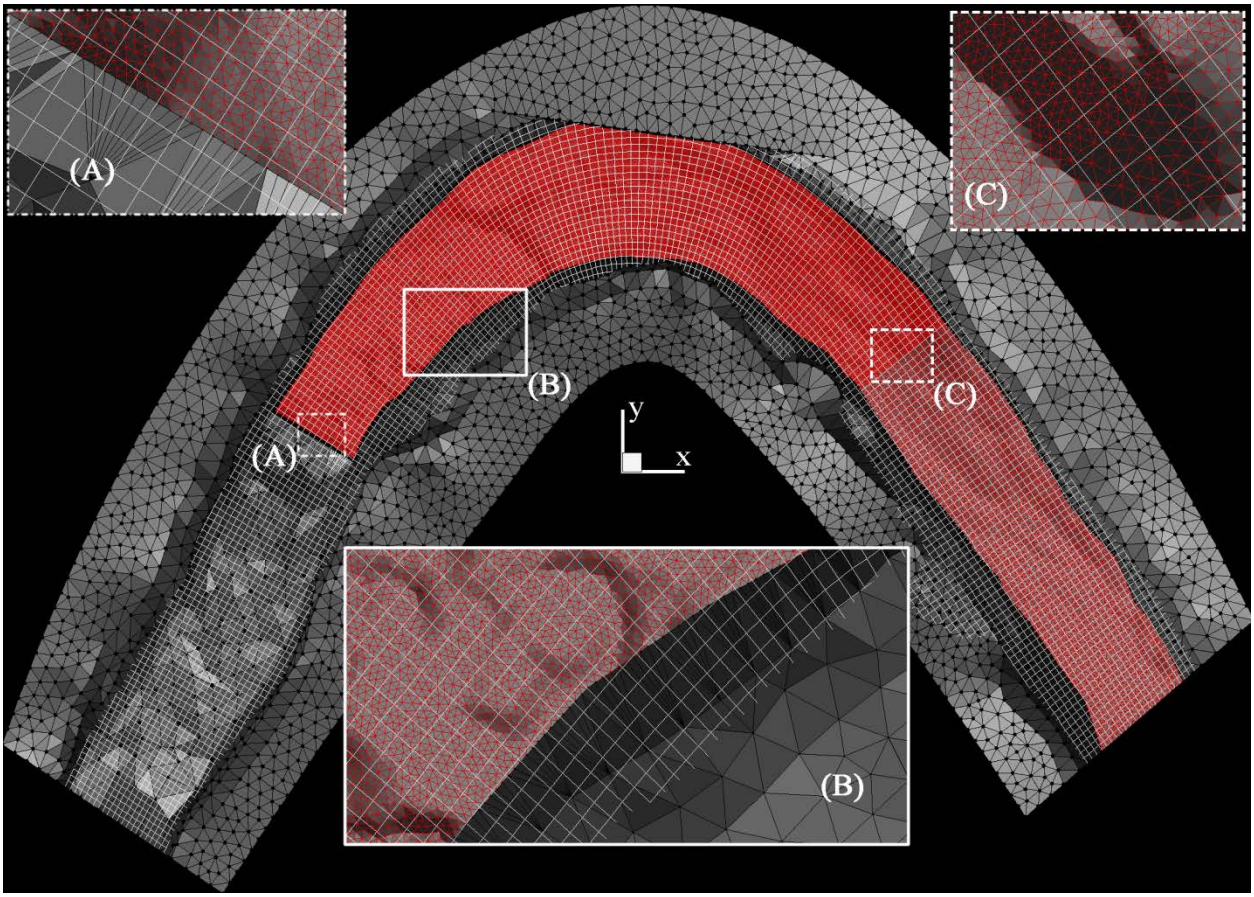

Figure 6. Computational mesh for the OSL with a longitudinal wall at the outer bend of the meander (*OSL-W1* test case). Bed morphodynamics is solved on the unstructured red triangular mesh, the white structured mesh is the background mesh on which the flow field is solved. The white square background mesh is skipped by a factor of 5 for the sake of visual clarity. The black-dots are the points surveyed in the OSL to produce the geometry of the OSL. Flow is from left to right. The grid resolution is almost uniform in all directions and is about 1.5 cm.

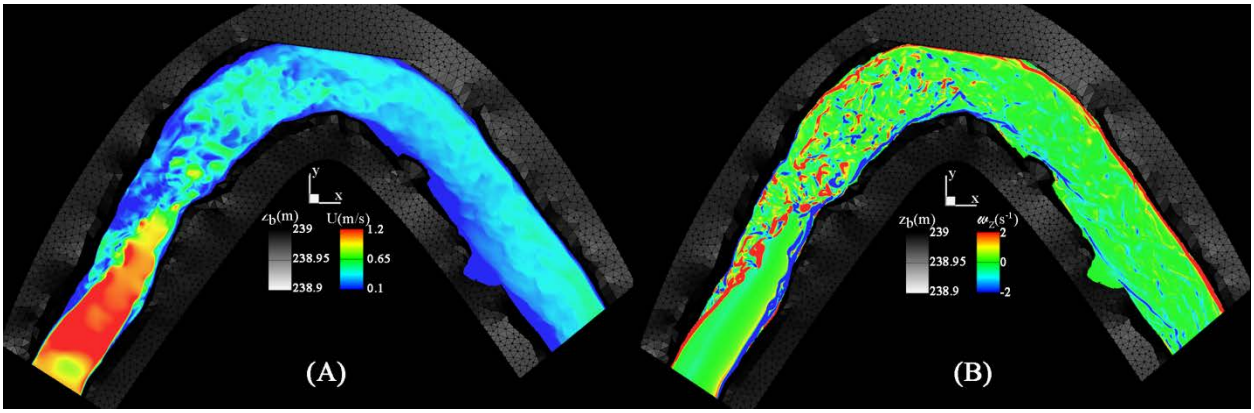

Figure 7. Simulated instantaneous velocity (A) and vorticity (B) fields for the W1 test case of the OSL. (A) Contours of velocity magnitude at the free-surface. (B) Contours of out-of-plane vorticity at the free-surface. Flow is from left to right.

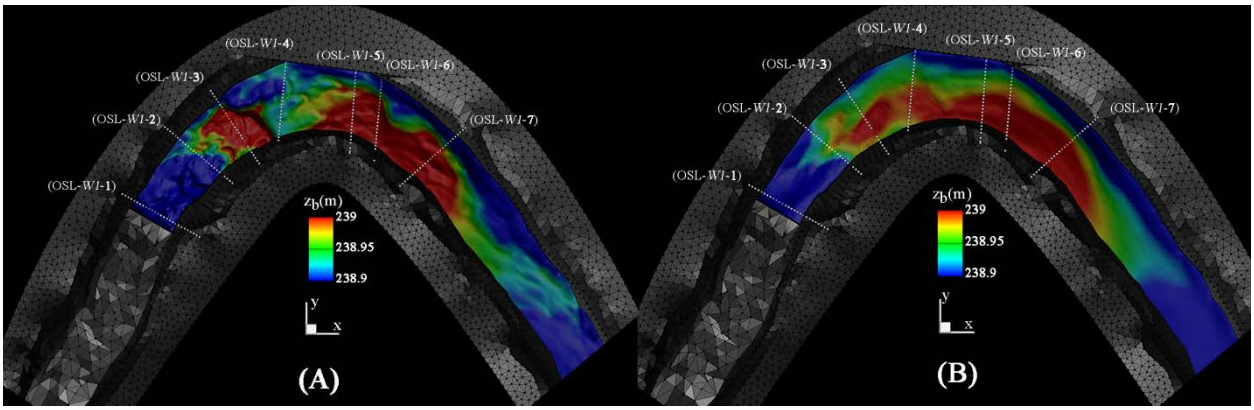

Figure 8. Simulated contours of bed elevations: (A) instantaneous morphology at t ~5 hours; and (B) time-averaged for the *W1* test case of the OSL. The simulated and measured bed elevations will be quantitatively compared along the seven cross sections shown in (A) and (B): "*OSL-W1-1*" to "*7*". "W1" stands for the wall 1 case. Flow is from left to right.

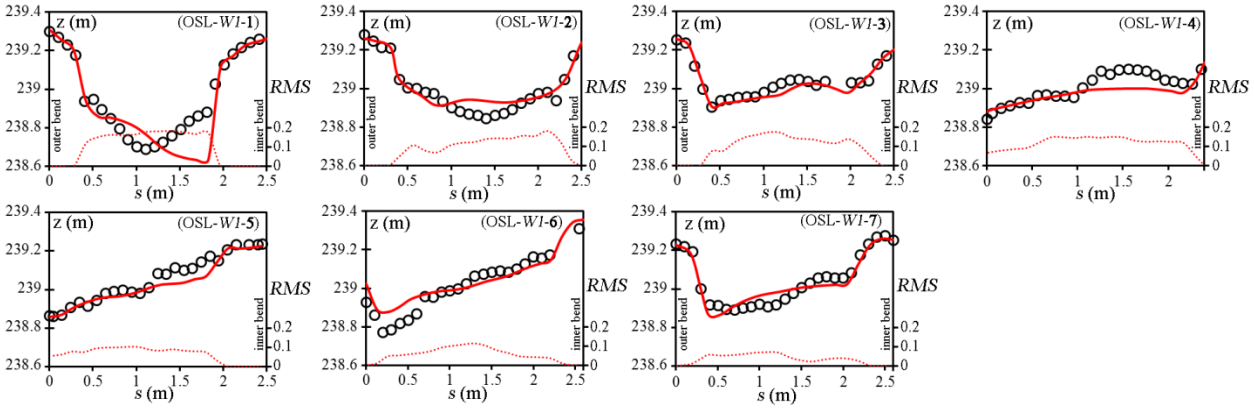

Figure 9. Simulated (time-averaged) (red lines) and measured (instantaneous) (black circles) bed elevations (z) along cross-sections *OSL-W1-1* to *7* in Fig. 8. The vertical axis on the right represents the *RMS* of bed fluctuations (red dotted-line) for the simulated bed morphology and s (in m) is the vector along each cross-section. Note that since the stream banks are almost stationary, the *RMS* of fluctuation near the stream banks approaches zero. While in the mid-channel where migrating bedforms are present in the simulations the *RMS* value varies between 0 and 0.2.

E.1.3. Numerical simulation of the W2 test case: OSL with a longitudinal wall 2

As the last validation test case in this section we present the coupled simulation results for an experiment in the OSL in which a different longitudinal wall was installed. The flow and sediment characteristics used in this experiment and the corresponding simulation were the same as other two test cases. The only difference is the orientation and location of the longitudinal wall in the OSL, which is shown in Fig. 10.

In Fig. 11 we plot the simulated flow and bed morphodynamics of the *OSL-W2* test case. As shown in Fig. 11 (B), the numerically captured bedforms migrate through the OSL and lead to significant fluctuations in bed elevation. The computed time-averaged bed elevations in Fig. 11 (C) are used to compare the simulations with the point measurements data for the bed profiles along the seven cross-sections in Fig. 12.
Notwithstanding the discrepancies between the measurements and simulations results for the bed profiles in Fig. 12 at the first two cross sections, the bed profiles are predicted with a mean error of about 8 percent.
Given the level of accuracy in these bed morphology simulations, we will employ the present coupled flow and morphodynamics model to perform numerous numerical experiments to quantify the scour depths adjacent to various longitudinal walls in meandering and straight rivers.

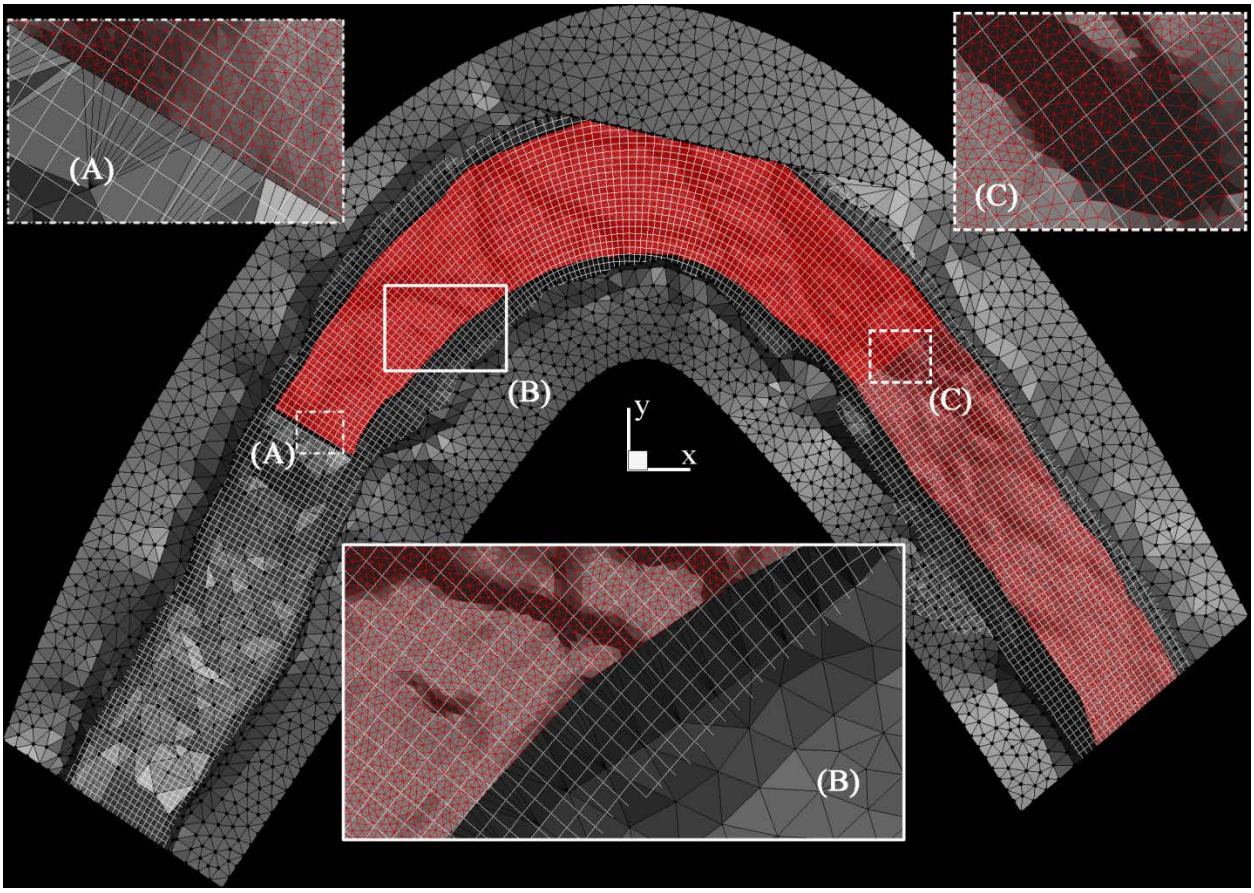

Figure 10. Computational mesh for the OSL with a longitudinal wall at the outer bend of the meander (OSL-W2 test case). Bed morphodynamics is solved on the unstructured red triangular mesh, the white structured mesh is the background mesh on which the flow field is solved. The white square background mesh is skipped by a factor of 5 for the sake of visual clarity. The black-dots are the points surveyed in the OSL to produce the geometry of the OSL. Flow is from left to right. The grid resolution is almost uniform in all directions and is about 1.5 cm.

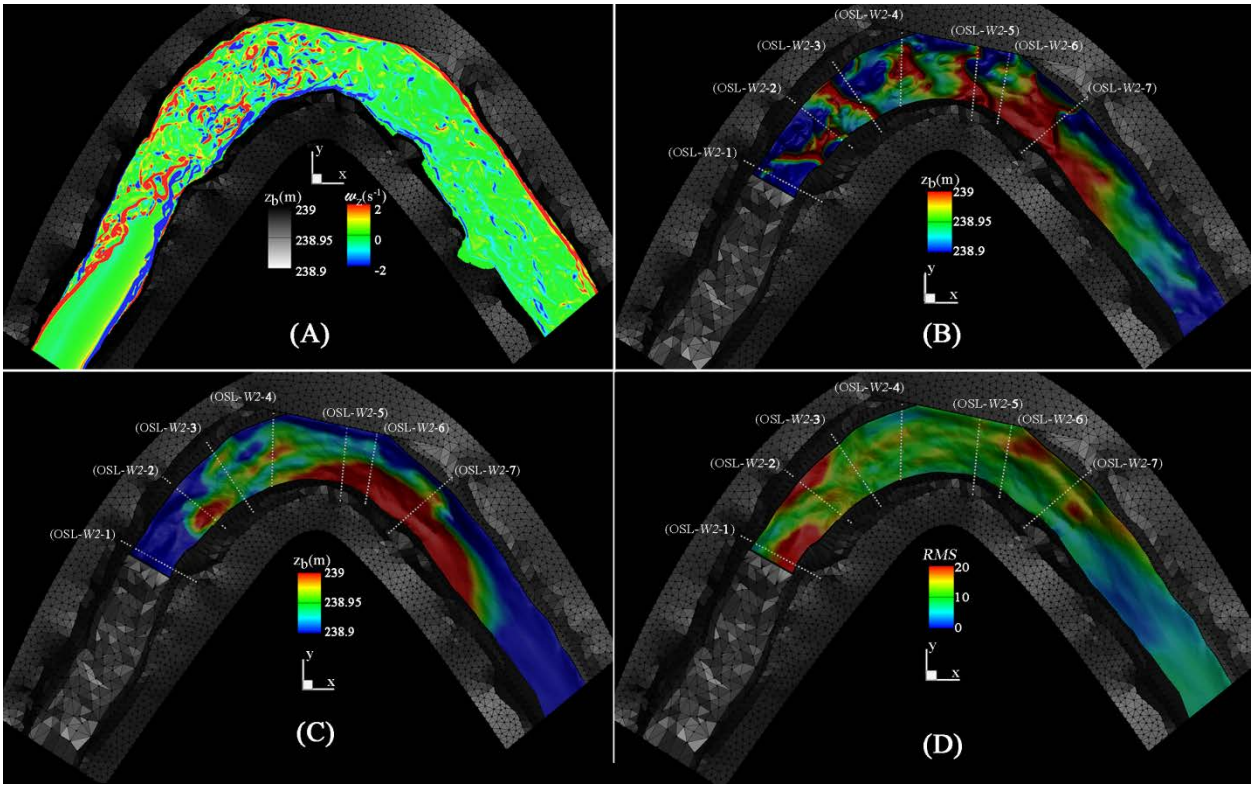

Figure 11. Simulated results of the coupled flow and bed morphodynamics for the OSL wall 2 (*OSL-W2*) test case: (A) instantaneous vorticity field showing the contours of out-of-plane vorticity at the free-surface; (B) a snapshot of the simulated bed morphology illustrating the migration of numerically captured bedforms in contours of bed elevation; (C) color map of the time-averaged bed elevation; and (D) computed *RMS* (percent) of bed fluctuations. Flow is from left to right.

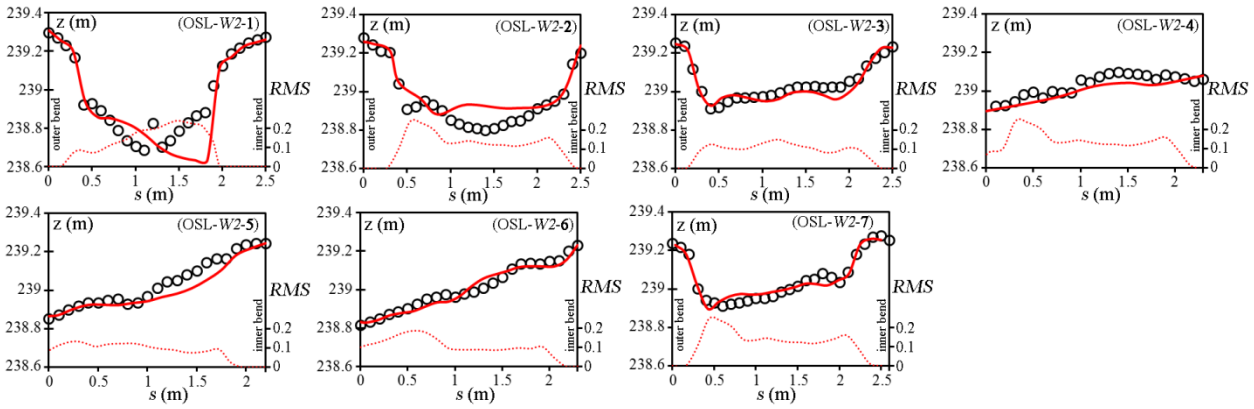

Figure 12. Simulated (time-averaged) (red lines) and measured (instantaneous) (black circles) bed elevations (z) along cross-sections *OSL-W2-1* to *7* in Fig. 11 (B-D). The vertical axis on the right represents the *RMS* of bed fluctuations (red dotted-line) for the simulated bed morphology and s (in m) is the vector along each cross-section. Note that since the stream banks are almost stationary, the *RMS* of fluctuation near the stream banks approaches zero. While in the mid-channel where migrating bedforms are present in the simulations the *RMS* value varies around 0.1 with a maximum of ~0.2.

We note that the computed *RMS* can be a good representative for the amplitude of the numerically captured bedforms. For all cases in this validation study including baseline, W1, and W2 cases the *RMS* near the mid-channel varies between 0.1± 0.05 with a maximum of about 0.2 (see Figs. 5, 9, and 12). If this is true, then the amplitudes of the simulated bedforms should vary between 0.05 m to 0.15m with a maximum of 0.2 m. Numerically captured bedforms in Figs. 8(A) and 11(B) show that the simulated bedforms are about 0.15 m high, which verifies this hypothesis.

E.2 Model validation using small-scale experimental data

As mentioned in Appendix D, a series of experiments were carried out in an indoor flume at the Lehigh University in which the clear-water scour around the upstream (sharp) edge of longitudinal wall is extensively investigated. We simulated three of these experiments to compare the numerical captured scour pattern and maximum scour depth with the measured data. The three test cases are as follows (for details see Table 2 in Appendix D):

(a) Small-scale experiment: Run G1 with 29^o side wall and smooth longitudinal wall (G1)

(b) Small-scale experiment: Run G2 with 29^o side wall and rough longitudinal wall (G2)

(c) Small-scale experiment: Run G5 with 35^o side wall and smooth longitudinal wall (G5)

The roughness of the longitudinal wall in (b) is 0.6 mm. The experiments start from a flatbed throughout the channel. For all of the above experimental cases ((a) to (c)), the mean flow velocity, mean flow depth, flow discharge, longitudinal bed slope, *Fr* number, and d_{50} of bed material in the experiment are 0.466 (m/s), 0.17 (m), 80 (lit/s), 0.0025, 0.361, and 3.6 (mm), respectively (see Table 2 of Appendix D for details of the experiments).

Starting from a flatbed condition, it takes approximately 2 hours until the scour pattern reached quasi-equilibrium. Once at quasi-equilibrium, the experimental team measured the maximum scour depth and bed profiles two lines starting from the upstream edge of the longitudinal wall in sapnwise and streamwise directions (see Appendix D for a descriptive illustration of the two directions).

E.2.1 First attempt to simulate the indoor flume via conventional bed shear stress

We employed the URANS module of the model along with the $k-\omega$ turbulence model coupled with the morphodynamics model to simulate the flow and sediment transport within the indoor flume. Since the experiment is under clear-water scour condition, we only used the bed-load module of the morphodyanmics mode. The computational grid system used for this validation study consist of ~2.7 million grid nodes, which is a 701×133×33 grid system in streamwise, spanwise, and vertical directions, respectively. Given the vertical (~0.2 (m)), spanwise (0.85 (m) plus 0.35 (m) of sloped side bank), and longitudinal (~10 (m)) dimensions of the simulated channel. Thus, the spatial resolution of the employed grid system is about 0.01 m, which is fine enough to capture most of the energetic large scale vertical structures that contribute to the sediment dynamics within the channel.

Despite the fine resolution of the simulations, our simulation results for all three cases with the current conventional methods used in our turbulence model and morphodynamics module showed no movement of sediment in the indoor flume. This can be seen in Fig. 13, where the bed elevation change after several hours of physical time of the simulations is zero everywhere. Ostensibly, the simulated flow fields in these simulations obtain bed shear stresses that are well below the threshold values for the sediment particles on the channel bed. However, we know from the experiment that the bed should be destabilized. The reason for the failure of the coupled model in capturing the bed change in these cases can be attributed to the incapability of the URANS models in predicting the vertical structures that form near the upstream edge of the longitudinal wall. Such energetic vertical flow structures created a zone of high turbulent kinetic energy with fluctuating shear stresses that exceed the threshold of the motion of the sediment particle in the experiment.

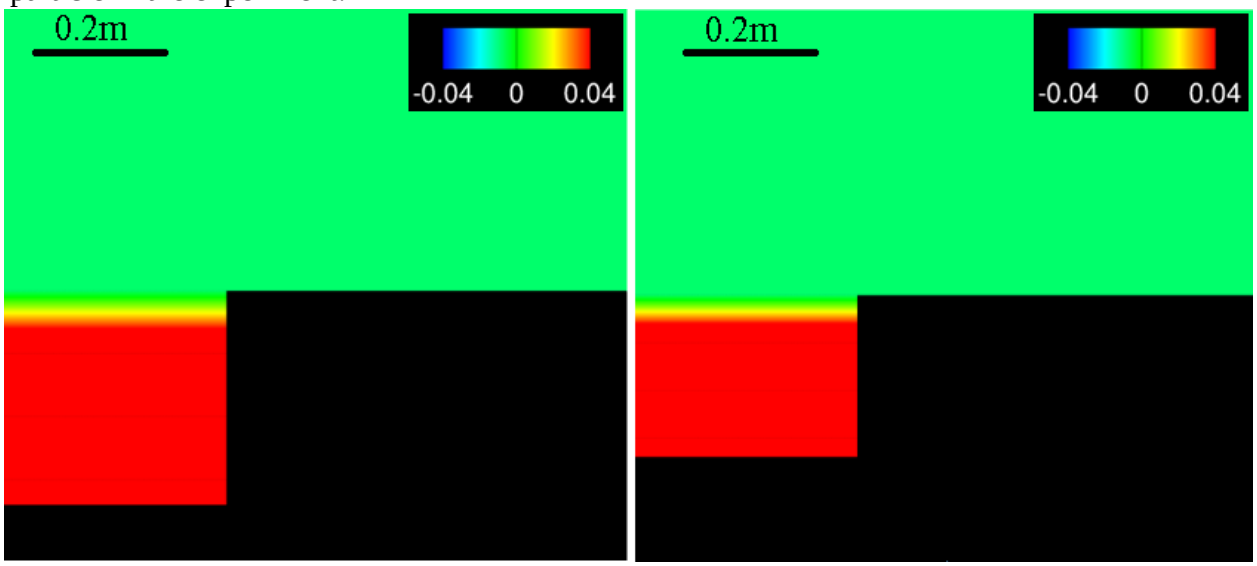

Figure 13: Simulated bed elevation of the indoor flume for the two cases of Run G1 (left) and G5 (right) from top view. Part of the flumes with the longitudinal walls and the sloping side bank are shown, while part of the flume on the left bank that has no longitudinal wall and the side bank is vertical is not shown in the pictures. The two pictures are focused on the region near the upstream edge of the longitudinal wall and flow is from left to right.

E.2.2 Development of a physics-based relationship for effective bed shear stress

In order to address the shortcoming of the turbulence model and to be able to capture the scour pattern near the upstream edge of the longitudinal wall, we developed and employed a physics-based ad-hook relationship for the effective bed-shear stress. The effective bed shear stress (τ_e) can be expressed as follows:

$$\tau_e = \tau_0 + \tau_a \tag{1}$$

where τ_0 is the conventional bed shear stress obtained from wall model based on the velocity field that is computed from URANS and the $k-\omega$ turbulence model and τ_a is the additional bed shear stress due to the presence of high-energy votical structures at the leading edge of bluff bodies, e.g. the upstream edge of the longitudinal wall in this study. The additional bed shear stress is a function of turbulent kinetic energy ($\hat{k}$) in the water column and the relative strength of vertical component of the velocity ($\widehat{w}$) on the local bed cell (Jia et al., 2002 and Khosronejad et al., 2012). Therefore, the additional bed shear stress in an ad-hook manner can be written as follows:

$$\tau_a = \frac{5}{24} c_s \, \rho \, \|\widehat{w}\| \, \hat{k} \tag{2}$$

where ρ is the density of water, c_s is a constant (=1.5 in this work). $\hat{k}$ is usually obtained by integrating the equation of mixing length of the eddy viscosity model over the water depth (see, e.g., Jia et al., 2002), however, because we solve the transport equation of turbulent kinetic energy, we already have the value of turbulent kinetic energy in water depth. $\hat{k}$ in this work is then computed by averaging the value of turbulent kinetic energy over half depth above each local bed cell. $\widehat{w}$, on the other hand, is computed using the velocity field on the bed surface as follows:

$$\widehat{w} = \frac{\widetilde{w}}{\sqrt{u^2+v^2+\widetilde{w}^2}} \tag{3}$$

where u and v are the streamwise and spanwise vertical vectors, respectively, at the leading edge of the bed-load layer obtained using wall-model approach (see Khosronejad et al. 2011, 2012,

2013, 2014). The two velocity components of u and v are parallel to the bed surface, while $\widetilde{w}$ is the mean velocity perpendicular to the bed surface computed as follows:

$$\widetilde{w} = \frac{\bar{w} - u\,\frac{\partial z}{\partial x} - v\,\frac{\partial z}{\partial y}}{\sqrt{\frac{\partial z}{\partial x}\,\frac{\partial z}{\partial x} + \frac{\partial z}{\partial y}\,\frac{\partial z}{\partial y} + 1}} \tag{4}$$

where *x*, *y*, *z* are the streamwise, spanwise, and vertical directions and *z* represents the bed elevation of the bed surface, as well. $\bar{w}$ is the vertical component of flow velocity, which averaged over lower half of the flow depth. At distances away from a bluff body, or a hydraulic structure in general, the $\widehat{w}$ term rapidly approaches zero and thus the additional bed shear stress (Eq. (2)) becomes zero. In the meantime, due to such trend, the effective bed shear stress in Eq. (1) becomes equal to τ_0 .

E.2.3 Numerical simulation of Indoor flume with newly developed effective bed shear stress approach

Using the effective bed shear stress relationship in Eq. 1, we simulated the three test cases: G1, G2, and G5. A similar grid system to the one in our first attempt is employed for these simulations. The sediment dynamics in all cases takes about 2 hours of physical time to get to quasi-equilibrium.

As shown in Fig. 14, use of the newly developed bed shear stress resulted in scour patterns near the upstream edge of the longitudinal walls. In Fig. 14 we plot the time-averaged bed elevation of the channel near the upstream edge of the longitudinal wall, where nearly all of the sediment transport takes place. Time-averaging of the bed elevation is done after the bed reached the quasi-equilibrium.

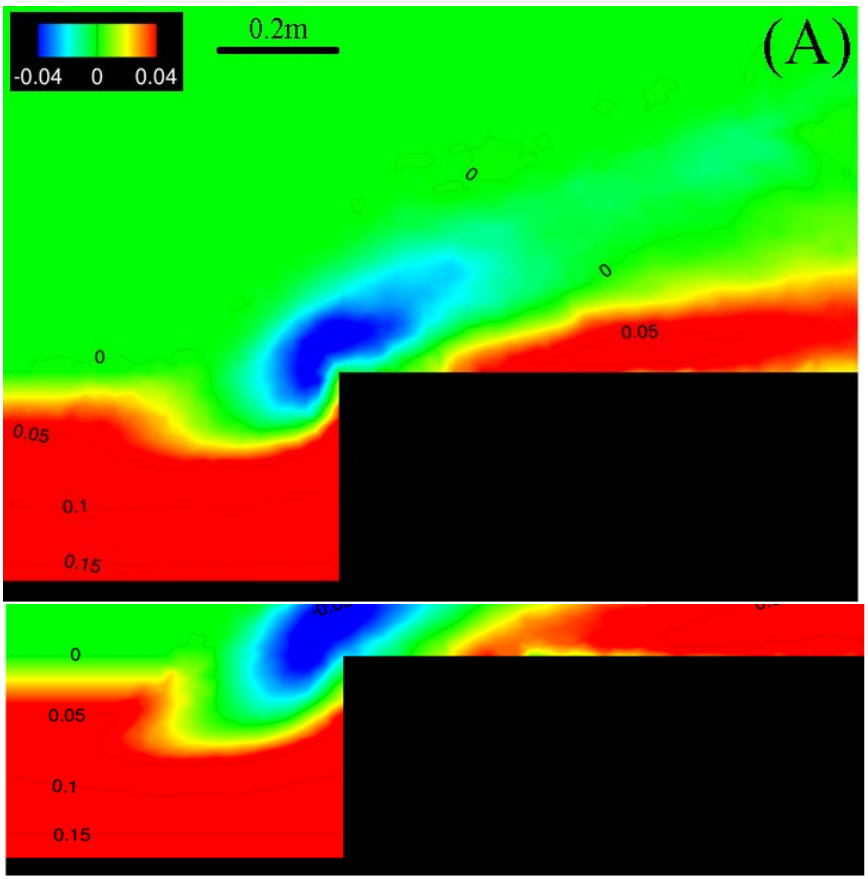

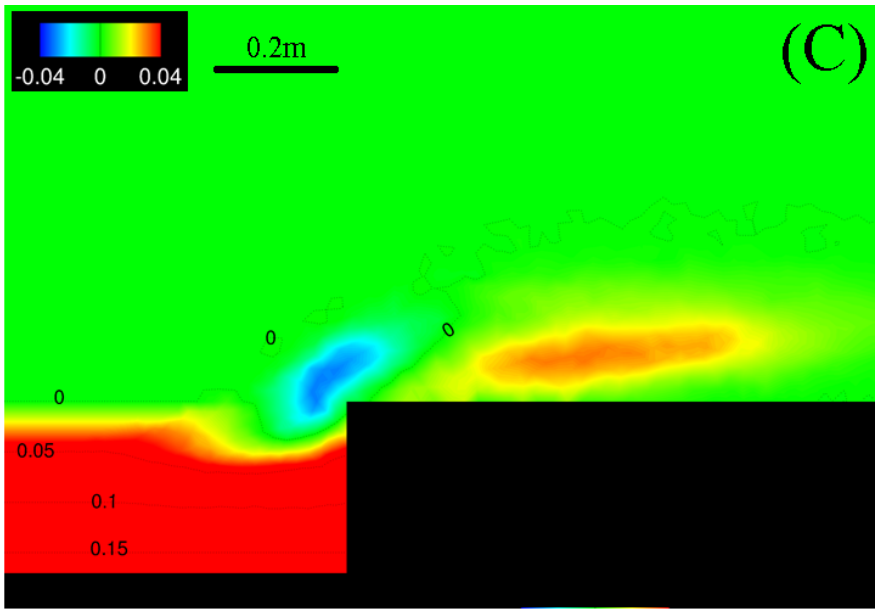

Figure 14. Simulated bed elevation (time-averaged) of the indoor flume for the Run: (A) G1, (B) G2, and (C) G5 from top view. Parts of the flumes bed surface where sediment dynamic takes place are shown. Therefore, pictures are focused on the region near the upstream edge of the longitudinal wall and flow is from left to right. The magnitude of the computed maximum sour depth near the upstream edge of the longitudinal walls for (A) to (C) is 0.042 (m), 0.053 (m), and 0.030 (m), respectively. Contour lines are in meters.

In Table 1 we show a comparison between the measured and computed values for the maximum scour depth near the upstream edge of the longitudinal wall. An important factor in these simulations is the activation of avalanche model in the coupled simulations. As we shown in Fig. 15, lack of an avalanche model can results in a significantly different scour pattern. Due to the mobile bank slope upstream of the wall, the avalanche model very often becomes activated to

account for the slopes that constantly exceed the angle of repose of the sediment material. The avalanche model used in these simulations is developed based on the mass balance of sediment by distributing the mass of avalanched sediment among the three neighboring cells. The higher the frequency and the larger the magnitude of sediment movement in avalanche events, the more difficult it is to successfully simulate the physics of the phenomena. For the higher bank slope of 35, it is therefore more difficult to accurately simulate such avalanched. This is evident in Table 1 where the maximum scour depths for the 28 degree bank cases are predicted with a paramount accuracy, while for the 35 degree bank slope the maximum scour depth is over estimated. However, overall, the maximum scour depth in all three cases is reasonable good.
In order to show the accuracy of the coupled model is predicting the transient development of the scour patterns, in Figs. 16 to 18, we plot the simulated versus measured bed profile for the three test cases along the spanwise (y) and streamwise (x) direction at different instants in time.

Table 1. Comparison of the measured and simulated maximum scour depth (|S|) near the upstream edge of the longitudinal walls in the indoor flume experiments of Lehigh University. For details of flow and sediment characteristics of Runs G1, G2, and G5 see Table 2 of Appendix D.

Run #	**Bank angle (^{o})**	**Roughness**	**Measured |S| (m)**	**Computed |S| (m)**
G1	28	smooth	0.053	0.052
G2	28	rough	0.42	0.043
G5	35	smooth	0.019	0.030

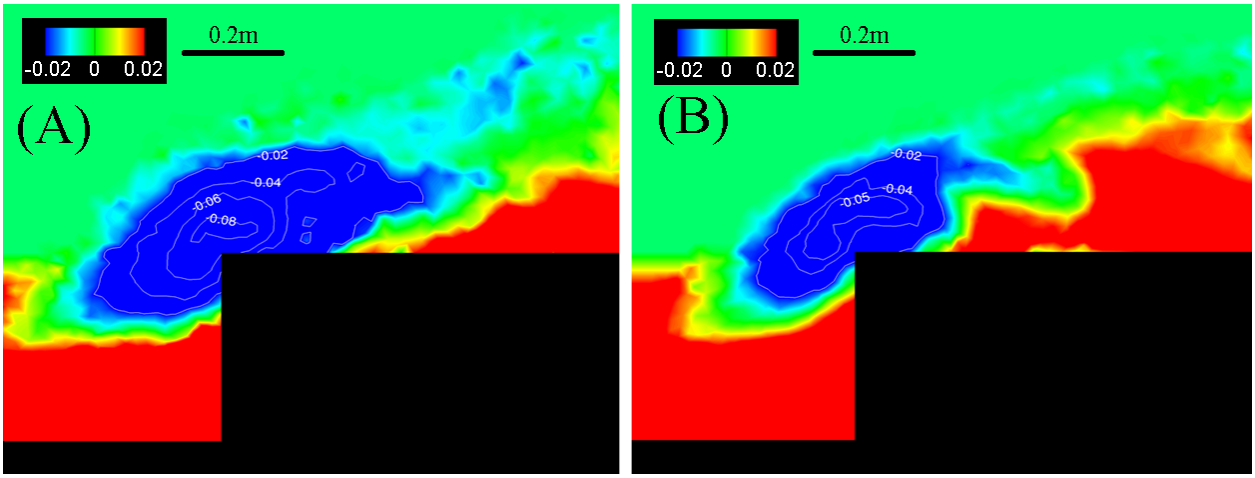

Figure 15. Simulated bed elevation (instantaneous) of the indoor flume for the Run G1without (A) and with (B) avalanche model. Parts of the flumes bed surface where sediment dynamic takes place are shown. Therefore, pictures are focused on the region near the upstream edge of the longitudinal wall and flow is from left to right. The magnitude of the computed maximum instantaneous sour depth near the upstream edge of the longitudinal walls without avalanche

model (A) exceeds 0.08 m, while for the case with avalanche model (B) it is about 0.05 m. Contour lines are in meters.

As shown in Figs. 16 to 18, the instantaneously captured bed elevation profiles are in good agreement with those that are observed experimentally. To have a quantitative evaluation of the coupled model's accuracy in predicting these profiles, we computed the mean absolute error of the simulations based on the data presented in Figs. 16 to 18. The calculated error percentage is about 5.2 percent, which--consideration the complexity of the scour near the sloped side bank of the indoor flume--is reasonably small.

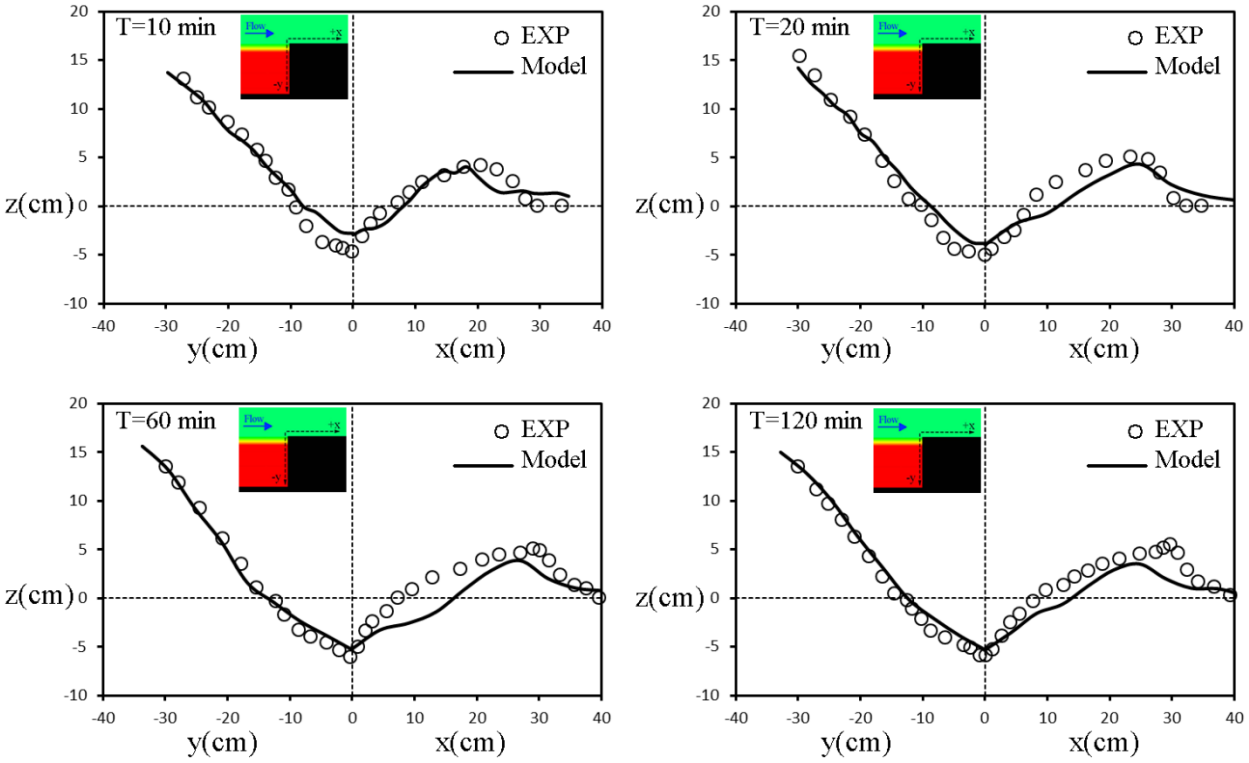

Figure 16. Simulated (black-lines) and measure (circles) bed elevation profiles along x and y directions at different instants in time for the tests case G1.

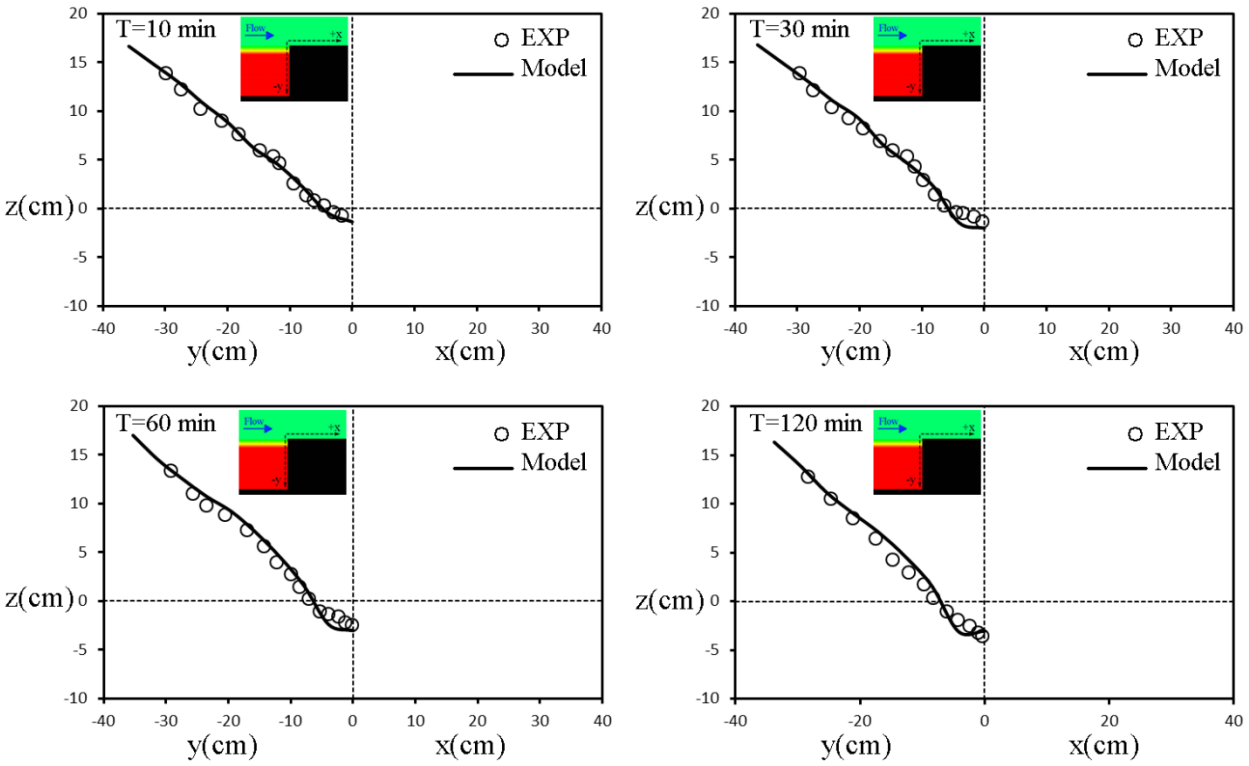

Figure 17. Simulated (black-lines) and measure (circles) bed elevation profiles along x and y directions at different instants in time for the tests case G2. Because of lack of visibility (as the sand papers were installed for roughening the wall) the bed profile data along x direction are not probed and thus no comparison is made for that region.

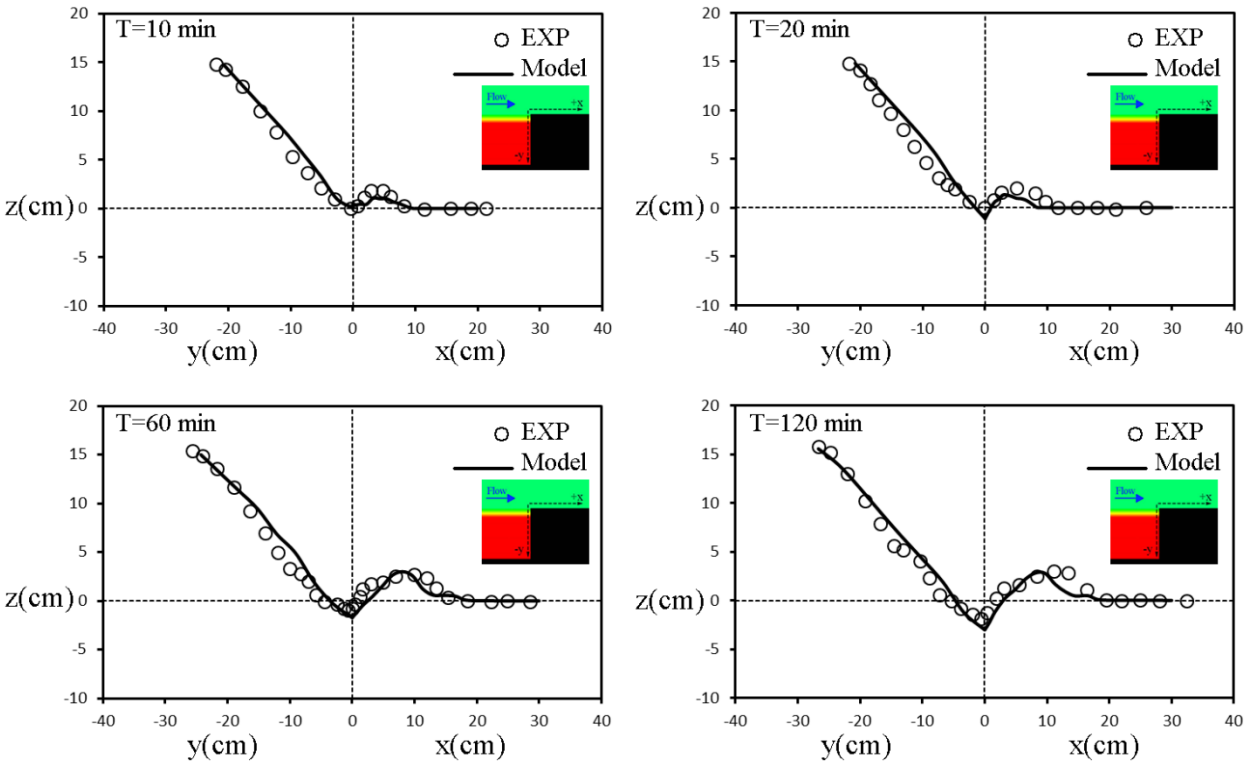

Figure 18. Simulated (black-lines) and measure (circles) bed elevation profiles along x and y directions at different instants in time for the tests case G5.

In this section, in addition to validating the coupled modeling approach, we performed two separate simulations to evaluate the effect of two streamlined edges on the scour pattern near the upstream edge of the longitudinal walls. Based on the results of numerical and laboratory experiments on scour pattern around the sharp-edges, we hypothesize that use of stream-lined edges will lead to formation of less energetic vertical structures and consequently induction of less erosive forces, which will eventually result in smaller scour depth. To test this hypothesis, we simulated two test cases that in terms of flow, sediment, and channel characteristics are the same as G5. These two new test cases, however, have streamlined edges.

The first simulated hypothetical case (see Fig. 19 (A)) has an edge of quarter-circle with a radius that is equal to the mean-flow depth (=0.17m). The second case, on the other hand, has an edge that is tilted to, instead of being perpendicular to the mean-flow direction; make an angle of ~60 ^{o} with the mean-flow direction (see Fig. 19 (B)).

The two hypothetical cases are simulated and the time-averaged results for the bed elevation are shown in Fig. 19. As shown in Fig. 19, streamlining of the edge makes a significant difference in the magnitude of the maximum scour depth near the edge. More specifically, for the quarter-circle edge (Fig. 19 (A)) the maximum scour depth after time-averaging is about 0.008 (m), while for the other case the value is about 0.011 (m), which means 73 and 63 percent reduction in maximum scour depth, respectively, when compared with the baseline case of G5 that has a sharp-edge perpendicular to the mean-flow direction.

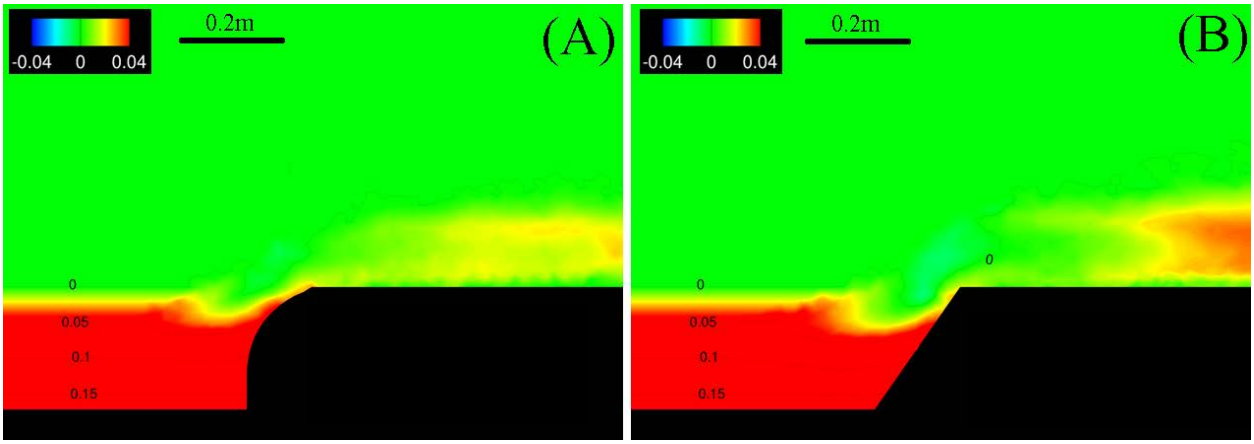

Figure 19. Simulated (time-averaged) scour patterns test case G5 with streamlined upstream edges: (A) quarter-circular edge and (B) tilted edge with and angle of 60^o with the mean-flow direction. Flow is from left to right and contour lines are in meters.

E.3 Numerical simulations of meandering rivers with longitudinal walls

In this section we present our simulation results for the four representative field-scale meandering and straight rivers. Building on the work completed for NCHRP 24-33, where two representative channels were selected as a typical meandering sand channel (S_m) and a typical meandering gravel channel (G_m) based on a range of measured field variables, we will include these virtual channels in our analysis. Additionally, because scour processes are expected to be different in meandering and straight channels (S_s and G_s for S and G rivers, while sub-s' stand for "straight" channels) two additional straight reach virtual channels will be used with similar characteristics to the meandering channels in terms of width, depth, slope, and discharge. Table 2 details the proposed channel characteristics for the four virtual channels to be used in the simulations.

The validated model (see section E.1 and E.2 for validation studies) is applied to systematically investigate the maximum scour depth in the vicinity of different longitudinal wall structures. Parameters such as the installation angle, sinuosity of rivers, sediment properties, flow condition, etc., are systematically investigated using the coupled hydro-morphodynamic module of VFS-Rivers in URANS mode (with $k-\omega$ turbulence model). More than 32 different cases, each using grids with 2-3 million nodes and simulating up to 3 months of sediment transport in physical time to reach quasi-equilibrium are completed over a period of 6 calendar months using SAFL's 2400-core computer cluster.

We base our systematic investigation of the factors influencing the maximum scour depth in the vicinity of the longitudinal walls on the following hypothesizes:

1- Geometrical and flow field characteristics of the rivers affect the scour pattern and the maximum scour depth in the vicinity of the longitudinal walls;

Table 2: Characteristics of the four stream channels chosen to install the longitudinal wall on their side bank in order to investigate the couple flow and scour conditions at the base of the longitudinal structure. All channels are chosen to be at their bankful flow conditions. In this table, d_{50} is median grain size of sediment material (mm), B is channel width (m), Q is flow discharge (m3/s), h is flow depth (m), S_0 is bed slope, s is sinuosity, and λ_m is wave length of meander (m).

Stream	d_{50}	**B**	**Q**	h	S_0	**s**	λ_m
G_m	32	27	36	0.9	0.0032	1.15	328.1
S_m	0.5	27	48.4	1.35	0.0007	1.5	266.7
G_s	32	27	36	0.9	0.0032	1	-
S_s	0.1	27	48.4	1.35	0.0007	1	-

2- The effective-roughness-height of longitudinal walls affects the strength of the energetic vertical flow structures that are capable of scouring the river bed and endangering the stability of the longitudinal walls. The roughness effective height can vary from a hydraulically smooth surface to a fully rough surface. In this investigation we will address the effect of this parameter by considering two longitudinal wall surfaces: hydraulically smooth and rough;

3- The installation angle of the longitudinal walls (or the angle of attack of the approaching mean-flow) plays an important role in strength of helical flow in rivers and therefore may influence the maximum scour depths near the walls. The effect of installation angle is studies by considering four different angles for each river.

In the two meandering rivers of S_m and G_m the longitudinal wall are installed at the apex with four angles within the range of -20 to 30 degrees, while for the two straight channels of S_s and G_s the four angles vary between 0 and 60 degrees. Fig. 20 shows a schematic of installation angle for the two rivers.

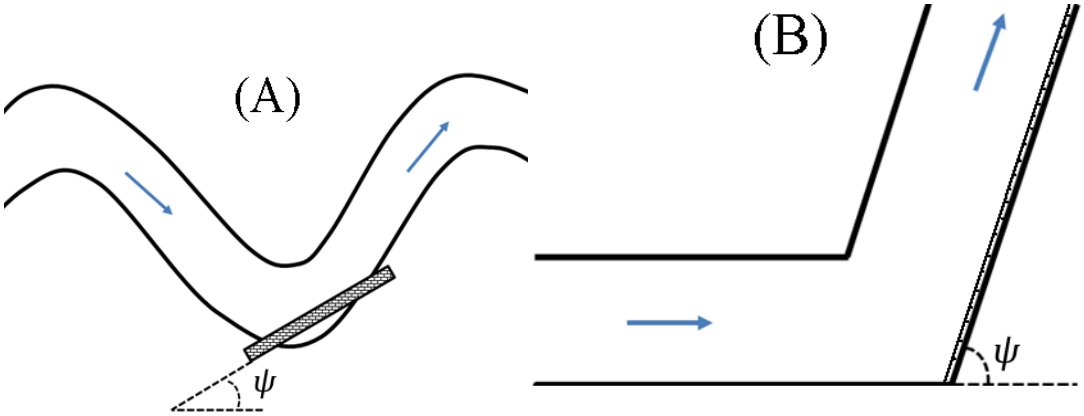

Figure 20. Schematic of the installation angles (ψ) of the longitudinal wall in (A) the meandering river of S_m and G_m and (B) straight channels of S_s and G_s.

We note that the total length and configuration of the longitudinal walls in each meandering river is determined based on the following criteria:

(a) The effective width of the river after installment of the longitudinal wall should be at least 70 percent of the original width of the river, i.e., the maximum width reduction due to installment of the longitudinal wall is 30 percent;

(b) The total length of the longitudinal wall is obtained by considering the installation angle (ψ in Fig. 20) and the maximum width reduction of 30 percent as mentioned above.

Hence, a matrix of numerical simulations, as shown in Table 3, is designed to investigate the above mentioned parameters that deemed most important.

Table 3. Matrix of scenarios for numerical simulations. Two effective roughness heights, various angles of attacks for meandering and straight channels. For the meandering channels the vertical wall are apex centered. The effective roughness height for the G and S rivers in rough simulations are equal to 0.096 (m) and 0.05 (m), respectively.

Stream	k_s	**Angle of installation, ψ (^{o})**	**# of simulations**
G_m	smooth, rough	0, 10, 20, -20	8
S_m	smooth, rough	0, 20, 30, -20	8
G_s	smooth, rough	0, 15, 30, 60	8
S_s	smooth, rough	0, 15, 30, 60	8
		Total	32

E.3.1 Simulation results for the meandering rivers of S_m and G_m

For each meandering river of G and S, three meander bends are considered in the simulations. The meandering length of a single bend for each river is given (λ_m) in Table 2. Simulations start with running solely the flow solver (with $k-\omega$ turbulence model) to obtain a steady state solution for the flow field. Once a steady state flow field is obtained for each test case, then the morphodynamic module is activated. The coupled hydro- and morpho-dynamics simulations are continued until the bed morphology reaches quasi-equilibrium, which on averaged takes about 2 to 3 months of physical time of the process. Depending on the number of computer cores utilized in parallel, CPU clock-time to get to quasi-equilibrium is also about 7 to 10 days for each test case.

After reaching quasi-equilibrium, we time average the bed morphology data to obtain statistically converged bed morphology for each test case. Presence of numerically captured bedforms throughout the rivers is often the main reason why we need to time-average the simulated bed morphology results.

At the inlet a uniform flow condition is applied, while at the outlet we employ a Neumann boundary condition. Free-surface of the water is treated as a rigid-lid surface and wall model approach is used for side banks and mobile bed boundary conditions. Out-flux of the sediment material is calculated at the outlet of each channel and fed into the river at its inlet cross section.

G_m river

In Fig. 21 we plot the simulated time-averaged morphology of the G_m river without any longitudinal wall. This case serves as our base-line case for the rest of the G_m cases with longitudinal walls.

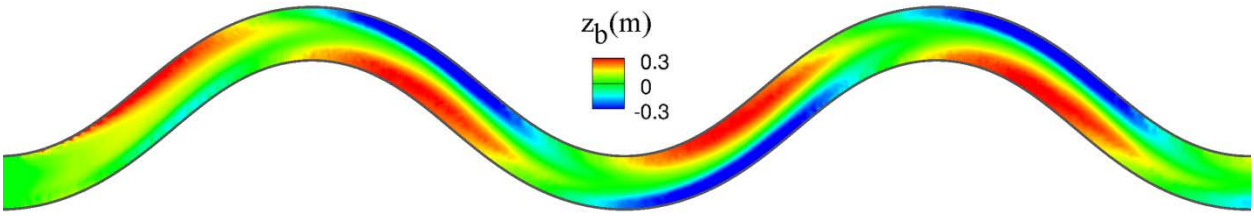

Figure 21. Plan view of the simulated (time-averaged) bed elevation (z_b) of the G_m river without longitudinal wall. Flow is from left to right and the body of water is not shown.

In Fig. 22 we show the simulated bed morphology of the G_m river with different longitudinal walls, which are hydraulically smooth. Typical patterns of degradation and sediment deposition in forms of scour and point bar near the inner and outer banks of the meander can be seen in this figure. However, for the longitudinal wall with installation angle of -20^o one can see an extended scour pattern that reaches upstream up until the middle of the base of longitudinal wall (Fig. 22 (D)). As we show in Fig. 22, for all of the installation angles the maximum scour depth in the vicinity of the longitudinal walls, the maximum scour depth occurs near the middle of the structures.

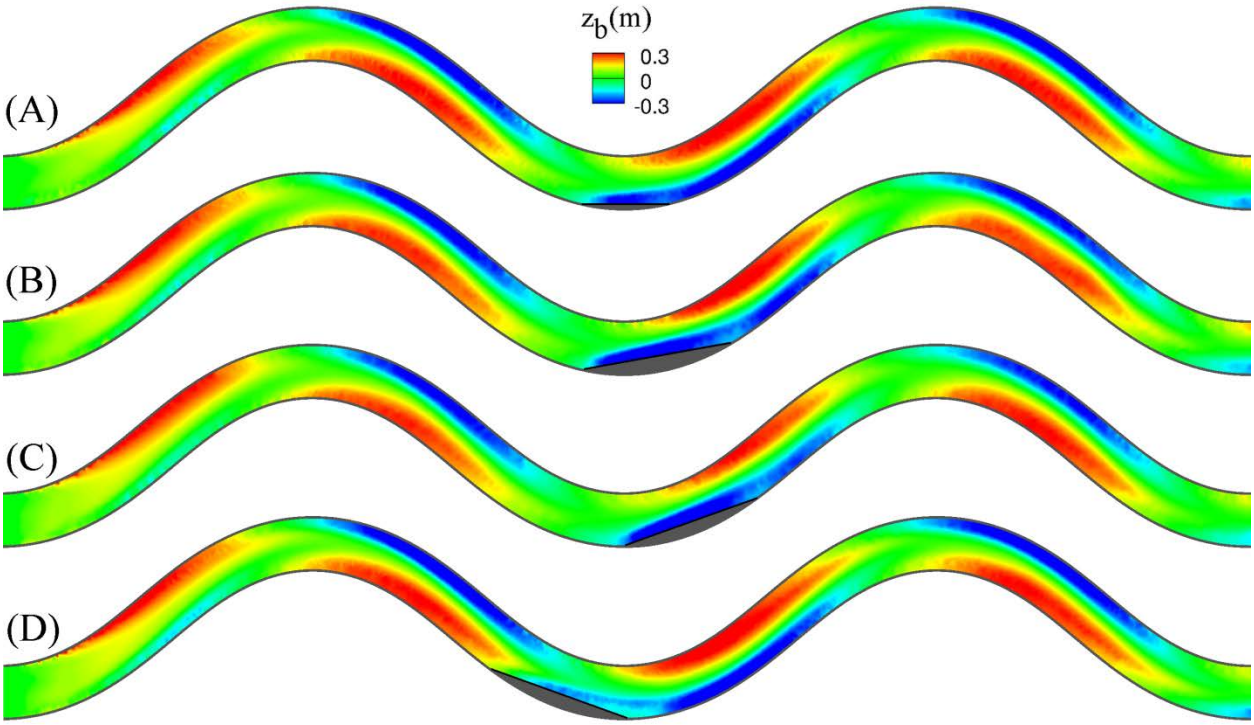

Figure 22. Plan view of the simulated (time-averaged) bed elevation (z_b) of the G_m river with hydraulically smooth longitudinal walls. Installation angle of walls in (A) to (D) are 0^o, 10^o, 20^o, and -20^o, respectively. Flow is from left to right and the body of water is not shown. Gray areas show the longitudinal walls.

In order to demonstrate the effect of the longitudinal walls on the overall scour patterns in G_m river, we compute the difference between each bed morphology and the bed morphology of the base line case (shown in Fig. 21) as $\Delta z_b = \langle z_b \rangle_{wall\ installed} - \langle z_b \rangle_{base-line}$.

In Fig. 23 we plot the computed difference between the base-line and wall installed cases, which show that, in all cases, placement of the longitudinal walls lead to a deeper scour hole in the region near the middle of the walls. One should note that, however, instead of being attached to the outer bank (in the base-line case), the location of maximum scours in Fig. 23 is slightly pushed toward the middle of channel.

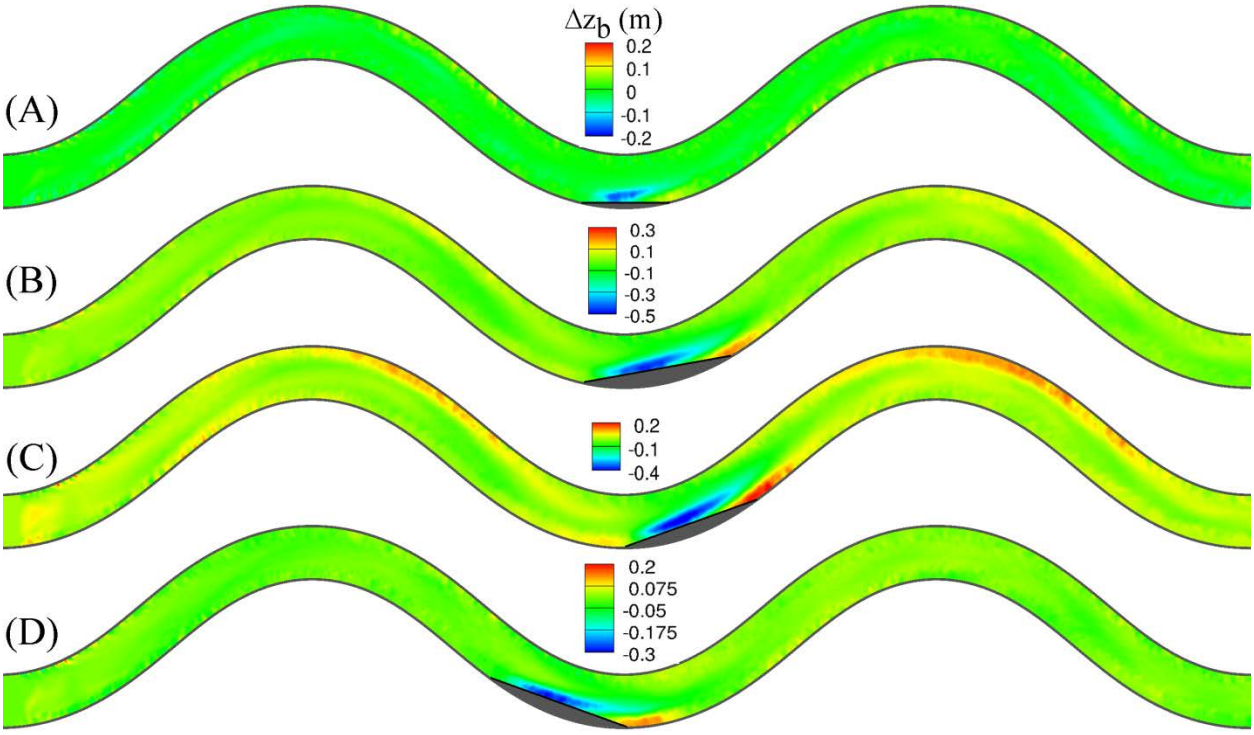

Figure 23. Plan view of the computed bed elevation difference between base-line and wall installed cases (Δz_b) for the G_m river. Installation angle of walls in (A) to (D) are 0^o, 10^o, 20^o, and -20^o, respectively. Flow is from left to right and the body of water is not shown. Gray areas show the longitudinal walls.

A similar pattern can be seen in Fig. 24 for the G_m river with similar installation angles but with hydraulically rough longitudinal walls. The maximum scour depth for rough walls is slightly greater but the overall scour patterns quite similar.

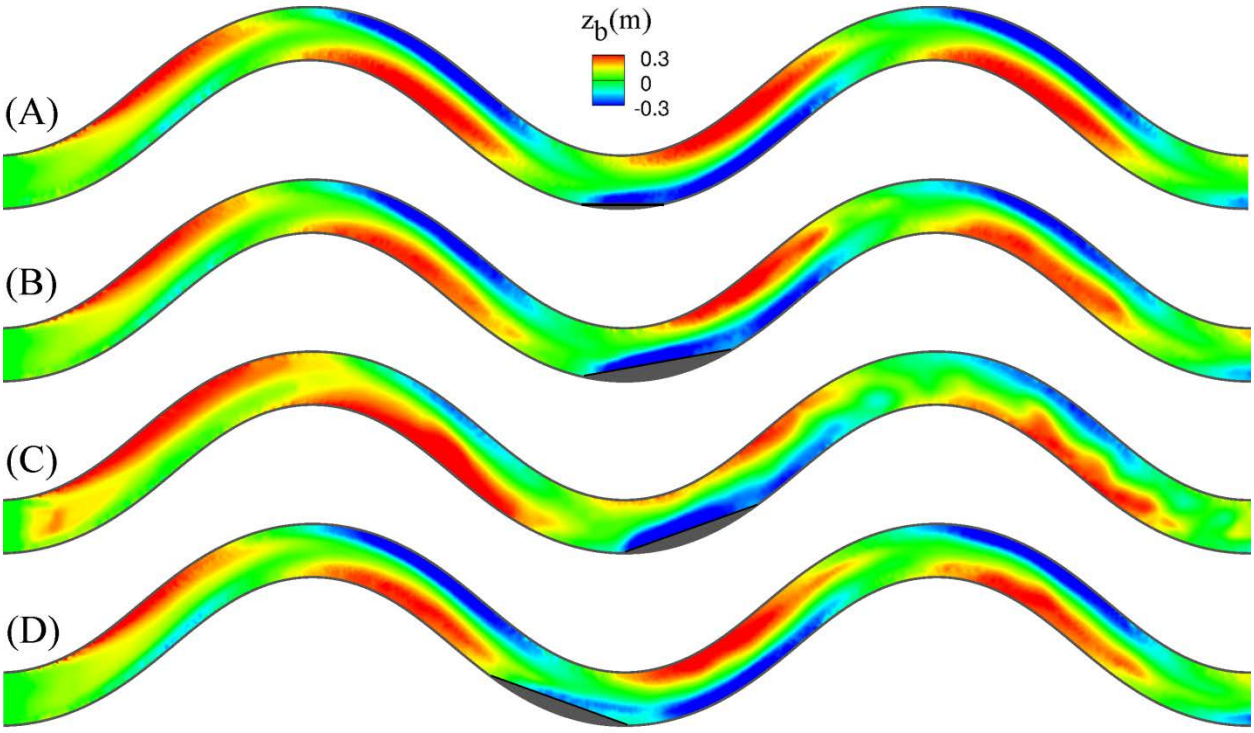

Figure 24. Plan view of the simulated (time-averaged) bed elevation (z_b) of the G_m river with hydraulically rough longitudinal wall. Installation angle of walls in (A) to (D) are 0^o, 10^o, 20^o, and -20^o, respectively. Flow is from left to right and the body of water is not shown. Gray areas show the longitudinal walls.

The range of the maximum scour depths for the G_m river varies between 0.2 (m) to 0.6 (m). The maximum scour depth data will be used in section E.4 to adapt a formula for the maximum scour depth around the longitudinal walls.

S_m river

As for the S_m rivers, in Fig. 25 we plot the simulated bed morphology of the base-line case in which degradation and deposition (point bar) areas can be seen near the outer and inner banks, respectively.

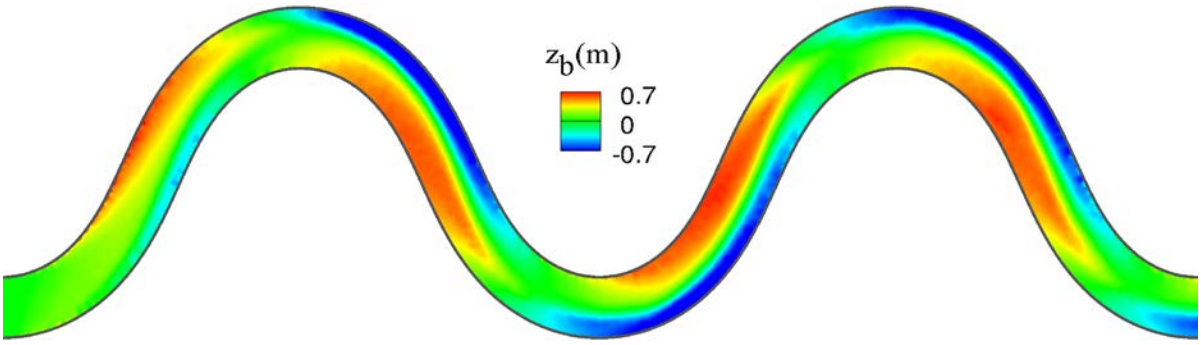

Figure 25. Plan view of the simulated (time-averaged) bed elevation (z_b) of the S_m river without longitudinal wall. Flow is from left to right and the body of water is not shown.

We placed the four hydraulically smooth longitudinal walls with installation angles of 0^o, 20^o, 30^o, and -20^o near the apex of the middle meander and completed the coupled simulations. The time-averaged bed morphology of these test cases are shown in Fig. 26, where even time averaging could not completely remove the footprint of the numerically captured bedforms. For the two installation angles of 20^o and 30^o in which the longitudinal walls have caused a relatively more pronounced width constriction, relatively larger bedforms are created and thus longer time averaging is required to completely remove them.

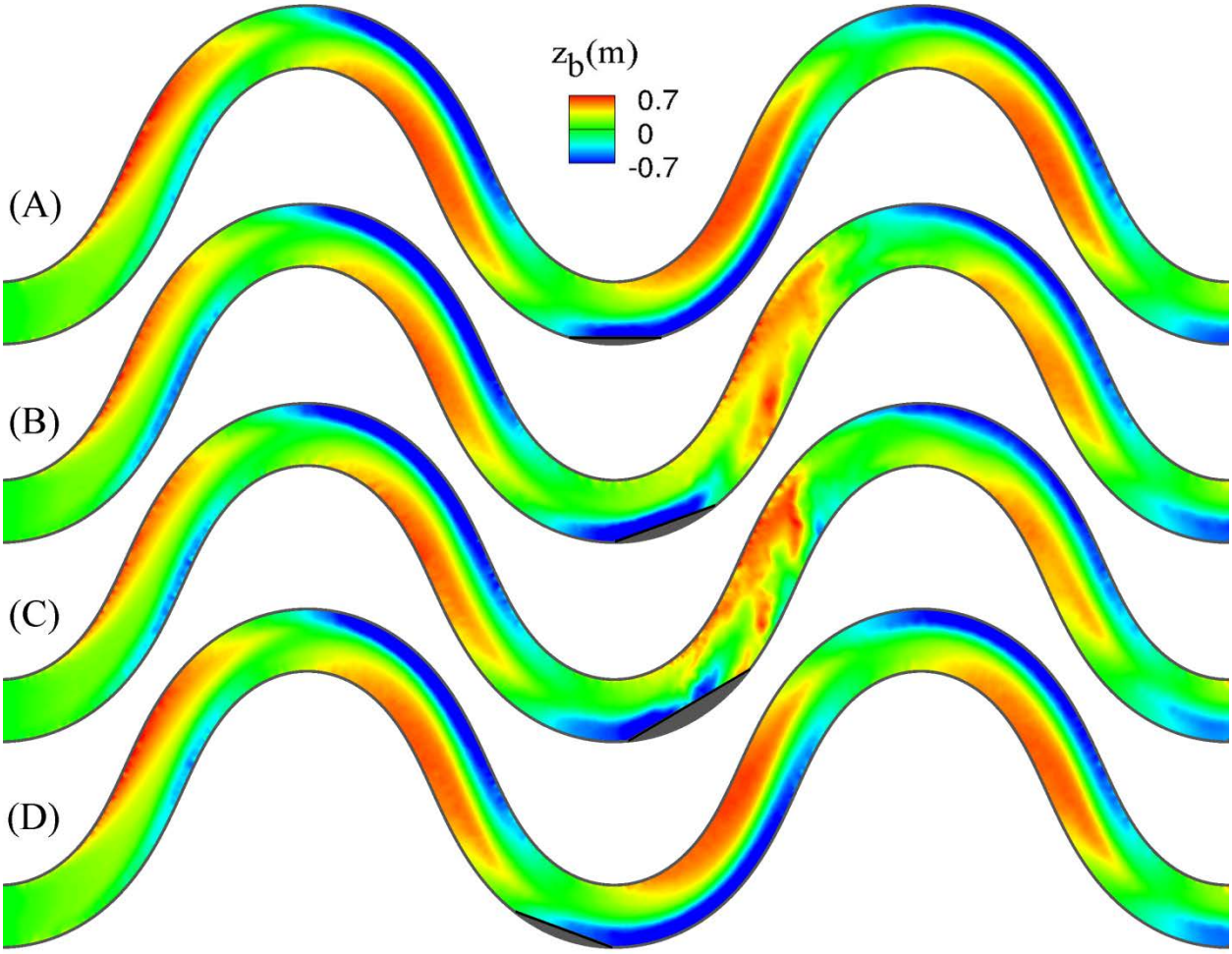

Figure 26. Plan view of the simulated (time-averaged) bed elevation (z_b) of the S_m river with hydraulically smooth longitudinal walls. Installation angle of walls in (A) to (D) are 0^o, 20^o, 30^o, and -20^o, respectively. Flow is from left to right and the body of water is not shown. Gray areas show the longitudinal walls.

Plots of bed elevation difference between base-line (in Fig. 25) and wall installed cases (Fig. 26) for the S_m river are shown in Fig. 27. As shown in this figure, similar to the G_m river placement of the longitudinal wall has led to a relatively deeper scour depth near the middle of the longitudinal walls.

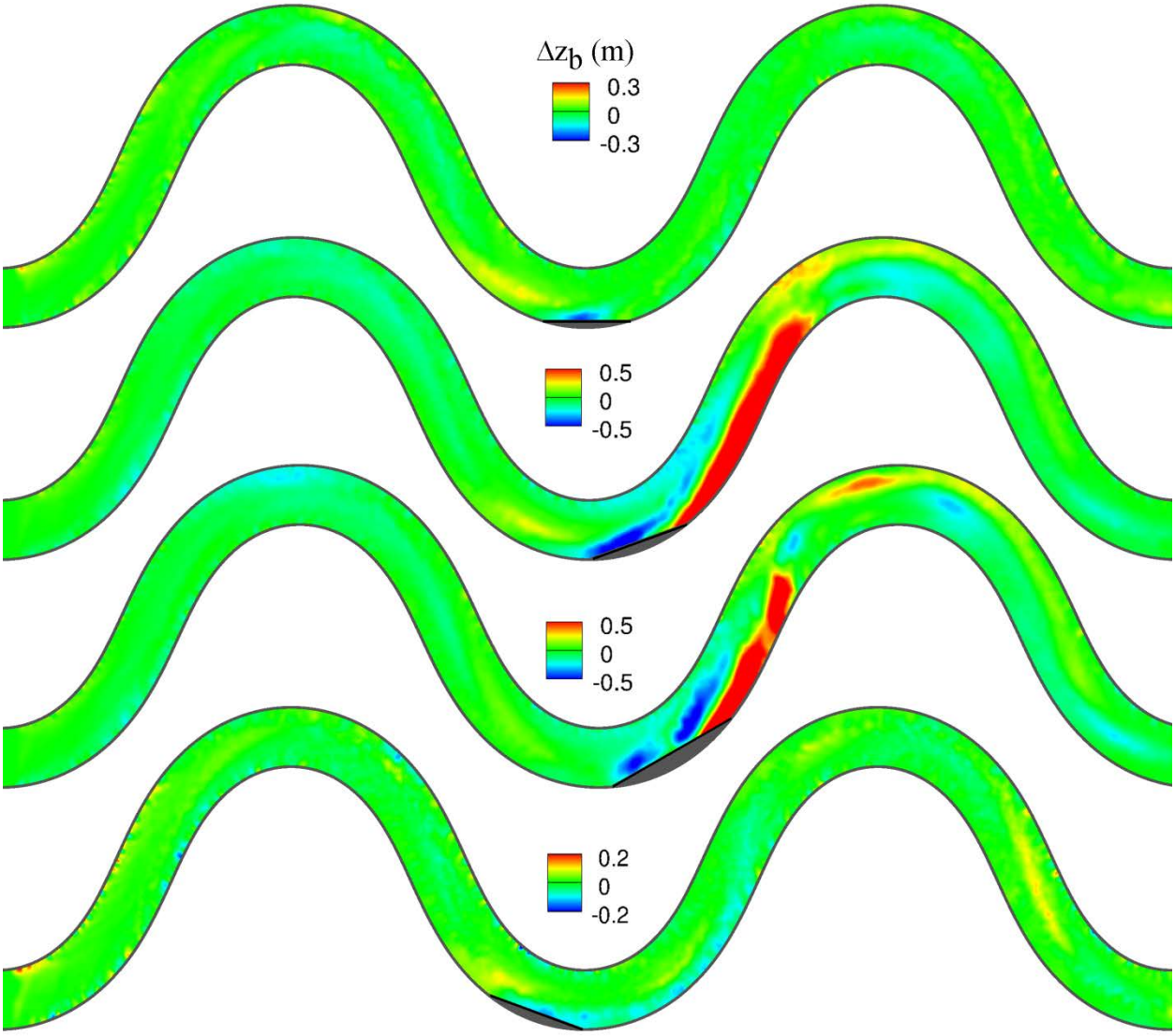

Figure 27. Plan view of the computed bed elevation difference between base-line and wall installed cases (Δz_b) for the S_m river. Installation angle of walls in (A) to (D) are 0^o, 20^o, 30^o, and -20^o, respectively. Flow is from left to right and the body of water is not shown. Gray areas show the longitudinal walls.

Adding roughness to the longitudinal walls in S_m river, we simulated the four scenarios and the time-averaged bed morphology are plotted in Fig. 28. Comparing to the smooth walls, the rough walls has led to about 1 to 5 percent increase in maximum scour depth. However, as one can see

in the Figs. 26 and 28 the general scour patterns for the two smooth and rough cases are quite similar. The maximum scour depths for the S_m river varies between ~0.6 (m) and ~1.3 (m) and the bulk of these data along with the data obtained for the G_m river will be utilized in section E.4 to extract a general formula for the maximum scour depth around longitudinal walls in meandering rivers.

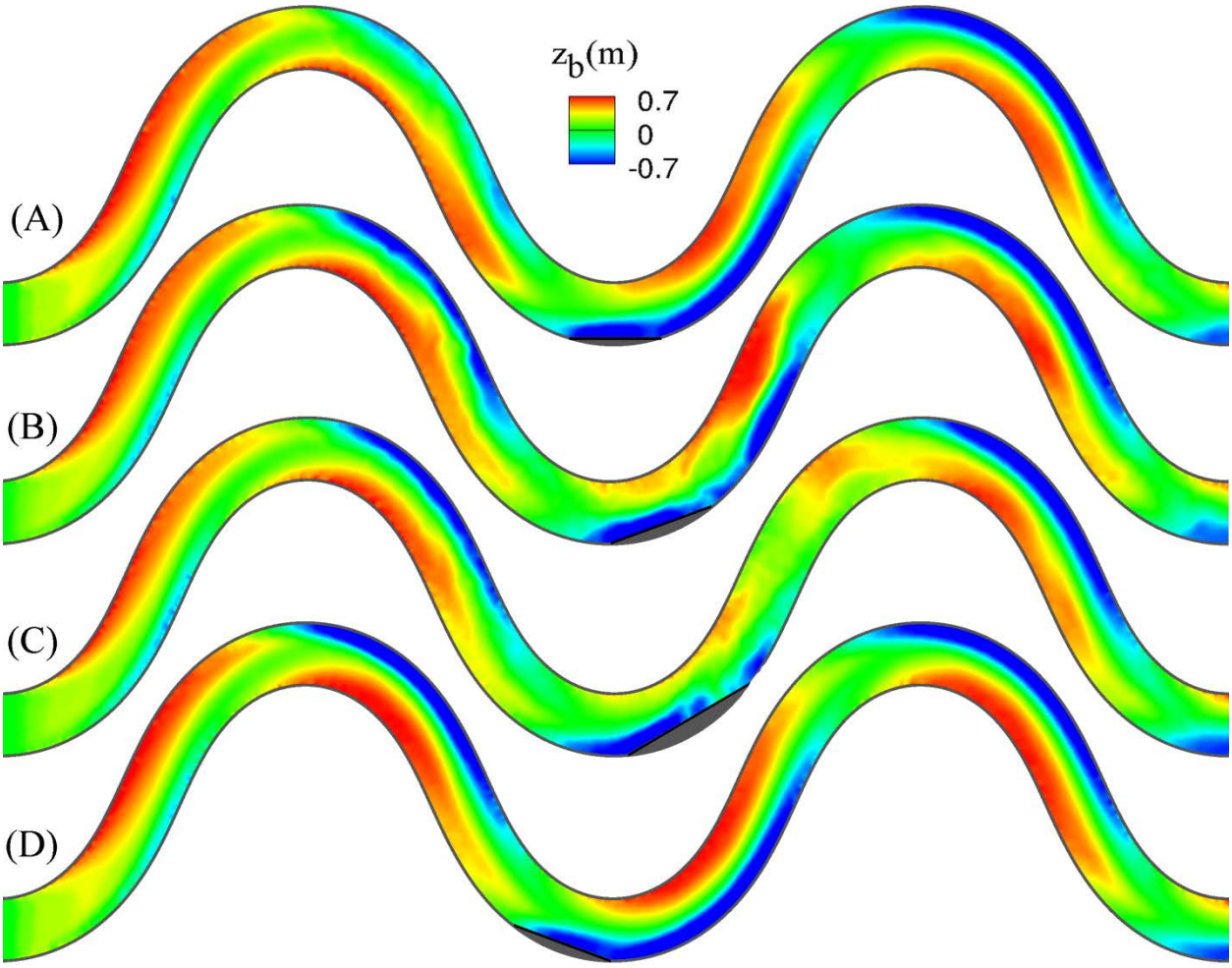

Figure 26. Plan view of the simulated (time-averaged) bed elevation (z_b) of the S_m river with hydraulically rough longitudinal walls. Installation angle of walls in (A) to (D) are 0^o, 20^o, 30^o, and -20^o, respectively. Flow is from left to right and the body of water is not shown. Gray areas show the longitudinal walls.

E.3.2 Simulation results for the straight rivers of S_s and G_s

For each of straight G and S rivers, four different angles of installation, which follows the river bank, is considered (Fig. 20 (B)). The overall length of the straight rivers is shorter than their alternative meandering rivers. The reason for this is that for the meandering rivers we considered three meander bend so that the middle meander, where we install the structures, is far enough

from the inlet and outlet of the channels. While for the straight cases the structures are installed on the entire angled bank. Simulations start with running solely the flow solver (with $k-\omega$ turbulence model) to obtain a steady state solution for the flow field. Soon after steady state condition for the flow field is reached, the fully coupled hydro- and morphodynamic model is started. Coupled simulations are continued until the bed morphology reaches quasi-equilibrium, which on averaged takes about 1 to 2 months of physical time of the process. Depending on the number of computer cores utilized in parallel, CPU clock-time to get to quasi-equilibrium is about 6 to 8 days. Boundary conditions are identical to those we employed for the meandering rivers of G and S.
Even though the flow, sediment characteristics, and channel width (=27 (m)) of the two straight rivers of G and S are the same as those of meandering channels, the total length of straight channels is shorter than the meandering rivers. Depending on the angle of the walls, the total length of the straight channels vary between ~200 (m) and ~300 (m). The greater the angle of installation the longer is the channel.

Gs river

We ran the simulation for this test case and observed no significant sediment movement except for the tow installation angles of 30 and 60 degrees. However, the scour and deposition processes occur only near the sharp angle on the opposite side of the longitudinal walls (near left banks) (see Fig. 27). As we show in Fig. 27, because of the large size of the sediment particles in the G rivers, when placed in a straight channel, no sediment movement occurs. While in a meander bend, as shown for the G_m rivers, the same sediment particle size would move and thus we observe various scour patterns in Fig. 22. The main reason for this disparity is the present of strong helical flows in the meandering rivers and that the flow pattern near the mobile bed is such that causes the formation of point bars and scour region near the outer and inner banks, respectively. We obtained literally identical simulation results for the hydraulically smooth and rough longitudinal walls.

Gs river with much finer bed material

As we showed in Fig. 27, the existing bed shear stress is not high enough to excite a meaningful bed martial transport in the *Gs* river, which virtually consists of such a large particle size of d_{50}=3.5 cm (see Table 2). In order to bring the bed material in this river to the brink of movement and to figure out potential transport pattern associated with such bed material transport, we employed bed materials with a grain size that is one order of magnitude finer ($d_{50} = 0.35\ cm$). Having said, all other characteristics such as flow, river, and sediment material properties are kept the same as those of *Gs* in Table 2.
With the new particle size, the particles start to be destabilized and this is shown in our simulations results in Fig. 28. In about a day or two of physical time of simulations, the bedforms cover the whole length of the river. After around a month of physical time the bedfroms reach their dynamic-equilibrium in which even though the bed elevation is constantly changing but it follow the wavy-shape trend of dune movement.
The time-averaged results of the simulated bed elevation in this case has an *rms* of bed fluctuation of about 50 percent. Given the high *rms* of bed elevation fluctuations, we argue that

the maximum scour depth for this case is better to be predicted based on the minimum bed elevation during the passage of a sand wave near the longitudinal wall (bed elevation at the trough of the bedforms). Therefore, the maximum scour depth for the four installation angles of 0, 15, 30, and 60 degrees (Fig. 28) are computed as 0.25 (m), 0.26 (m), 0.28 (m), and 0.31 (m), respectively. Our simulation results for this case with the hydraulically rough longitudinal wall in terms of maximum scour depth and the simulated bedforms are literally the same.
The data points associated with G_s river with angle of 0 degree (for rough and smooth walls), which are similar to a meandering river with a sinuosity of 1.0, will be used in the next section to develop a scour depth relationship.

Ss river

The simulation results for this test case with four hydraulically smooth walls and different angles of installations are shown in Fig. 29. Soon after coupled flow-morphodynamics simulations start, numerically captured sand waves form and continue to grow in size. The size of these bed forms grows until they reach to an equilibrium size that is about 1.4 (m) m in amplitude, i.e. the trough the sand waves is about 0.7 (m) below the initially flatbed elevation.
By time-averaging the bed elevation results we computed maximum scour depths of the four installation angles of 0, 15, 30, and 60 degrees (Fig. 29) to be 0.31 (m), 0.21 (m), 0.34 (m), and 0.81 (m), respectively. As one can see in Fig. 29, the entire channel bed in all cases is covered with the numerically captured bedforms and the computed *rms* of the bed elevation fluctuations, in all cases, is more than 60 percent. Such a high *rms* number show that one must be careful interpreting these maximum scour depths.

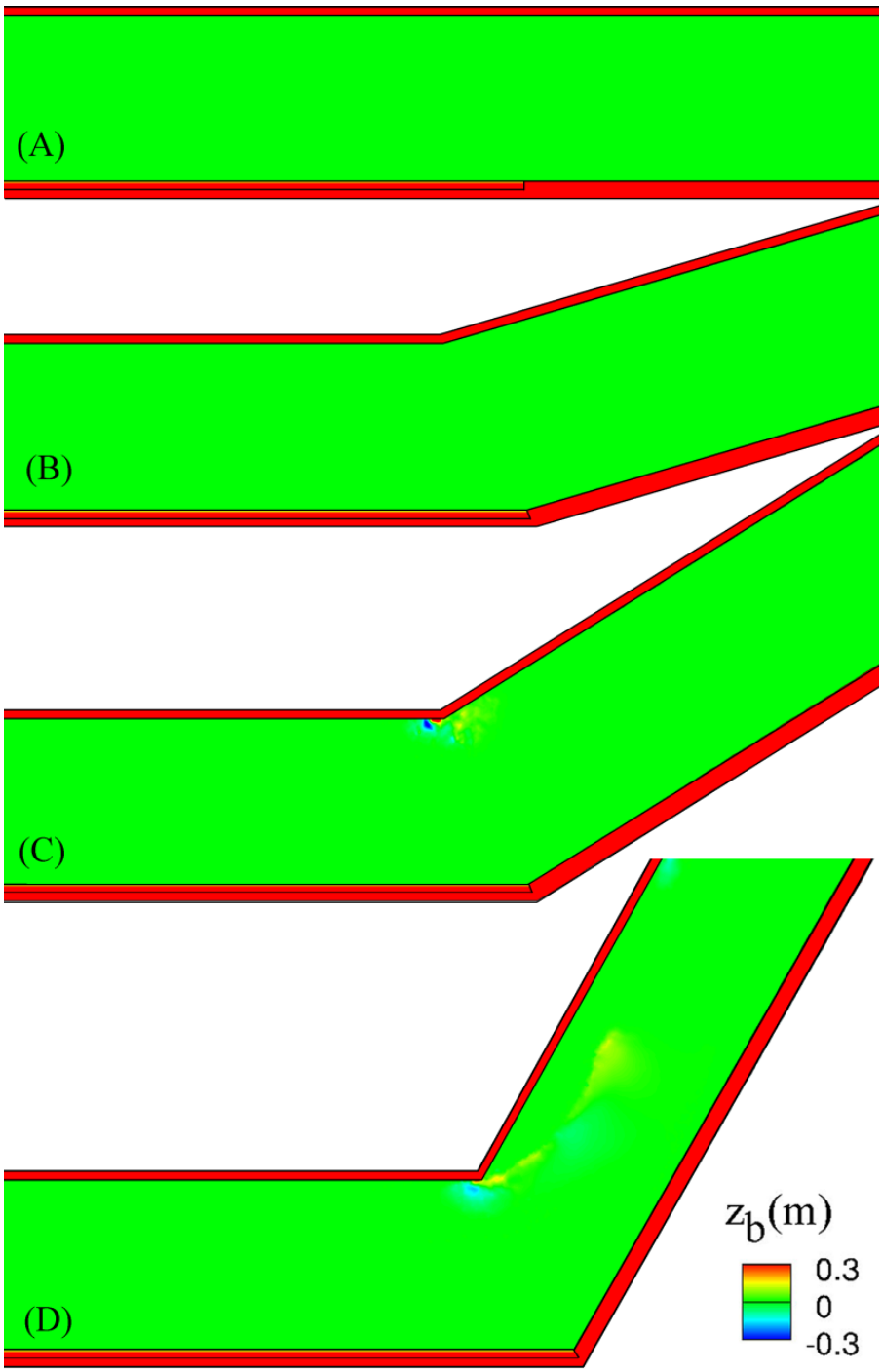

Figure 27. Plan view of the simulated (instantaneous) bed elevation (z_b) after 2 months (physical time) of the G_s river with hydraulically smooth longitudinal walls, which is identical to those of the rough walls. Installation angle of walls in (A) to (D) are 0^o, 15^o, 30^o, and 60^o, respectively. Flow is from left to right and the body of water is not shown. The sediment movement regions

exist only for the two cases with 30 and 60 degrees angle of installation and these movement regions are limited to zones near the sharp angle on the opposite side of the longitudinal walls.

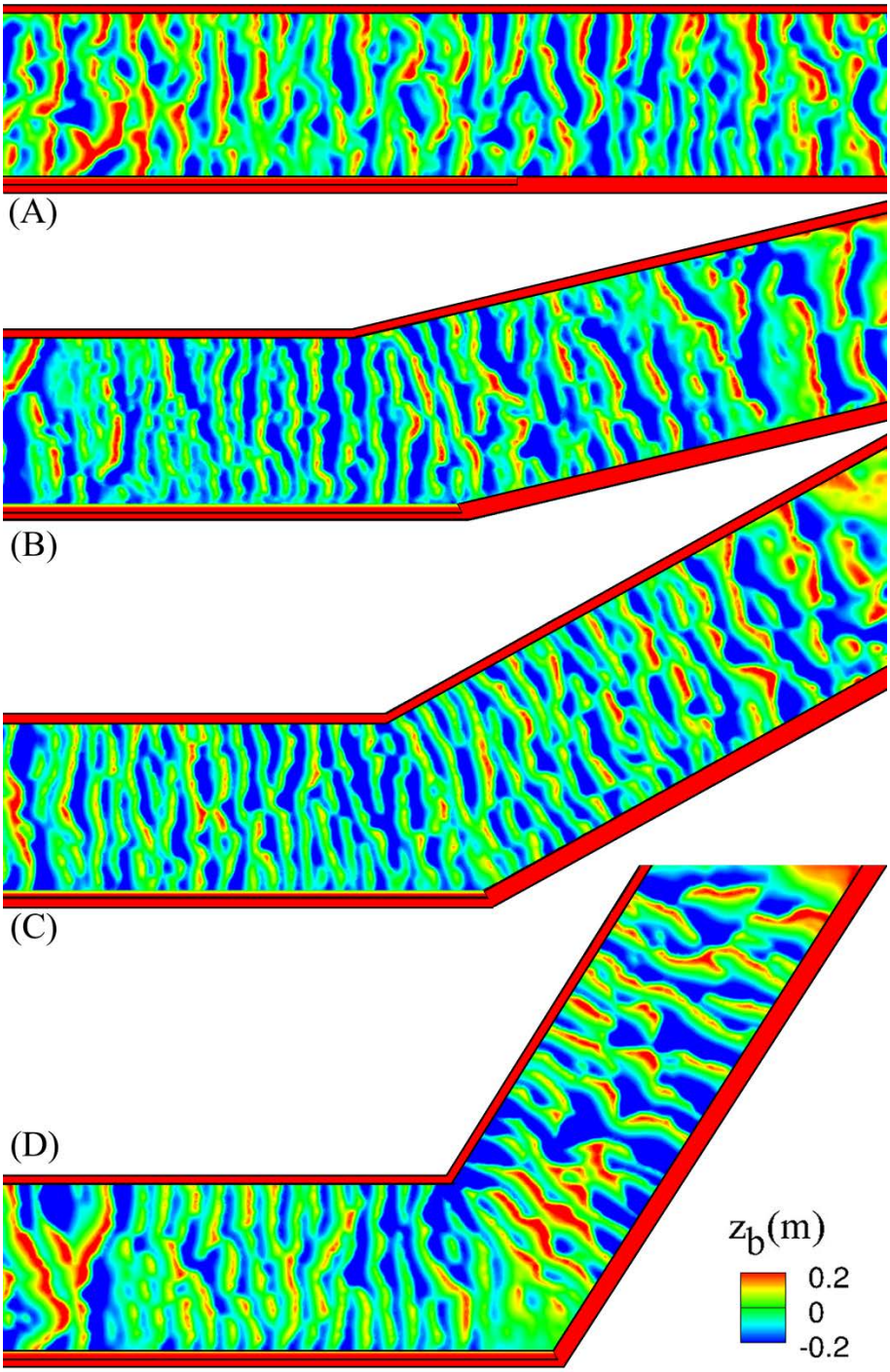

Figure 28. Plan view of the simulated (instantaneous) bed elevation (z_b) after 1.5 months (physical time) of the G_s river with hydraulically smooth longitudinal walls. Installation angle of

walls in (A) to (D) are 0^{o}, 15^{o}, 30^{o}, and 60^{o}, respectively. Flow is from left to right and the body of water is not shown.

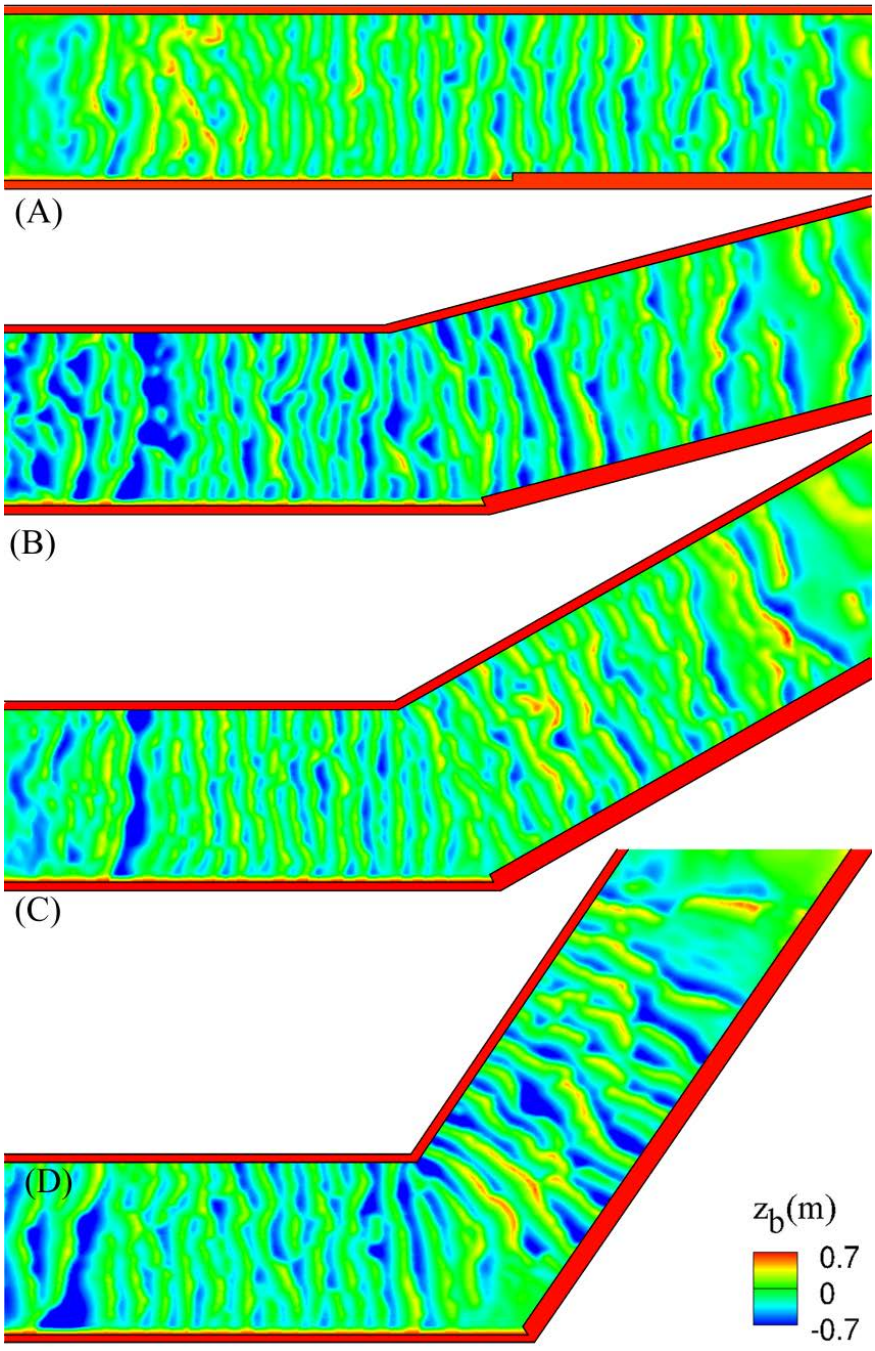

Figure 29. Plan view of the simulated (instantaneous) bed elevation (z_b) after about 1.5 months (physical time) of the S_s river with hydraulically smooth longitudinal walls, which is similar to those of the rough walls. Installation angle of walls in (A) to (D) are 0^o, 15^o, 30^o, and 60^o, respectively. Flow is from left to right and the body of water is not shown.

To have a conservative estimation, one may use the norm of the maximum scour depth computed from time-averaged results and the amplitude of the bedforms. Therefore, the following maximum scour depth can be obtained for each case: 0.7 (m), 0.7 (m), 0.7 (m), and 0.81 (m), for the installation angles of 0, 15, 30, and 60 degrees, respectively. The simulations results for the hydraulically rough longitudinal walls obtained identical results in terms of characteristics of the bedform and the computed maximum scour depth.
We note that the maximum scour depth data points for the S_s river with angle of 0 degree (rough and smooth walls), which are similar to a meandering river with a sinuosity of 1.0, will be used in the next section to develop a scour depth relationship.

E.4 Development of scour relationships based on the numerical experiment and OSL data

The simulation results for maximum scour depth near longitudinal wall in E.3 and also scour data from OSL experiments in Appendix C are used to produce an empirical relationship for general scour. As shown in Table 3, these data points include are 24 and include G_m (8 data points), S_m (8 data points), G_s (2 data points), and S_s (2 data points) river data. Note that only the zero degree straight channels are used in developing the equation as they are similar to the meandering channels except that their sinuosity is 1.0. For the OSL experiments, we have 4 data points, which are explained in Appendix C.
Via dimensional analysis, parameters influencing the maximum scour depth along the length of the walls are as follows:

$$H_s = f(d_{50}, U, H, S_0, \lambda_m, A_m, Q, g, k_s, \psi) \tag{5}$$

where H_s is the maximum scour depth, d_{50} median grain size of the sediment material, U is the mean-flow velocity, H is the mean-flow depth, S_0 is the channel bed slope, λ_m is the wavelength of the meander bend, A_m is the amplitude of the meander bend, Q is the flow discharge, g is the acceleration of gravity, k_s is the effective roughness height on the longitudinal wall, and ψ is the angle of installation of the longitudinal wall.
Performing a series of analysis, we found that the maximum scour depth can be best found if scaled with d_{50}. The characteristics of a meander bend can also be best expressed via its sinuosity, which is a function of λ_m and A_m. Thus, Eq. (5) in its non-dimensional form can be rewritten to obtain:

$$H_s/d_{50} = f(Fr, Fr_d, tan\,(\psi), s, k_s/H) \tag{6}$$

where $Fr = U/\sqrt{gH}$ is the Froude number, $Fr_d = U/\sqrt{gd_{50}}$ is the particle Froude number, and s is the meander sinuosity.

We analyzed numerous methods to best represent the bulk of these data in one empirical relationship (see Fig. 30) and found that the following equation provides the best overlap:

$$H_s/d_{50} = 1909\ (Fr\ s\ \vartheta)^{-10/9} + \frac{8}{5}\ Fr_d - \frac{3\pi}{2}\,\mathrm{e}^{(k_s/H)^{1/10}} \tag{7}$$

In which ϑ for the G and S rivers is defined in Eqs. (8) and (9), respectively.

$$\vartheta = Max\{150, (\tan\psi)^{-2}\} \tag{8}$$

$$\vartheta = Max\{100, (\tan\psi)^{-2}\} \tag{9}$$

Equation (7) has a correlation coefficient of r^2 = 0.821 and has the following important limitations:

1- It is only applicable for rivers and streams with non-cohesive material;
2- It is developed for rivers under bankfull flow conditions and thus use of this equation for base-flow condition can result in misleading predictions;
3- It is best applicable for the rivers that have geometry, flow, and sediment characteristics within the range of the rivers we studied in this project (see Table 2);
4- Scour hole due to the intrusion of the upstream edge of the longitudinal wall is not considered in obtaining these data and such scour depth needs to be determined based on the laboratory experiments (see Appendix D) and added to the maximum scour depth obtained from Eq. (7);
5- As we discussed in section E.3, the effective roughness height plays a minor role in predicting the maximum scour depth. Therefore, even though we do not recommend, but for the sake of simplicity one can drop the last term on the right hand side of the Eqn. (5).

We also show in Fig. 31 the source of each data point used in this analysis to obtain the correlation associated with the maximum scour depth formula in Eq. (7). As we discussed above, these data base include 24 data points from our two different sources: numerical (20 points) and OSL (4 points) experiments.

Thus, we propose the use of Eq. (7) as a formula to calculate the maximum scour depth at the base of longitudinal walls in meandering rivers. To avoid misleading predictions, it is important, however, that the five limitations (mentioned above) to be considered.

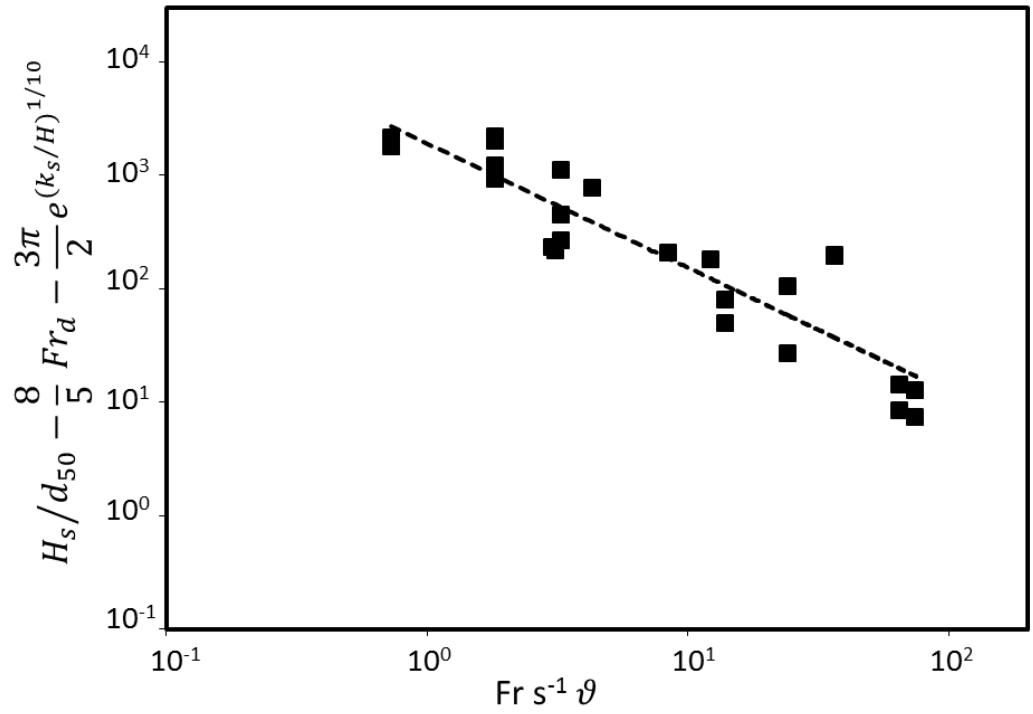

Figure 30. Maximum scour depth data obtained from numerical experiments and OSL experiments (dots) and the regression equation overlapping the data (dashed-line). r^2 of the regression is 0.821.

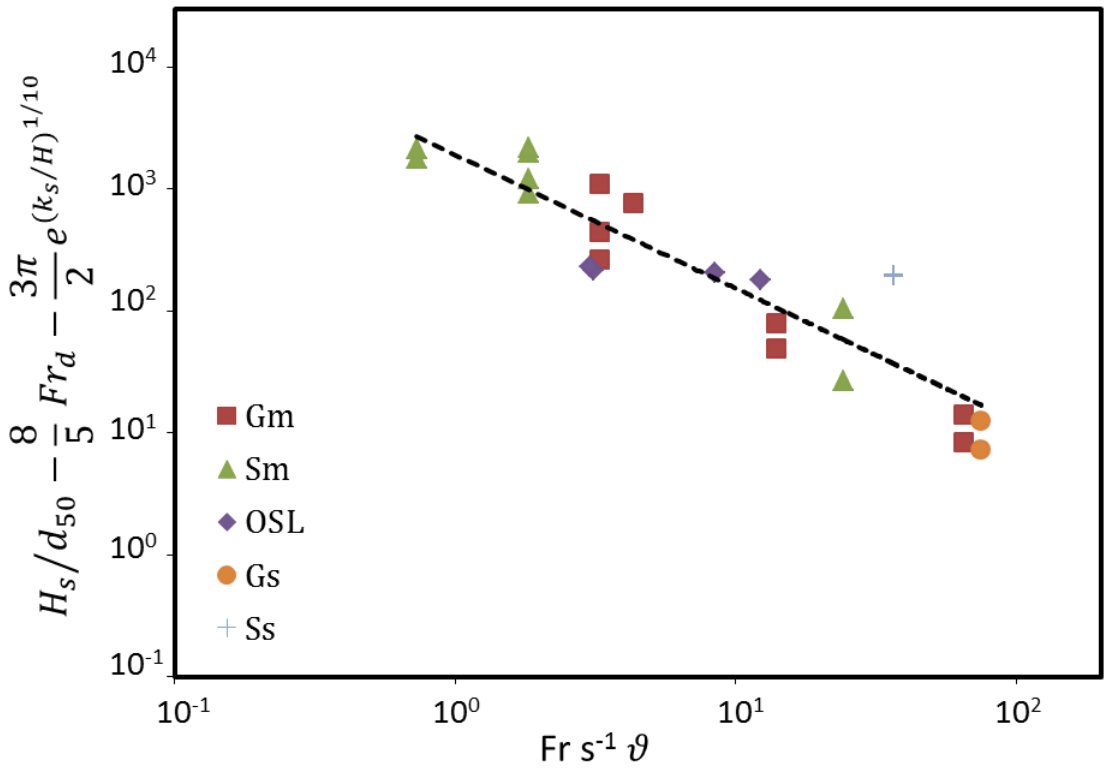

Figure 31. Maximum scour depth data obtained from numerical and OSL experiments (purple diamonds) and the regression equation overlapping the entire data points (dashed-line), which has a goodness of $r^2 = 0.821$. Green-triangles, red-squares, orange-circles, and blue-plus signs represent the numerical data points associated with the S_m, G_m, G_s, and S_s virtual rivers.

E.5 References

Jia Y, Xu Y, Wang S.Y. (2002). Numerical simulation of local scouring around a cylindrical pier. In: Proceedings of ICSF-1, *1st International Conference on Scour of Foundations*, 2002, Texas A&M University, Texas, USA.

Khosronejad, A., Kang, S., and Sotiropoulos, F., 2012. Experimental and Computational Investigation of Local Scour around Bridge Piers. Advances in Water Resources, 37, 73-85.

Appendix F

List of variables

A_m	Amplitude of the meander bend;
d_{50}	Median grain size of sediment material;
Fr	Froude number;
Fr_d	Grain-size Froude number;
g	Acceleration of gravity;
H	Mean-flow depth;
H_s	Maximum Scour depth at the base of longitudinal wall;
H_{sl}	Maximum scour depth due to local scour mechanism;
H_{sg}	Maximum scour depth due to general scour mechanism;
k_s	Effective roughness height of the surface of longitudinal wall;
Q	Flow discharge;
R_C	Radius of curvature of meander bend;
Re_p	Sediment particle Reynolds number;
S	Waterway bed slope;
s	Sinuosity of the waterway;
U	Mean-flow velocity;
W	Width of the waterway;
θ	the angle between the impinging flow direction and the vertical wall;
ψ	Angle of installation of longitudinal wall in meandering rivers;
λ_m	Wavelength of the meander bend;
ρ_s	Density of sediment material;
ρ	Density of fluid, which, in this work, is water;
υ	Kinematic viscosity of water.